DISS. ETH No 23170

Role of the CXCR4/SDF-1 Chemokine Axis in Metastasis Formation in Osteosarcoma

A thesis submitted to attain the degree of

DOCTOR OF SCIENCE of ETH ZURICH

(Dr. sc. ETH Zurich)

presented by

Olga Neklyudova

Dipl. Biol. Siberian Federal University

born on 04.12.1985

citizen of Germany/Russia

accepted on the recommendation of

Prof. Dr. Ernst Hafen, ETH Zurich

Prof. Dr. Josef Jiricny, ETH Zurich

Prof. Dr. Pancras Hogendoorn, LUMC Leiden

Prof. Dr. Bruno Fuchs, Uniklinik Balgrist, Zurich

Prof. Dr. Marcus Thelen, IRB Bellinzona

2015

To my family

Table of Contents

Summary

Osteosarcoma (OS) is a highly malignant primary bone tumor with a high propensity for lung metastasis being the main cause of death in patients with OS. The introduction of chemotherapy in the late 70s improved the survival of OS patients with localized disease dramatically. The five-year survival rate of patients who present with metastasis at diagnosis, however, plateaued at about 20% and has not been increased since that time. Therefore, we urgently need to gain a better understanding of the molecular mechanisms underlying OS metastasis in order first to develop new efficient targeted therapies aiming at the inhibition of metastatic spread and second to improve survival and life quality of OS patients suffering from metastatic disease.

The involvement of the SDF-1/CXCR4 chemokine axis in the metastatic process of various cancers has been widely investigated. It has been shown that CXCR4 positive metastatic cells migrate towards SDF-1 concentration gradient to the sites of secondary lesions. It is not clear, however, if the same mechanism applies to OS cells originating from the bone, where SDF-1 is constitutively expressed by bone marrow cells. Further, inconclusive results of the correlation between CXCR4 expression in OS samples and metastasis or patient survival have been reported. Therefore, the aim of this thesis was to investigate in more details the role of the SDF-1/CXCR4 chemokine axis in OS development *in vivo* in SCID mice. In order to do so, we interfered with the SDF-1/CXCR4 chemokine signaling in CXCR4 expressing 143-B human OS cells via stable expression of native SDF-1 or its genetically modified variants, P2G or SDF-1-KDEL. P2G is a competitive SDF-1 receptor antagonist, whereas SDF-1-KDEL is a fusion protein that prevents cell surface expression of CXCR4. Empty vector carrying cells were used as a control.

Our results revealed that expression of native SDF-1 did not affect OS tumor growth, but strongly promoted metastasis, whereas local interference with SDF-1/CXCR4 interaction through P2G or SDF-1-KDEL expression in 143-B cells significantly enhanced intratibial

tumor growth and inhibited lung metastasis. Interestingly, we observed that tumors grown from P2G and SDF-1-KDEL expressing 143-B cells contained larger numbers of CXCR4 expressing tumor cells. These results were supported by the increased levels of CXCR4 encoding mRNA detected in these tumors compared to control. Apparently, CXCR4 expression in OS cells promoted tumor cell retention within primary tumors rather than metastatic dissemination, which was reflected by an increased primary tumor size and a decreased number of metastasis in P2G- and SDF-1-KDEL- tumor-bearing mice. Intriguingly, further analysis of mouse lungs revealed an enrichment in CXCR4 expressing disseminated tumor cells in all experimental groups. These findings provide evidence that SDF-1/CXCR4 signaling might be crucial for survival and proliferation of OS cells in later steps of the metastatic process, thus revealing a dual role of the SDF-1/CXCR4 pair in the metastatic cascade of OS. In conclusion, our results provide new insights into the role of the SDF1/CXCR4 chemokine pair in OS, thereby defining the basic rationale for local CXCR4 targeted anti-metastatic therapy in the lungs.

Zusammenfassung

Das Osteosarkom ist ein bösartiger primärer Knochentumor. Es verursacht Lungenmetastasen, welche die Haupttodesursache der Osteosarkompatienten sind. Nach der Einführung der Chemotherapie in den Siebzigerjahren hat sich das Überleben der Osteosarkompatienten mit einem lokalisierten Tumor dramatisch verbessert. Bei den Patienten, bei denen Metastasen festgestellt wurden, blieb die 5-Jahres-Überlebensrate unverändert bei nur 20 Prozent. Die Prognose hat sich für die Patienten mit Metastasen seitdem nicht verbessert. Um neue, effektivere und gezielte Therapieansätze zu entwickeln um die Lebensqualität der Patienten mit Metastasen zu verbessern, bedarf es eines besseren Verständnisses von den molekularen Mechanismen der Osteosarkommetastasierung.

Es wurde wissenschaftlich nachgewiesen, dass das Chemokin SDF-1 und dessen Rezeptor, CXCR4, bei der Metastasierung von verschiedenen Krebsarten involviert sind. Tumorzellen, die den Rezeptor CXCR4 haben, migrieren entlang eines Gradienten von SDF-1, das im Sekundärgewebe produziert wird. Es ist nicht klar, ob der gleiche Mechanismus bei Knochentumoren eine Rolle spielt, weil SDF-1 permanent im Knochenmark produziert wird. Die Zusammenhänge zwischen CXCR4-Expression des Primärtumors und das daraus resultierende metastatische Potential eines Osteosarkoms oder der allgemeinen Überlebensrate der Patienten, sind noch unklar. In dieser Dissertation wurden daher die Funktionen des Chemokines SDF-1 und dessen Rezeptor CXCR4 in der Pathogenese des Osteosarkoms *in vivo* in SCID Mäusen untersucht. Zu diesem Zweck haben wir humane 143-B Osteosarkomzellen manipuliert damit sie natives SDF-1 oder dessen genetisch modifizierte Formen, P2G und SDF-1-KDEL, stabil exprimieren und dadurch die Wechselwirkung zwischen SDF-1/CXCR4 unterbunden wird. P2G ist ein kompetitiver Hemmer des Chemokines SDF-1, und SDF-1-KDEL ist ein Fusionseiweiss, welches verhindert, dass der Rezeptor CXCR4 an die Zellmembran gelangt. Als passende Kontrolle haben wir auch 143-B Zellen mit einem leeren Infektionsvektor generiert.

Unsere Resultate zeigen, dass die Expression von nativem SDF-1 das Wachstum des Tumors nicht verändert hat, aber die Lungenmetastasierung stark gefördert hat. P2G und SDF-1-KDEL haben das Wachstum der primären Tumore gefördert, allerdings die Metastasierung reduziert. Wir haben auch beobachtet, dass die Tumore, die aus den 143-B P2G und 143-B SDF-1-KDEL Zellen gewachsen sind, mehr CXCR4-positive Tumorzellen aufwiesen als die Kontrolltumore. CXCR4 wurde mit Hilfe von Flusscytometrie und PCR bestimmt. Offensichtlich wurden die Osteosarkomzellen durch deren CXCR4 Rezeptor und das vom Knochenmark produzierte SDF-1 in den Primärtumoren behalten. Dadurch haben die 143-B P2G und 143-B SDF-1-KDEL Zellen grössere Primärtumore und weniger Metastasen entwickelt. Interessanterweise hat die Analyse der Mauslungen aller experimenteller Gruppen

gezeigt, dass die Metastasen mit CXCR4-positiven Tumorzellen angereichert wurden. Unsere Resultate weisen darauf hin, dass CXCR4 sehr wichtig für das Überleben der Tumorzellen in der neuen Umgebung sein könnte und dass CXCR4 eine duale Rolle im Metastasierungsprozess des Osteosarkoms spielen könnte. Schliesslich liefert unsere Studie neue Erkenntnisse über die Rolle, die SDF-1 und CXCR4 in der Pathogenese des Osteosarkoms spielen könnten und deutet an, dass eine örtliche, auf CXCR4 abgezielte Therapie eine attraktive Option darstellt.

Preface

The focus of this thesis was to investigate the role of the SDF-1/CXCR4 chemokine axis in OS metastasis. The introduction part gives an overview on OS and the metastatic process and includes the description of animal models used for studying OS. CXCR4/SDF-1 chemokine biology as well as its implication in carcinogenesis is also detailed in the introduction section.

The result part is split into two parts. The first part is presented as a manuscript:

Altered CXCL12 expression reveals a dual role of CXCR4 in osteosarcoma tumor growth and metastasis

The second part contains further results that were not included in the manuscript and additional studies written as separate chapters:

- **Role of the SDF-1/CXCR4 axis in OS metastasis**
- **Pulmonary administration of an SDF-1 neutralizing ligand for targeted treatment of lung metastasis in an intratibial metastasizing OS mouse model: a pilot study**
- ***In vivo* characterization of K12 *lacZ*, K7M2 *lacZ*, and MOS-J *lacZ* OS models**

- **Establishment of highly metastatic mouse K7M2 *lacZ* and MOS-J *lacZ* OS models**

The result section is followed by the discussion where major findings of the studies "*In vivo* characterization of K12 *lacZ*, K7M2 *lacZ*, and MOS-J *lacZ* OS models" and "Establishment of highly metastatic mouse K7M2 *lacZ* and MOS-J *lacZ* OS models" are summarized. In the Conclusion/Synthesis part of the discussion, I focus on the study "Altered CXCL12 expression reveals a dual role of CXCR4 in osteosarcoma tumor growth and metastasis". In this section, I restate the results without lengthy description and provide logical explanation of the findings.

In the Outlook/Future direction section, I provide a summary of the preliminary data of the study "Pulmonary administration of an SDF-1 neutralizing ligand for targeted treatment of lung metastasis in an intratibial metastasizing OS mouse model: a pilot study" and discuss clinical implications of our findings.

1. Osteosarcoma (OS)

1.1 OS clinical presentation

Osteosarcoma (OS) is a malignant tumor of mesodermal origin defined by the presence of highly proliferative malignant cells producing osteoid and/or immature bone (Klein and Siegal 2006). OS is the most common non-hematopoietic primary bone tumor in children and adolescents with a high propensity for lung metastasis. Lesions with different histological and anatomical features are distinguished. By its anatomical location OS is classified into central, surface, gnathic, multifocal (all osseous OSs), intramuscular or other location (soft tissue sarcomas). Central OS is further divided in high-grade or low-grade subtypes. High-grade OS comprises conventional, telangiectatic, small cell, epithelioid, osteoblastoma-like, chondrosarcoma-like, fibrohistiocytic, and giant cell-rich OS. OS is a relatively rare tumor with an incidence of 2-3 cases per million people per year. The peak incidence is seen in the second and the third decade, most likely associated with the growth phase in puberty. The second peak is seen at the age of approximately 50 years and appears to be associated with Paget disease and exposure to radiation of the bone (Klein and Siegal 2006).

Characteristic symptoms of OS include local pain, often associated with swelling in the involved region and limitation in movement of affected joints (Marina, Gebhardt et al. 2004). In patients with osteolytic tumors, bone fractures are frequently observed. Most commonly, OS occurs in the metaphyses of long bones, in the distal femur, the proximal tibia, and the proximal humerus, with 50% of the cases originating around the knee. Approximately 15% of OS patients present with radiologically detectable metastases, predominantly in the lung, at the time of diagnosis. Similar to other mesenchymal tumors OS metastasizes through the circulation.

OS is most frequently diagnosed by X-ray and subsequent tumor tissue biopsy (Marina, Gebhardt et al. 2004; Klein and Siegal 2006). In most cases OS appears in its classic or

conventional form consisting of spindle-like or polyhedral cells. Conventional OS is characterized by the ability to produce different amounts of cartilage matrix and fibrous tissue. Based on these features OS is subdivided into osteoblastic, chondroblastic, and fibroblastic OS depending on the type of extracellular matrix and the types of cells that produce it. In fact, in most conventional OS all three cell types are detected, but the cell type which is most predominant defines a histological subtype of OS (Klein and Siegal 2006; Ritter and Bielack 2010).

1.2 OS therapy and prognosis

Current therapy of OS patients includes preoperative (neoadjuvant) chemotherapy, complete surgical removal of all detectable tumor sites, and postoperative (adjuvant) chemotherapy (Marina, Gebhardt et al. 2004). Chemotherapy usually includes doxorubicin, high-dose methotrexate, cisplatin and ifosfamide. Despite the fact that OS was long considered as radiotherapy resistant tumor, recent data suggest that radiotherapy might be beneficial for patients with incomplete tumor resection. Despite improved treatment success after the introduction of neoadjuvant chemotherapy in the late 70s, patients with metastatic or recurrent disease continue to have a very poor prognosis with a 5-year survival rate of only approximately 20% (Isakoff, Bielack et al. 2015). The current treatment of metastatic or recurrent disease is similar to that applied for localized disease combining complete surgical removal of all visible metastases and second-line chemotherapy including ifosfamide, etoposide and/or carboplatin (Marina, Gebhardt et al. 2004; Mialou, Philip et al. 2005; Kansara and Thomas 2007; Walkley, Qudsi et al. 2008). Although the location of the primary tumor and tumor size, response to chemotherapy and surgical remission are of a prognostic value, the presence of metastases appears to be the only a reliable prognostic factor. The fact that 80% of OS patients eventually develop metastases suggests that most of them have nondetectable micrometastases already at the time of diagnosis. Therefore, there is a

continued need for better understanding of molecular mechanisms of OS in order to identify therapeutic targets and to develop new effective agents and treatment strategies for OS patients suffering from metastatic disease in order to improve the outcome for those patients.

1.3 OS origin/Etiology

Although, the situation of OS patients was significantly improved during the past years, the etiology of OS remains largely unknown. Giving the fact that OS arises early in lifetime, it is unlikely that slow progressive accumulation of carcinogenic changes leads to occurrence of this type of tumor (Fuchs and Pritchard 2002; Mohseny, Szuhai et al. 2009). Oncogenic viruses, such as Rous sarcoma virus encoding for the v-Src protooncogene, were first found to be related to the development of sarcomas. FBJ virus was shown to be very potent in inducing spontaneous OS in mice. Later, radiation, electrical burn and several chemical agents, such as beryllium oxide and methylcholanthrene were found to be associated with OS. More recently, significant effort has been made in order to delineate etiological factors and genes that may contribute to the pathogenesis of OS, let to the identification of several genetic predispositions such as hereditary retinoblastoma, Li-Fraumeni syndrome, Rothmund-Thomson syndrome, Bloom syndrome, and Werner syndrome (Fuchs and Pritchard 2002; Walkley, Qudsi et al. 2008). All these syndromes are associated with mutations in genes regulating the cell cycle and DNA repair and metabolism. Genomic instability and chromosomal abnormalities with significant cell-to-cell variation and heterogeneity are common in OS. For example, chromothripsis was documented in 25% of OS (Forment, Kaidi et al. 2012). It is suggested that chromotripsis occurs in a single, catastrophic event early in cancer cell development which precedes loss of heterogeneity (Figure 1). However, it remains to be determined at which stages of tumorigenesis chromotripsis usually takes place and which mechanisms trigger the rearrangement of chromosomes. Most of the cells undergoing chromotripsis *in vitro*, die due to the DNA damage-induced apoptosis. The minority of the cells that escape

apoptosis and survive could potentially become cancerous. Moreover, double-stranded breaks in cells where G1/S cell cycle check point arrest in not efficiently induced (for example, in *p53*-deficient cells) become a substrate for chromosomal rearrangements (Forment, Kaidi et al. 2012). Indeed, a strong association between p53 mutations and chromotripsis for acute myeloid leukaemia patients has been reported. Conventional cytogenetic analysis, molecular analysis of allelic imbalance, comparative genomic hybridization (CGH), and array-based CGH identified regions of gene loss, amplification, and rearrangement in OS. Genetic alterations observed in OS are common in other cancers and are not specific for OS (Fuchs and Pritchard 2002; Kansara and Thomas 2007; Chen, Zhou et al. 2015). They include the deletion of *p53* and mutations in *Rb* tumor suppressor genes, as well as an overexpression of oncogenes such as *myc, c-fos, src*, and *Her-2.* In a recent study it has been shown that osteoblast-restricted loss of *p53* and/or *pRB* led to the development of OS in mice with p53 mutations being dominant (Walkley, Qudsi et al. 2008). Mouse double minute 2 (MDM2) and cyclin-dependent kinase 4 and 6 (CDK4/6) genes were also reported to be amplified or overexpressed in OS (Kansara and Thomas 2007; Sakamoto and Iwamoto 2008). Wnt/β-catenin signaling plays a central role in the control of developmental gene expression (Kansara and Thomas 2007). It is falsely regulated in many cancers and false regulation appears to correlate with OS metastasis. The SDF-1/CXCR4 chemokine axis was shown to play an important role in migration and adhesion of OS cells *in vitro*, as well as in the development of lung metastases in an *in vivo* mouse model (Wang 2005; Tang, Song et al. 2008). Some pathways and regulatory molecules involved in OS pathogenesis are illustrated in Figure 1.

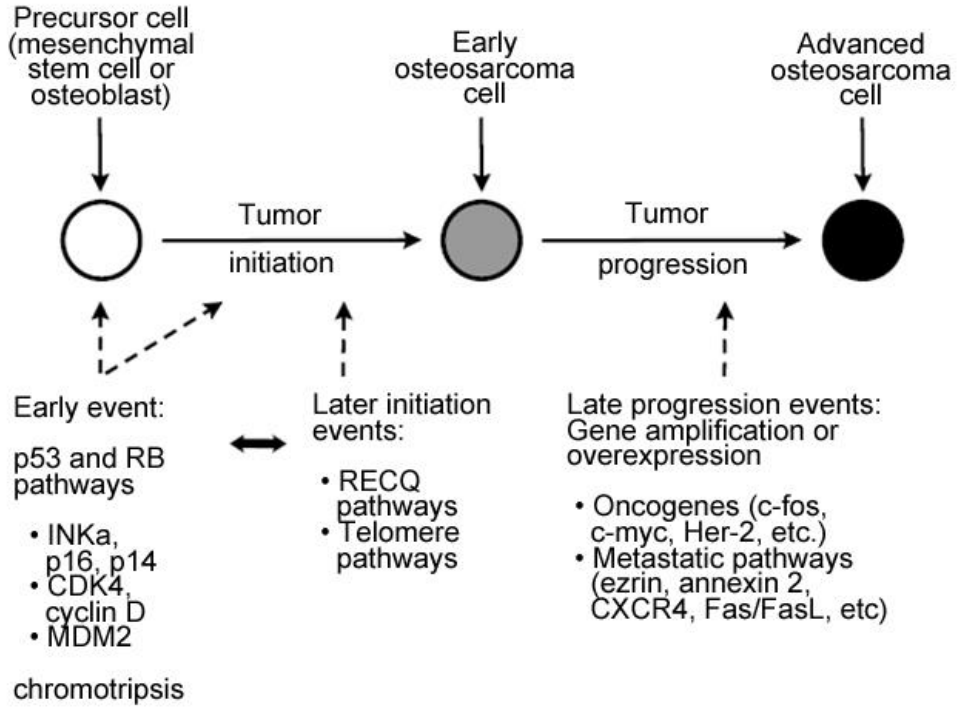

Figure 1: Schematic representation of pathways and molecules involved in OS pathogenesis. Dotted arrows indicate that the exact timing of these events is not known. The two-headed arrow indicates specific interactions between pathways (adapted from Wang 2005; Forment, Kaidi et al. 2012).

Most of the OS tumors are sporadic and the cells of origin remain a much debated topic in OS. Patane et al. demonstrated experimentally that overexpression of the *MET* oncogene in primary human osteoblasts transformed these cells into tumorigenic and invasive OS cells (Patane, Avnet et al. 2006). Moreover, it induced cytogenic and chromosomal aberrations in OS cells. Suppressed expression of HGF, of its receptor MET, or inhibition of receptor dimerization abrogated the transformed phenotype of OS cells. More recently, mesenchymal stem cells (MSCs) were proposed as cells of origin in OS. Homozygous loss of *cdkn2* region was shown to mediate MSCs malignant transformation *in vitro* (Mohseny, Szuhai et al. 2009).

2. *In vivo* models of OS

Tumor tissue heterogeneity and considerable genetic instability are important characteristics of OS and contribute to the deficits in our knowledge on the etiology of OS. Therefore, it is of a great importance to have animal models available that closely mimic the human disease and allow the dissection of pathophysiological mechanisms, the design of novel therapeutic strategies and adequate drug screening. Moreover, a valuable *in vivo* model of OS must be reliable and reproducible. Numerous *in vivo* OS models have been developed in the past.

First, OS models in mice have been generated by radiation-induced or chemical-induced lesions. Several genetically-modified mouse models, including *p53*-deficient germline, have been reported (Walkley, Qudsi et al. 2008). The disadvantage of these models is their unpredictability. Alternatives to this model are xenotransplantation models or the models where established cell lines are injected either subcutaneously, intravenously, or orthotopically into mice. Several human-derived OS cell lines have been established, including U2OS (Ponten and Saksela 1967), SAOS (Jia, Worth et al. 1999), HOS (McAllister, Gardner et al. 1971) and its highly metastatic derivate 143-B (Bacchetti and Graham 1977). The limitation of these mouse models is that relationships between tumor and immune system cannot be studied.

Immunocompetent mouse models based on the mouse-derived cell line can help overcome this problem. Several mouse-derived OS cell lines have been also reported, including K7 (Schmidt, Strauss et al. 1988), K12 and K7M2 (Khanna, Prehn et al. 2000), Dunn (Dunn and Andervont 1963) and its more aggressive derivate LM8 (Asai, Ueda et al. 1998), and MOS-J (Joliat, Umeda et al. 2002). K7M2 OS transplantation model was shown to be highly tumorigenic, and metastatic, however a very high speed of primary tumor formation makes it difficult to study metastatic process (Khanna, Prehn et al. 2000).

The murine osteosarcoma MOS-J cell line was derived from spontaneously occurring chondroblastic osteosarcoma in a C57BL/6J mouse. Intratibial injections of MOS-J cells into

immunocompetent syngeneic mice reveal primary tumors in bone however no metastases in lung or other organs were formed (Joliat, Umeda et al. 2002). Development of a highly metastatic MOS-J cell line would be much appreciated in the light of recent improvements in the generation of genetically modified mice on the C57BL/6J mouse genetic background. It would be very attractive to study a role of conditionally altered alleles in a cell-specific manner in the development of OS in syngeneic transplantation or cell inoculation mouse models.

3. Metastasis

3.1 Metastasis genes

Metastasis is a multistep process that includes local invasion, intravasation, survival in the circulation, extravasation, and colonization of a distant organ (Chambers, Groom et al. 2002). Different tumor types share these processes and mechanisms, but the organs targeted by metastasizing tumor cells and the kinetics of metastatic progression are remarkably different. This indicates that tumor cells need to acquire different properties to invade different organs and to develop metastases in organ-defined microenvironments. The time period between organ invasion and colonization, defined as latency, varies considerably.

Genes involved in the metastatic process can be divided into three categories: metastasis initiation, metastasis progression and metastasis virulence genes (Nguyen, Bos et al. 2009). Metastasis initiation genes are involved in the epithelial-mesenchymal transition (EMT), promote degradation of the extracellular matrix needed for tissue invasion, and stimulate angiogenesis (Nguyen, Bos et al. 2009; Valastyan and Weinberg 2011). Metastasis progression genes promote extravasation of circulating metastatic cells, invasion into the site of the secondary lesion and survival in new parenchyma. Although these genes are needed to successfully infiltrate distant tissues, they can already be expressed at the site of the primary

tumors, where they might have different functions. There are no rigid borders between metastasis initiation and metastasis progression genes: the genes that enable cells to proliferate within the primary tumor site can also confer metastatic phenotype of the cells. Thus metastasis progression gene expression at the primary tumor site might predict to which organ a certain type of tumor will metastasize (Nguyen, Bos et al. 2009). Expression of the metastasis virulence genes becomes prominent only in those cells that successfully disseminated and invaded a distant organ. These genes do not give any advantage to tumor cells in primary sites and therefore they do not contribute to the expression signature that would predict organ-specific metastasis formation in the primary tumor (Bernards and Weinberg 2002; Nguyen, Bos et al. 2009).

There are two different approaches *in vivo* that help to model and study the metastatic processes. Tumor cells are either injected orthotopically or intravenously. The first model includes spontaneous metastasis and closely mimics the metastatic disease in patients. The second model of experimental metastasis is useful to study metastasis formation undergoing processes in the target organ, but is not able to clarify which genes and molecules play a role at the initial steps of metastasis formation, when tumor cells acquire metastatic signatures and leave primary tumor site (Chambers, Groom et al. 2002).

3.2 Organ-specific metastasis and self-seeding

Once tumor cells enter the circulation they encounter several stresses, including physical damage from blood shear forces, attack of the immune system, and loss-of-detachment evoked death, or anoikis. However, considering the rather short period of time the metastatic cells remain in the circulation, the relevance of anoikis is unclear (Gupta and Massague 2006; Valastyan and Weinberg 2011). In order to escape from immune surveillance, metastatic cells attract platelets, which protect them from attacks of the immune system (Gupta and Massague 2006).

The most common metastatic sites include bone marrow, lungs, liver and brain. Stephen Paget proposed a "seed and soil" theory of metastatic dissemination (Gupta and Massague 2006). According to this theory, the outcome of cancer metastasis depends on the interactions between tumor cells ("seeds") and the secondary organ to which the cells metastasize ("soil"). In 1929, James Ewing suggested that the anatomical layout of the vasculature determines site specific metastasis (Chambers, Groom et al. 2002). However, these theories are not mutually exclusive. Dissemination of metastatic cells is partially influenced by the physiological blood flow pattern and by specific molecular interactions between the metastatic cells and endothelial cells lining the capillary walls of a specific organ that dictate infiltration (Gupta and Pillarisetti 1999; Bernards and Weinberg 2002; Chambers, Groom et al. 2002). Capillary vessels of the bone marrow and the liver are highly permissive, whereas endothelial cells of lung capillaries are surrounded by basement membrane and alveolar cells. Therefore, the circulating tumor cells metastasizing to the lung need to express particular molecules that mediate migration through the lung endothelial layer. Mediators of lung endothelial transmigration include for example epiregulin, prostaglandin G/H synthase 2 (PTGS2 or COX2), matrix metalloproteinases (MMP1 and MMP2), cytokine angiopoetin-like 4 (ANGPTL4), etc (Bernards and Weinberg 2002; Chambers, Groom et al. 2002). Stromal cell derived factor 1 (SDF-1, also called CXCL12) interacting with its receptor CXCR4 was shown to mediate lung-specific metastasis of breast cancer (Muller, Homey et al. 2001). The mechanism of site-specific metastasis mediated by the SDF-1/CXCR4 axis in breast and other cancers will be discussed later.

Cancer cells that detached from the primary tumors and entered the circulation can return to the site of the primary tumor and thereby contribute to its growth and size. Alternatively, cancer cells can undergo self-seeding following proteolysis of extracellular matrix and reattachment to the tumor mass without passing through the circulation. In both cases self-

seeding leads to the formation of high-density cells conglomerates, which form independent loci of growth that contribute to a larger overall tumor size (Norton and Massague 2006).

3.3 Time course of metastasis

Some types of tumors such as lung and pancreatic adenocarcinoma, skin melanoma and osteosarcoma have a short relapse period (Nguyen, Bos et al. 2009). The short period of recurrence implies that the metastatic competence genes either are already expressed in premalignant cells or acquired earlier during malignant transformation. Mediators enabling cells to rapidly establish secondary lesions in different organs have been proposed for some tumor types (Garraway, Widlund et al. 2005; Nguyen, Bos et al. 2009). For example, it has been suggested that microphthalmia-associated transcription factor (MITF) predisposes the melanocyte lineage to malignant transformation. In addition, some of the embryonic stem cell modules, such as transcriptional factor SNAI2, were linked to the disease relapse (Gupta, Kuperwasser et al. 2005; Nguyen, Bos et al. 2009).

On the contrary, other tumors are capable of invading distant organs, but have a long period of latency (Nguyen, Bos et al. 2009). Such tumors exhibit long disease-free intervals. Breast and prostate cancers are examples for such tumors. Breast cancer cells reside in the lung as single cell micrometastases or form non-proliferating cell clusters. This state is called proliferative dormancy or tumor mass dormancy. Dormancy is influenced by both, intrinsic properties of the metastatic cells and the organ tissue microenvironment. Importantly, metastatic cells must not only survive during latency and bypass senescence, but also reinitiate growth once the conditions are favorable. The acquisition of competence by dormant cells to reinitiate tumor growth can be intrinsic to the tumor cells or driven by selective pressures that the organ imposes to the dormant cells (Chambers, Groom et al. 2002; Gupta and Massague 2006). Additional functions that dormant cells can acquire stochastically under such a pressure contribute to the site-specific metastatic process.

In order to explain dormancy, Judah Folkman proposed that apoptosis and proliferation rates of micrometastasis are balanced because micrometastases fail to become vascularized (Chambers, Groom et al. 2002). These micrometastases were consequently named preangiogenic micrometastases. Moreover, dormant cells can occur in a state of non-dividing solitary cells. Dormant and non-dormant cells can exist at the same time at the secondary site. When non-dividing breast cancer cells were isolated from the secondary lesions in liver and reinjected into the mouse fat pads, they were able to reinitiate primary tumor growth indicating that dormant cells retain functions that contribute to the primary tumor growth (Chambers, Groom et al. 2002).

Hematogenous metastatic spread to the lung remains the major cause of death of OS patients. However, the molecular processes underlying the metastatic process of OS remain to be clarified. Chemokines are known to regulate cell migration, adhesion, and proliferation in different types of cancer and have been reported to be involved in OS pathogenesis (Liao, Zhou et al. 2013).

4. Chemokine and chemokine receptors

4.1 Chemokines, structure and classification

Chemokines are a family of nearly 50 small secreted cytokines (7-14 kDa) that belong to the cytokine family (Balkwill 1998; Laing and Secombes 2004; Bachelerie, Ben-Baruch et al. 2014). Chemokines are best known for their ability to regulate leukocyte trafficking. They also play essential roles in cell proliferation, differentiation, death and maturation, as well as in embryonic development, angiogenesis, tissue regeneration, etc. (Balkwill 1998). Moreover, chemokines augment pathophysiological processes by recruiting different leukocyte subsets to a site of tissue injury. Thus, chemokines play a fundamental role in myocardial infarction,

rheumatoid arthritis, psoriasis, glomerulonephritis and HIV infections (Furie and Randolph 1995; Horuk 2001). All chemokines bind to proteoglycans on endothelial cells, which mediate their localization at the site of inflammation and avoid that they are removed by the blood flow (Adams and Lloyd 1997; Mantovani, Bonecchi et al. 2006).

Two categories of chemokines, homeostatic and inflammatory chemokines, have been defined based on their functions. Some chemokines are produced and stored as inactive pro-peptides and are activated by enzymatic cleavage at an inflammatory site (Berahovich, Miao et al. 2005; Nomiyama, Osada et al. 2011). Homeostatic chemokines are constitutively expressed and secreted by a wide variety of non-inflamed tissues and are mainly involved in controlling lymphocyte trafficking and homing under physiological conditions. Inflammatory chemokines are expressed in response to a pro-inflammatory stimulus and control the migration of leukocytes to the site of inflammation. Some chemokines that act as both inflammatory and homeostatic chemokines are called dual-function chemokines (Nomiyama, Osada et al. 2011).

Structurally, chemokines are divided into four subfamilies, named CXC, CC, XC (C), and CX_3C according to the arrangement of four conservative cysteine residues in their amino acid sequence (Nomiyama, Osada et al. 2011; Bachelerie, Ben-Baruch et al. 2014). These cysteine residues are involved in the formation of disulfide bonds. CXC and CC are the main subfamilies. In the CXC and CX_3C subfamilies the first two of four cysteine residues are separated by one or three amino acids, respectively. In the CC subfamily the first two cysteine residues are adjacent to each other. Chemokine of CXC, CX_3C and CC families form two disulfide residues. The XC (or C) subfamily lacks the first and the third cysteine residues and forms therefore only one disulfide bond. CXC chemokines are further subdivided into ELR+ and ELR– subgroups depending on the presence or absence of the three amino acid residues glutamine-leucine-arginine adjacent to the CXC motif (Laing and Secombes 2004). ELR+

chemokines include CXCL1, CXCL2, CXCL3, CXCL5, CXCL6, CXCL7, and CXCL8 and display neutrophil attracting ability. ERL– chemokines include CXCL4, CXCL9, CXCL10, CXCL11, CXCL12/SDF-1, CXCL13, CXCL14, and CXCL16. These ERL– chemokines attract neutrophils only with a low efficiency. All ERL+ chemokines can induce angiogenesis, whereas ERL– chemokines are anti-angiogenic with the exception of CXCL12/SDF-1, which was shown to induce angiogenesis.

Chemokine secretion is upregulated by pro-inflammatory cytokines such as IL-1, IL-2, TNFα, γ-interferon, and the bacterial product, lipopolysaccharide, and inhibited by TGFβ, IL-4, and IL-10. However, the response depends on the individual chemokine (Adams and Lloyd 1997).

4.2 Chemokine receptors

Chemokine receptors belong to the superfamily G protein-coupled cell-surface receptors GPCRs (also termed 7-transmembrane or heptahelical receptors) that share a seven-transmembrane-spanning α-helix architecture with each of the seven segments displaying a high level of hydrophobicity, an extracellular N-terminus and an intracellular C-terminus. Conserved overall domain structure of GPCRs was revealed by X-Ray crystallography. This includes DRY, ERY and NPXXY motifs that keep GPCRs in an inactive state until binding of an agonist (Lodowski and Palczewski 2009). The extracellular domains, consisting of the amino-terminal domain and three loop structures constitute the high-affinity ligand binding site and the intracellular serine/threonine-rich carboxy-terminal domain and three intracellular loop structures interact with signaling molecules and mediate receptor internalization.

The ligation of an agonist is the first step in the signal transduction through G-protein coupled chemokine receptors which initiates a cascade of intracellular events. The binding of the ligand leads to the conformational changes in the receptor which involves disruption of the ionic interactions between the third and the six trans-membrane loops of the receptor, followed by the hydrolysis of GTP and its exchange for GDP. Dissociated Gα and Gβγ

subunits bind to cellular effector enzymes, such as phospholipases and regulate second messenger molecules which in turn regulate activity of other enzymes thus ultimately leading to the cellular response (Kroeze, Sheffler et al. 2003; Lodowski and Palczewski 2009). There are at least 18 different types of Gα, 5 types of Gβ, and 11 types of Gγ proteins known to which GPCRs can be bound (Kroeze, Sheffler et al. 2003).

Downstream signaling molecules interacting with chemokine receptors include Rho, Rac, Cdc42, adenylcyclases A2, C and D, as well as MAPK depending on the individual chemokine receptor and the cell type in which it is expressed (Balkwill 1998; Mantovani, Bonecchi et al. 2006). Some "silent" or atypical chemokine receptors such as ACKR3 (also known as CXCR7/RDC1), ACKR1 (DARC), ACKR2 (D6), and ACKR4 (CCX-CKR) have been described (Mantovani, Bonecchi et al. 2006; Bachelerie, Ben-Baruch et al. 2014). These receptors serve as decoy and scavenger receptors and thus fine-tune the actions of cytokines and other chemokine receptors.

Chemokine receptors are classified and named based on their specificity for the different CXC, CC, XC (C), CX_3C, and CX chemokine subfamilies (Zlotnik and Yoshie 2000; Bacon, Baggiolini et al. 2002). Their names are composed of the name of the family of chemokines they recognize followed by the letter "R" for "receptor" and a number indicating the chronology of identification.

All chemokine receptors are encoded by a single exon with the exception of CCR2, which is encoded by two separate exons (Balkwill 1998). Compared to the chemokines, chemokine receptors are well conserved across the species (Laing and Secombes 2004; Nomiyama, Osada et al. 2011; Bachelerie, Ben-Baruch et al. 2014). Twenty three human and 24 mouse chemokine receptor genes have been identified so far, including six atypical (non-signaling) chemokine receptors. Only one major cluster containing 14 genes encoding for human chemokine receptors was found on the chromosome 3p21. Some chemokine receptor genes

were mapped individually to miniclusters (Horuk 2001; Nomiyama, Osada et al. 2011), including CCR6 and CCR7 which were mapped to the human 6q27 and 17q12-21.2 chromosomes respectively (Horuk 2001). CXCR1, CXCR2 and pseudogene for CXCR2 were found on the human 2q35 chromosome, whereas CXCR4 was found to be located to the human 2q21 chromosome.

Chemokine receptors are expressed by a variety of tissues and cell types, including hematopoietic cell types, lymphoid organs (CCR5, CCR6), neurons (CCR5, CXCR4), epithelial and endothelial cells (CCR5), etc. (Horuk 2001). Chemokine receptors can be upregulated upon stimulation with their ligands; hypoxia can modulate the expression of some chemokine receptors.

4.3 Chemokine evolution

Chemokines are present in vertebrates and microorganisms (Laing and Secombes 2004; Nomiyama, Osada et al. 2011), although the latter is probably the result of a host-virus gene copy transfer (Nomiyama, Mera et al. 2001; Nomiyama, Osada et al. 2010). Thus, it is likely that chemokine-mediated control of the immune response arose and evolved with the evolution in vertebrates.

Inflammatory chemokines possess highly redundant and promiscuous ligand-receptor relationships, whereas homeostatic chemokines tend to undergo more specific ligand-receptor interactions. Indeed, taking into consideration the complexity of leukocyte recruitment and the importance of the immune response to the host survival, it is not surprising that multiple mechanisms have evolved, resulting in the observed redundancy (Adams and Lloyd 1997). Phylogenetic analysis demonstrated that homeostatic chemokines are much older than inflammatory chemokines. Therefore the individual genetic and functional features of inflammatory chemokines are supposed to be attributed to their recent evolution (Mantovani 1999; Nomiyama, Mera et al. 2001).

The major CC chemokine gene cluster is located on the human chromosome 17 and contains 17 CC chemokine genes, including one pseudogene, DL78γ/SCYA3L2, whereas in mice the CC chemokine gene cluster is mapped to chromosome 11 and contains only 12 genes (Naruse, Ueno et al. 1996; Nomiyama, Mera et al. 2001; Nomiyama, Osada et al. 2010). Two regions can be distinguished within human CC cluster: MIP and MCP. Mouse counterparts of the human MIP and MCP have been identified. Human and mouse CXC clusters are mapped to the chromosomes 4 and 5, respectively and contain two regions: CXCL10 and GRO. Interestingly, chemokines that cluster in the same region, mostly interact with the same chemokine receptors. For example, CC chemokine genes which are located in the MIP region mostly use CCR1 and CCR5 for their signaling whereas chemokines which genes are located within the MCP region mostly interact with CCR2 and CCR3. Similarly, CXC chemokines clustered in GRO region utilize CXCR1 and CXCR2, whereas chemokines clustered in CXCL10 region utilize CXCR3 and CXCR5. It indicates a coevolution of the chemokines and their receptors. Importantly, chemokine genes probably arose through different types of gene duplications and rearrangements. Those chemokine genes that have a higher level of sequence similarity to their neighboring genes within the same cluster than to their probable orthologous in the other species were probably generated through a tandem duplication. These species-specific rearrangements of the chemokine genes might have taken place after the diversification of the human and rodents and could be driven by the need of the defense system against the viral molecular mimicry. Another example of such species-specific rearrangements is the absence of some human counterparts in a mouse genome. Other chemokine genes were evolved through a duplication of the whole segment. These genes, for example the genes clustered in the CXCL10 region, are relatively well conserved across the species and this type of duplication in block may be attributed to their essential role in the maintenance of the homeostatic traffic of some leukocytes (Nomiyama, Mera et al. 2001).

5. SDF-1 and CXCR4

5.1 SDF-1 chemokine, structure, expression and regulation

SDF-1 (stromal cell-derived factor, also known as CXCL12) has been first isolated from mouse bone marrow stromal cells by using a signal sequence trapping strategy (Tashiro, Tada et al. 1993). A fusion protein carrying a Tac (α chain of human interleukin-2 receptor) was designed to specifically recognize NH_2-terminal signal sequence that is shared between most precursors for secreted factors. Thus, newly synthesized protein was redirected by the secretory signal sequence to the plasma membrane where the fusion protein was detected by anti-Tac antibody. Six human (SDF-1α, SDF-1β, SDF-1γ, SDF-1δ, SDF-1ε, SDF-1φ) and 3 mouse (SDF-1α, SDF-1β, SDF-1γ) isoforms of SDF-1 have been identified and arise from a single gene transcript by alternative splicing (Jiang, Zhou et al. 1994; Shirozu, Nakano et al. 1995; Yu, Cecil et al. 2006). They belong to the CXC chemokine subfamily. The major human SDF-1 isoform, SDF-1α, encodes an 89 amino acid protein with a 21 amino acid cleaved signaling peptide, which is identical in all the SDF-1 isoforms. In fact, all the human SDF-1 isoforms share the first three exons, but they differ in the exon 4, which is in each case derived from a different region of the SDF-1.

SDF-1 was originally characterized as a pre-B cell stimulating factor (Tashiro, Tada et al. 1993; Nagasawa, Kikutani et al. 1994). It was reported that SDF-1 induced chemotaxis of CD34+ human progenitor cells, therefore it was concluded that SDF-1 may play a unique role in the trafficking and homing of lymphocytes and hematopoietic cells (Aiuti, Webb et al. 1997). The genes encoding human and mouse SDF-1 were mapped to the chromosomes 10 and 6, respectively (Shirozu, Nakano et al. 1995; Nagasawa 2014). This chromosomal localization of the SDF-1 genes is unique, since the human and mouse genes encoding other CXC chemokines are clustered on the chromosomes 4 and 5, respectively. Human SDF-1α and SDF-1β are abundantly expressed in different tissue, but the highest expression was detected in liver, pancreas and spleen. Unlike SDF-1β, SDF-1α is also detected in the brain,

but it is rapidly hydrolyzed by proteases in the blood stream (Janowski 2009). Human SDF-1γ is predominantly expressed in the heart and only weakly expressed in some other tissues of adult organisms. During embryogenesis, SDF-1α can be found in different fetal tissues, whereas SDF-1β expression is mainly restricted to the fetal spleen. SDF-1δ is ubiquitously expressed in fetal tissue with the highest expression level found in fetal liver. SDF-1ε and SDF-1φ are weakly expressed in fetal kidneys (Yu, Cecil et al. 2006). Mouse SDF-1 isoforms are ubiquitously expressed among mouse tissues of adult animals. Mouse SDF-1β is expressed at different levels in highly vascularized adult mouse tissues such as kidneys, liver, heart, spleen and muscles, whereas SDF-1γ encoding transcripts were found in lung, heart, brain, and muscle tissue (Jiang, Zhou et al. 1994).

The three-dimensional structure of SDF-1α isoform was determined by X-ray and NMR spectroscopy (Crump, Gong et al. 1997; Dealwis, Fernandez et al. 1998). SDF-1 has three major domains: the N-terminus, the central core region made of three antiparallel β-sheets, and the C-terminal α-helix. SDF-1 is constitutively expressed in a variety of different tissues and exists as a monomer. Degradation of the C-terminus of SDF-1α by carboxypeptidase-N in the blood does not inactivate SDF-1α, but reduces its activity by 50%. In particular, it decreases the efficiency of SDF-1α binding to glycosaminoglycans (GAGs). This type of degradation is unique for the SDF-1α isoform and only occurs in the circulation. Degradation of the N-terminus of SDF-1 is slow and is mediated by cellular proteases and fully inactivates the peptide. This process occurs in both, tissues and blood, and it is isoform-independent (Janowski 2009). Binding of SDF-1 to GAGs protects the N-terminus from degradation possibly through SDF-1 oligomerization.

All SDF-1 splice variants bind to GAGs, but the binding affinities of the different isoforms vary considerably depending on the length of their C-terminus. For example, kinetic analysis demonstrated that the residence time of the SDF-1α on the heparin sulfate was shown to be 9

s, whereas the residence time of SDF-1γ was 525 s (Luo, Luo et al. 1999; Laguri, Arenzana-Seisdedos et al. 2008; Janowski 2009). SDF-1 binding domains in GAGs are localized within the highly sulfated regions. Negatively charged GAGs are covalently bound to core proteins on the cell surface and in the extracellular matrix. GAGs attract, bind and thereby stabilize SDF-1 protein. SDF-1-heparin sulfate binding is mediated by basic amino acids along the polypeptide chain of SDF-1 (Laguri, Arenzana-Seisdedos et al. 2008; Janowski 2009). Mutagenesis analysis, *in vitro* binding assays and molecular modelling demonstrated that SDF-1 binds to GAGs through its β-strands and the binding does not compromise ligandreceptor interaction (Amara, Lorthioir et al. 1999; Laguri, Arenzana-Seisdedos et al. 2008). However, Ziarek et al. demonstrated, by biophysical and mutation analyses, that SDF-1/GAG interactions depend on amino acids that partially overlap with the amino acids needed for receptor binding (Ziarek, Veldkamp et al. 2013). Moreover, interaction of SDF-1 with soluble heparin results in the formation of SDF-1 oligomers, which abolished SDF-1-mediated cardioprotective effects in an *ex vivo* rat heart model of myocardial infarction. SDF-1 chemokine binding to GAGs reveals chemotactic gradients within tissues and disruption of this interaction is believed to cause diffusion of SDF-1 and, consequently, abolition of the chemokine gradient (Laguri, Arenzana-Seisdedos et al. 2008).

SDF-1 is expressed by multiple cell types of the bone marrow, including CAR (CXCL12 abundant reticular) cells, osteoblasts, endothelial and nestin-expressing cells (Nagasawa 2014). It has been demonstrated that expression of SDF-1 in the bone marrow is regulated by rhythmic secretion of adrenergic hormones by the nerves of the sympathetic nervous system in the bone marrow (Scadden 2008; Giudice, Caraglia et al. 2010). Binding of adrenergic hormones to the β3-adrenergic receptor on the surface of SDF-1-producing stromal cells leads to dephosphorylation of the Sp1 transcription factor, which in turn decrease the expression of SDF-1. It has therefore been suggested that modulation of SDF-1 expression in the bone

marrow is not regulated by proteolytic enzymes, but by rhythmic oscillation of the release of neurotransmitters.

5.2 CXCR4 chemokine receptor

CXCR4 was isolated independently by different research groups and called hFB22 (human fetal brain 22), L5, D2S201E, HM89, or LESTR (leukocyte-derived seven-transmembrane receptor) (Rimland, Xin et al. 1991; Federsppiel, Melhado et al. 1993; Herzog, Hort et al. 1993; Jazin, Yoo et al. 1993; Nomura, Nielsen et al. 1993; Loetscher, Geiser et al. 1994). D2S201E/HM89/LESTR was identified as a seven-trans-membrane receptor and was found to be expressed mostly on human leukocytes and monocytes subsets. Later, in 1996 Feng et al. found that human-derived GPCR is required for entry of HIV-1 and fusion between cells expressing HIV-1 and CD4+ cells (Feng, Broder et al. 1996). This receptor was called fusin. Moreover, it was shown that overexpression of fusin in nonhuman CD4+ cells allows these cells that are otherwise resistant to HIV-1 infection to undergo fusion. These results were later confirmed by another group (Berson, Long et al. 1996).

The fact that fusin played a major role in HIV-1 infection raised a great interest on this scientific topic. In 1996, two groups independently discovered that SDF-1/PBSF serves as a ligand for LESTR/fusin receptor and blocks T-tropic HIV-1 cell entry (Bleul, Farzan et al. 1996; Oberlin, Amara et al. 1996). LESTR/fusin was therefore called CXCR4 according to the chemokine-receptor nomenclature established at the 1996 Gordon Conference on chemotactic cytokines. Importantly, Bleul et al. showed that SDF-1 induced chemotaxis of lymphocytes acting through GPCR LESTR/fusin/CXCR4. Later Nagasawa et al. isolated a murine analogue of the human CXCR4, and identified SDF-1 as a ligand for it (Nagasawa, Nakajima et al. 1996). It was shown that although murine PB-CKR/CXCR4 did not allow HIV-1 entry and infection, it was responsive to both, human and mouse SDF-1 and binding of SDF-1 to PB-CKR/CXCR4 induced Ca^{2+} influx.

The analysis of the human and mouse CXCR4 genes showed that they only contain one intron of 2.13 Kb and 2.3 Kb, respectively (Heesen, Berman et al. 1997; Wegner, Ehrenberg et al. 1998; Gupta and Pillarisetti 1999). However, splice variants of human and mouse CXCR4 have been identified (Heesen, Berman et al. 1997; Gupta and Pillarisetti 1999). Interestingly, the second isoform of human CXCR4, CXCR4-Lo (also known as CXCR4-1 or CXCR4a isoform), does not originate from classical splicing of alternative exons, but it occurs through alternative splicing into the single intron which gives rise to a unique 9-amino acids sequence (MSIPLPLLQ) in the N-terminal domain of CXCR4-Lo (Figure 3).

Very recently, two additional isoforms of human CXCR4, CXCR4-3 and CXCR4-4, that arise from similar alternative splicing, resulting in the extension of the N-terminus by 70 and 33 amino acids, respectively, has been reported (Sand, Jochemsen et al. 2015). These two CXCR4 isoforms were found to be expressed in tumor cells, including Ewing sarcoma cells, but also in the placenta. Interestingly, the expression of these two CXCR4 splice variants appears to be dependent on the expression of the major CXCR4 isoform (CXCR4b, or CXCR4-2). Although, CXCR4-3 and CXCR4-4 isoforms were mainly localized in the cytoplasm, it has been demonstrated that at least CXCR4-3 responds to SDF-1 stimulation by increased Ca^{2+} influx. However, the functionality as well as the expression of the more recently identified isoforms in mouse cell lines have to be further investigated.

CXCR4 is expressed in hematopoietic cells, including macrophages, monocytes, T and B cells, neutrophils, dendritic cells, hematopoietic and endothelial progenitor cells, and also in stem cells, including embryonic stem cells, in vascular endothelial cells and in neurons, etc. (Chatterjee, Behnam Azad et al. 2014).

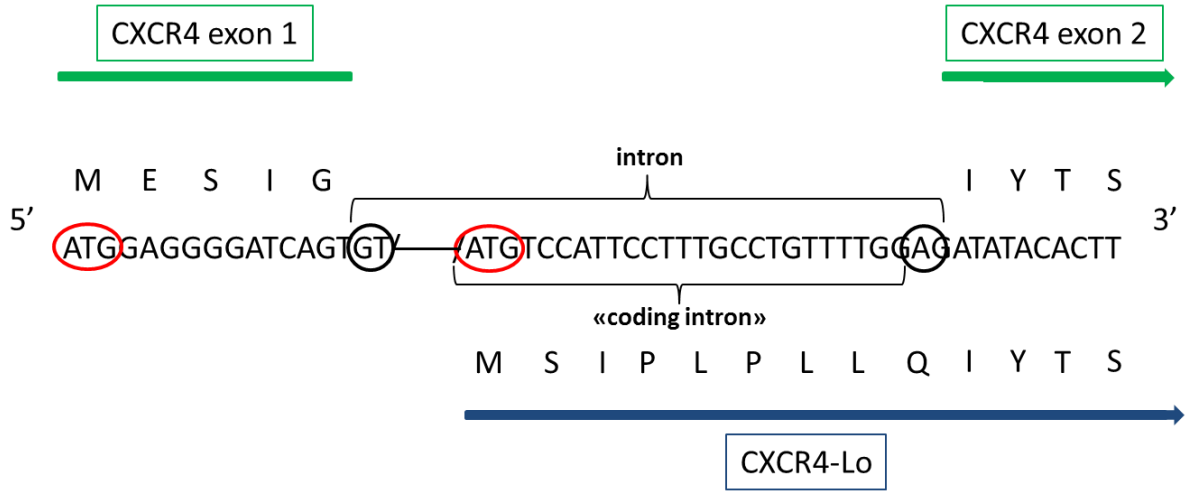

Figure 3: Partial N-terminal amino acid sequences of the CXCR4 (green) and CXCR4-Lo (blue) isoforms occurring through the indicated alternative splicing mechanism. The splice donor site (GT) and splice acceptor site (AG) indicated in the 2.13-kb intron are encircled in black. The alternative translation initiation codons ATG are encircled in red The figure is adapted from Gupta et al. (Gupta and Pillarisetti 1999).

5.3 Mechanism of SDF-1 binding to CXCR4

It has been demonstrated that N-terminus of SDF-1 is involved in receptor binding (Crump, Gong et al. 1997). The first SDF-1 receptor that has been identified is CXCR4 (Bleul, Farzan et al. 1996; Oberlin, Amara et al. 1996; Laguri, Arenzana-Seisdedos et al. 2008) and it was shown that SDF-1 binds to both splice variants of the mouse CXCR4 (Heesen, Berman et al. 1997). Chemokine receptor binding and receptor activation relies on a two-step mechanism. RFFESH amino acid sequence of SDF-1 binds to the N-terminus of CXCR4, while a N-terminal domain of SDF-1 interacts with the 2nd and the 3rd extracellular loop of the receptor leading to the receptor activation (Figure 2) (Laguri, Arenzana-Seisdedos et al. 2008). Importantly, the first two amino acids in the N-terminus of SDF-1, Lys-1 and Pro-2, are required for the receptor activation, whereas the following 6 amino acids (RFFESH) allow SDF-1 binding to its receptor (Crump, Gong et al. 1997; Janowski 2009). The stoichiometry of CXCR4/SDF-1 binding is 1:1. However, SDF-1 dimers also bind to CXCR4 as a partial agonist, whereas maximal activation requires monomeric SDF-1 (Kufareva, Stephens et al. 2014).

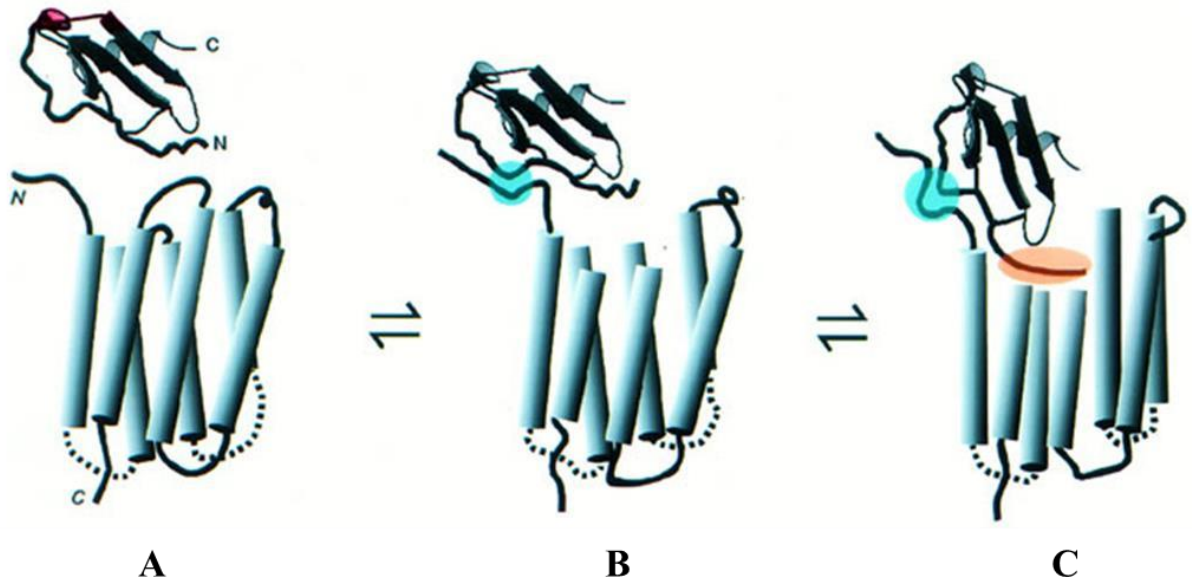

Figure 2: Schematic model of SDF-1 and CXCR4 interaction. The seven transmembrane helices of CXCR4 are represented as cylinders and connected by loop structures indicated in black. The N- and C-termini of SDF-1 are indicated. The amino acid sequence RFFESH of SDF-1 interacts with the N-terminus of CXCR4 (the first binding site is indicated in blue). The N-terminus of SDF-1 binds to an extracellular groove in CXCR4 (indicated in orange) and thereby activates signaling. The figure is adopted from Crump et al. (Crump, Gong et al. 1997).

5.4 SDF-1/CXCR4 signaling and its regulation

Binding of SDF-1 to CXCR4 activates Gi heterotrimers and multiple intracellular signaling pathways including those illustrated in Figure 4. After dissociation from the Gαβγ complex, the Gαi subunit inhibits adenylyl cyclase activity and, in parallel activates mitogen-activated protein kinases (MAPK) and phosphatidylinositol-3-kinase (PI3K) (Pawig, Klasen et al. 2015). Gβγ in turn has been shown to activate PI3K-γ, PKB/Akt and MAPK pathways (Thelen 2001; Delgado-Martin, Escribano et al. 2011; Munk, Ghosh et al. 2011) and to mediate the production of phosphatidylinositol 4,5-bisphosphate (PIP_2), diacylglycerol (DAG) and inositol triphosphate (IP_3). However, the Gαi subunit can also stimulate the production of these molecules (Pawig, Klasen et al. 2015). This illustrates that SDF-1 can simultaneously regulate several intracellular signaling processes as it has been demonstrated in human mature dendritic cells (Delgado-Martin, Escribano et al. 2011). For example, activation of PKB/Akt

inhibits the downstream FOXO protein and thereby regulates cell survival. In other cellular settings, PKB/Akt modulates the activity of the Tuberous sclerotic protein 2 (TSC2), which is an inhibitor of the mammalian target of Rapamycin complex 1 (mTORC1). Inhibition of TSC2 by PKB/Akt stimulates the activity of mTORC1, which regulates cell motility and survival (Figure 4). Altogether, CXCR4 signaling is complex and varies in different cell types. Along these lines, CXCR4 has recently been shown to also interact with other Gα subunits, including Gαq and $G\alpha_{12}$ (Pawig, Klasen et al. 2015). Interestingly, CXCR4 uses other signaling pathways than CCR7 to control the same cell responses, for example chemotaxis. It has been demonstrated that different intracellular loops (ICL) of CXCR4 are involved in activating different signaling pathways (Roland, Murphy et al. 2003; Delgado-Martin, Escribano et al. 2011). For example, ICL3 alone supports the binding of CXCR4 to G-proteins, whereas ICL2 and ICL3 together are essential for chemotaxis response. ICL1 and ICL2 play also a role in receptor folding.

Upon activation by SDF-1, CXCR4 is rapidly phosphorylated by G protein-coupled kinases (GPKs) and internalized (Busillo and Benovic 2007). Internalized CXCR4 is ubiquitinated and sorted to lysosomes for degradation. CXCR4 recycling back to the plasma membrane occurs rarely upon SDF-1 activation. Interestingly, a unique mechanism of SDF-1/CXCR4 complex internalization has been demonstrated in human endothelial bone marrow cells that resulted in consequent removal of the intact chemokine (Dar, Goichberg et al. 2005). Thus, CXCR4 mediated re-use of SDF-1 independent from the *de novo* chemokine synthesis. CXCR4-dependent SDF-1 transcytosis was accompanied by increased homing of transplanted human hematopoietic $CD34^+$ progenitor cells to the bone marrow. It is worth mentioning that although intracellular ubiquitin binds to CXCR4 and thereby targets it for degradation, it can also act as a receptor agonist when it is present outside the cell. Importantly, extracellular ubiquitin binds to CXCR4 domains different from those of SDF-1 and, unlike SDF-1, it does not inhibit HIV-1 cell entry (Saini, Marchese et al. 2011).

Besides the classical interaction with SDF-1, CXCR4 has also been shown to bind viral CC chemokine, vMIP-II (Qin, Kufareva et al. 2015), ubiquitin as described above (Saini, Marchese et al. 2011), migration inhibitory factor (MIF), human β3-defensin (HBD-3), HI virus glycoprotein Gp120 (Pawig, Klasen et al. 2015), and CXCL14 (Tanegashima, Suzuki et al. 2013). However, CXCL14 binding to CXCR4 has not been confirmed (Otte, Kliewer et al. 2014).

Regulation of SDF-1/CXCR4 signaling occurs at different levels. RGS16 (regulator of G protein signaling 16) enhances the GTPase activity of Gαi and thereby mediates GTP to GDP exchange and termination of GPCR signaling. Moreover, β-arrestin can either terminate SDF1/CXCR4 signaling and facilitate receptor internalization or activate MAPK pathway thereby modulating SDF-1/CXCR4 signaling (Pawig, Klasen et al. 2015). Transcriptional regulation of CXCR4 is mediated by the opposite actions of two transcription regulators, nuclear respiratory factor 1 (NRF-1) and SP-1. In addition, calcium and cyclic AMP, some interleukins (IL-2, IL-4, IL-7, etc), TGFβ, basic fibroblast growth factor (bFGF), VEGF, EGF, HIF-1, NF-κB, TNFα, IFN-γ modulate CXCR4 expression (Busillo and Benovic 2007). Posttranscriptional regulation of CXCR4 functions is mediated by glycosylation and tyrosine sulfation. As described above, SDF-1 binds to GAGs, which facilitates SDF-1 oligomerization and thereby modulates SDF-1/CXCR4 signaling. In addition, ACKR3 (CXCR7), the second receptor for SDF-1, scavenges SDF-1, thus modulating CXCR4 signaling (Thelen and Thelen 2008; Abe, Mueller et al. 2014).

Immunoprecipitation experiments, bioluminescence and fluorescence resonance energy transfer, fluorescence and luminescence complementation assays, and the use of bivalent ligands indicated that SDF-1 can provoke CXCR4 dimerization in the cell membrane, which in turn activates the JAK/STAT pathway (Figure 4) (Thelen, Munoz et al. 2010; Kufareva, Stephens et al. 2014; Pawig, Klasen et al. 2015). In addition, CXCR4 can also heterodimerize

with other GPCRs, including ACKR3 and other chemokine receptors. This leads to the transinhibition of ligand binding and changes in G protein and β-arrestin coupling.

Heterodimerization of CXCR4 with $\alpha_{1A/B}$-adrenergic receptor (α_1-AR) in vascular smooth muscle cells has been demonstrated (Tripathi, Vana et al. 2015). Moreover, CXCR4 agonists (SDF-1 and ubiquitin) enhanced the activity of the α_1-AR agonist, phenylephrine, which led to increased blood pressure. It is not yet well understood what kind of functional consequences homo- and heterodimerization of CXCR4 may have, however, it has been proposed that homodimerization of CXCR4 is important for the G-protein-independent activation of the JAK/STAT signaling pathway. Homodimerization of CXCR4 also enhances CXCR4 response to SDF-1, for example cell migration (Busillo and Benovic 2007).

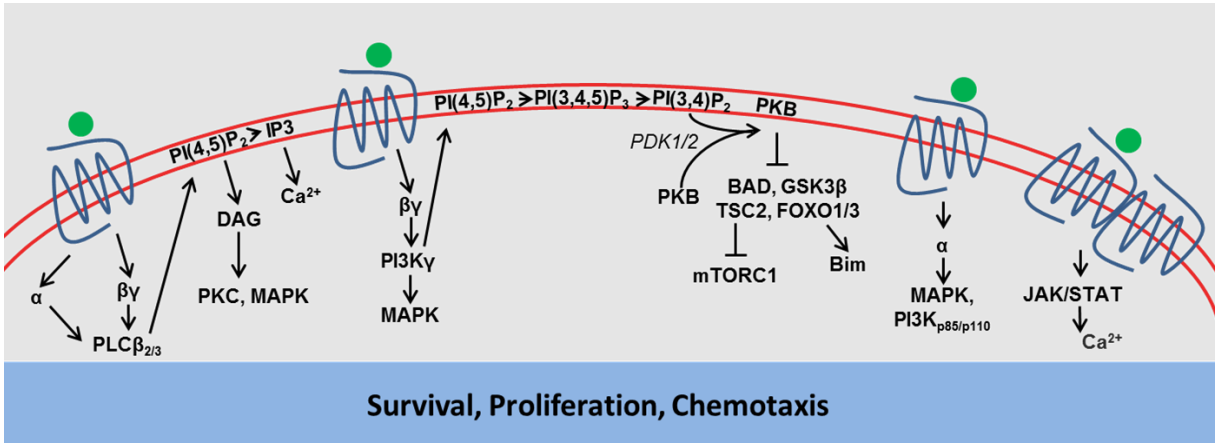

Figure 4: SDF-1/CXCR4 signaling mediating cell survival, proliferation and chemotaxis. SDF-1 (green) binds to CXCR4 (blue) on the cell membrane (red) and induces Gβγ-mediated activation of PI3Kγ and $PLC\beta_{2/3}$. Gα triggers activation of PI3Kp85/p110 and MAPK. Homo-dimerization of CXCR4 induces JAK/STATmediated signaling. Adapted from Thelen M., Pawig L. et al. and Delgado-Martin C. et al. (Thelen 2001; Delgado-Martin, Escribano et al. 2011; Pawig, Klasen et al. 2015). This scheme does not show all possible CXCR4 downstream signaling pathways; other effector molecules might be involved depending on cell type and environment.

5.5 Chemotaxis

Directed chemotaxis is the major function of chemokines and can for example be regulated by SDF-1/CXCR4 signaling (Van Haastert and Devreotes 2004). CXCR4 expressing cells sense the presence of SDF-1 and move towards SDF-1 gradients. Movements are occasionally

interrupted by tumbles. Chemotaxis is derived from ancient Greek chemia: “chemistry” and taxis: “marching forward” and is characteristic for both pro- and eukaryotic cells. Haptotaxis is a related process that is mediated by a gradient of insoluble molecules or chemokines bound to the ECM (Bussmann and Raz 2015). In terms of the cellular response, chemotaxis and haptotaxis are rather similar. Because of their relatively large size (10-20 μm in diameter), eukaryotic cells can sense both, spatial and temporal signals generated by a chemokine (Van Haastert and Devreotes 2004; Bussmann and Raz 2015). The formation of pseudopods on the leading edge of a cell is a response to a chemotactic gradient. Importantly, chemoattractants provoke the formation of pseudopods, but have a minor effect on their properties such as boundary size, formation frequency and lifetime. In the presence of a directional cue, a cell becomes polarized, which leads to pseudopod formation in the domain of the cell surface exposed to the highest concentration of a chemokine. This leading edge of a cell contains actin filaments, whereas retracting uropods in the rear of the cell contain myosin filaments. Chemotaxis is known to be mediated by Gβγ subunits, but, G-protein-independent chemotaxis has also been reported (Van Haastert and Devreotes 2004; Bussmann and Raz 2015). As described before, the second and the third intracellular loop structures of CXCR4 are involved in chemotaxis signaling, which is mediated by phosphatidylinositol-3-phosphate (PIP_3) and PKB/Akt. Pseudopods are preferentially formed in cell membrane domains that contain a patch of PIP_3, which appears to also influence the lifetime of the pseudopod. Chemokine signaling defines the site of actin polymerization by activating the Rac signaling protein through local PIP_3-dependent delivery of activated guanine-nucleotide-exchanging factors (GEFs) for Rac (for example, PREX1 and PAK-interacting exchange factor (PIX)). The formation of myosin filaments in the rear of a cell is mediated by ROCK and a cGMP-dependent kinase shown in neutrophils and in *D. discoideum*, respectively ((Van Haastert and Devreotes 2004).

5.6 Physiological and pathophysiological roles of SDF-1/CXCR4 signaling

SDF-1/CXCR4 signaling plays an important role during the ontogeny and in normal physiology of mammals (Nagasawa 2014; Nagasawa 2015). Mice lacking SDF-1 or CXCR4 exhibit almost the same phenotype, including disrupted B-cell lymphopoiesis (lack of $B220^{+}CD43^{+}$ progenitor cells), defects of cell proliferation and differentiation, and cardiac ventricular septum malformation. This suggests an essential role of CXCR4 and SDF-1 for the development (Nagasawa, Hirota et al. 1996; Ma, Jones et al. 1998; Takabatake, Sugiyama et al. 2009). SDF-1 and CXCR4 are essential for the migration of hematopoietic stem cells and progenitor cells (HSPCs) from the dorsal aorta to the fetal liver during ontogeny. During embryonic development, SDF-1/CXCR4 also mediates colonization of the gonads by primordial germ cells (Nagasawa 2014; Bussmann and Raz 2015). In an adult organisms, SDF-1 and CXCR4 play a role in the maintenance of hematopoietic stem cells (HSCs) in bone marrow (Nagasawa 2014). In addition, CXCR4/SDF-1 plays a role in antiviral immunity. The development and differentiation of different types of immune cells, including B cell precursors, plasmacytoid dendritic cells, megakaryocytic progenitor cells (Hodohara, Fujii et al. 2000), and NK cells (Robertson 2002; Noda, Omatsu et al. 2011), as well as homing of the end stage B- plasma cells to the bone marrow largely depends on SDF-1/CXCR4 signaling. In addition, homing of B cells to the lymph nodes is also CXCR4-dependent. The formation of T cells is SDF-1/CXCR4 independent, but SDF-1/CXCR4 mediates homing of hematopoietic progenitors to the postnatal thymus and thymic β-selection. SDF-1/CXCR4 is known to be also involved in the homing of T lymphocytes to sites of inflammation (Murdoch 2000; Munk, Ghosh et al. 2011). SDF-1/CXCR4 plays a role in the formation of the cardiac ventricular septum, in vascularization of the gastrointestinal tract, the skin, and the kidneys and in the formation of the lateral aortae and arterial-venous

network during brain vascularization. SDF-1/CXCR4 also plays a role in the formation of neuron assemblies in the cerebral cortex (Nagasawa 2014).

CXCR4 also contributes to various pathophysiological processes. CXCR4 is involved in Tcell-tropic and dual-tropic (T-cell and macrophage-tropic) HIV-1 infections, and SDF-1 was shown to inhibit CXCR4-mediated HIV-1 infection (Janowski 2009; Nagasawa 2014). Heterozygous mutations in the CXCR4 gene cause a rare combined immunodeficiency, WHIM (warts, hypogammaglobulinemia, immunodeficiency, myelokathexis), characterized by warts, hypogammaglobinemia, recurrent bacterial infection, and myelokathexis. Mutations affect the C-terminus of CXCR4 and impair desensitization and internalization of the receptor, enhance chemotaxis, and upregulate F-actin polymerization and calcium mobilization (Busillo and Benovic 2007). SDF-1 was reported to be involved in adult lung pathologies such as emphysema and chronic obstructive pulmonary disease (COPD) (Chen, Tzeng et al. 2010). It has been reported that SDF-1 prevents and rescues hypoxia-induced cardiopulmonary remodeling in neonatal mice (Young, Torres et al. 2009). Moreover, SDF1/CXCR4 chemokine signaling increases survival and proliferation of malignant cells and helps establishing site-specific metastasis in different types of cancer (Nagasawa 2014).

6. SDF-1/CXCR4 in cancer

Although the CXCR4/SDF-1 axis was originally recognized as a mediator of lymphocyte trafficking and hematopoiesis (Murdoch 2000), CXCR4/SDF-1 is adapted by neoplastic cells to promote tumor cell growth, angiogenesis, resistance to chemotherapy, invasion and formation of site-specific metastasis (Chatterjee, Behnam Azad et al. 2014). CXCR4 expression alone or together with SDF-1 was shown to be associated with more aggressive metastatic phenotype and poor overall and disease-free survival in patients suffering from different types of malignancies such as breast cancer (Liu, Lang et al. 2009; Zhou, Jiang et al.

2009), oral squamous cell carcinoma (Meng, Wuyi et al. 2010), lung adenocarcinoma (Wagner, Hyjek et al. 2009), pancreatic cancer (Thomas, Kim et al. 2008; Liang, Zhu et al. 2010), gastric cancer (Iwasa, Yanagawa et al. 2009), colorectal cancer (Speetjens, Liefers et al. 2009), renal cell carcinoma (Wehler, Graf et al. 2011), cervical carcinoma (Huang, Zhang et al. 2013; Yu, Shi et al. 2013), and ovarian carcinoma (Guo, Cui et al. 2011). In fact, CXCR4 overexpression occurs in more than 23 different human cancers (Chatterjee, Behnam Azad et al. 2014). Findings demonstrating a correlation between CXCR4 and SDF-1 expression in cancer and disease progression stimulated research investigating pathophysiological roles of CXCR4 in cancer progression. Muller et al. first demonstrated a successful CXCR4 antibody blocking therapy in experimental and spontaneous breast cancer metastatic mouse models (Muller, Homey et al. 2001). Administration through intravenous injection of CXCR4 blocking antibody in mice exhibited significantly reduced pulmonary metastasis. Targeting of the SDF-1/CXCR4 axis was shown to be a promising strategy for the treatment of different types of tumors such as colon carcinoma (Zeelenberg, Ruuls-Van Stalle et al. 2003), lung cancer (Phillips, Burdick et al. 2003; Fahham, Weiss et al. 2012), prostate cancer (Darash-Yahana, Pikarsky et al. 2004), renal cell carcinoma (Pan, Mestas et al. 2006), ovarian carcinoma (Kajiyama, Shibata et al. 2008), pancreatic cancer (Ma, Hwang et al. 2013), chondrosarcoma (Sun, Charbonneau et al. 2013), etc.

The SDF-1/CXCR4-stimulated signaling pathways used by cancer cells are the same as those described in non-malignant cells (Balkwill 2004). The concentration of SDF-1 needed to stimulate tumor cell migration and other CXCR4-mediated responses was reported to be comparable to those activating normal cells. However, it is not clear whether the affinity of SDF-1 in CXCR4 binding as well as the kinetics of signal transduction in malignant cells differ from those in normal cells.

In lung cancer, CXCR4 activation by SDF-1 stimulates migration, invasion and integrin-dependent cancer cell adhesion to bone marrow stromal cells (Burger and Kipps 2006). In hepatocellular carcinoma SDF-1/CXCR4 promotes metastasis by activating the secretion of MMP-9 and MMP-2 (Chatterjee, Behnam Azad et al. 2014).

The SDF-1/CXCR4 axis promotes tumor growth by activating canonical cell proliferation pathways employing MAPK/Erk and PKB/Akt (Balkwill 2003; Chatterjee, Behnam Azad et al. 2014). Moreover, SDF-1/CXCR4 signaling was shown to modulate the Wnt pathway in pancreatic (Guo, Wang et al. 2015) and colon cancer cells (Song, Gao et al. 2015) *in vitro*. In addition, SDF-1 was found to suppresses apoptosis through activation of NF-κB or inhibition of pro-apoptotic protein BAD. SDF-1 was also shown to indirectly stimulate the growth of ovarian cancer by upregulating the expression of TNF-α in malignant cells (Balkwill 2003).
The SDF-1/CXCR4 axis is further known to promote tumor angiogenesis through recruitment of endothelial progenitor, smooth muscle and hematopoietic progenitor cells and indirect upregulation of VEGF (Chatterjee, Behnam Azad et al. 2014; Guo, Wang et al. 2015). The tumor microenvironment consists of non-tumorigenic cells such as stromal fibroblasts, endothelial cells, immune cells, connective tissue and extracellular matrix. Interaction of tumor cells with their microenvironment through SDF-1/CXCR4 promotes their survival (Burger and Kipps 2006; Lazennec and Richmond 2010). For example, breast cancer associated fibroblasts, unlike normal mammary fibroblasts, express high levels of SDF-1 as demonstrated at the mRNA and protein levels. SDF-1 produced by cancer-associated fibroblasts promotes tumor cell growth, survival and angiogenesis.

The CXCR4/SDF-1 axis also plays a role in chemotherapeutic resistance by promoting proliferation, invasion, adhesion and the survival of tumor cells and by supporting a cancer stem cell (CSCs) phenotype (Burger and Kipps 2006; Sun, Cheng et al. 2010; Domanska, Kruizinga et al. 2013; Hattermann and Mentlein 2013). In prostate cancer, CXCR4-mediated

signaling enhances adhesion of cancer cells to endothelial cells and to fibronectin, laminin and collagen. In lung cancer cells, CXCR4 induces tumor cell adhesion to bone marrow stromal cells in an integrin-dependent manner, thereby protecting the cells from loss-of attachment cell death. In B-cell chronic lymphocytic leukemia, "nurselike cells" attract malignant cells in a CXCR4-dependent manner, thereby protecting them from drug-induced apoptosis. In a similar way, bone marrow cells attract CXCR4-expressing acute myelogenous leukemia (AML) cells. CXCR4 mediates VLA-4-dependent adhesion of AML cells to the bone marrow stromal cells thereby protecting AML cells from cytotoxic drugs. CXCR4-dependent adhesion of small-cell lung cancer (SCLC) cells to bone marrow stromal cells is thought to protect SCLC cells from chemotherapy. In addition, SDF-1/CXCR4 signaling induces the recruitment of myeloid bone marrow-derived and mesenchymal stem cells and thereby indirectly facilitates tumor recurrence and metastasis.

Importantly, SDF-1/CXCR4 signaling promotes site-specific metastasis in breast and other cancers (Guo, Wang et al. 2015). CXCR4-overexpressing cancer cells that lack SDF-1 expression respond to gradients of SDF-1 concentration and migrate to established metastatic sites, such as the lungs, brain, bone marrow and liver where SDF-1 is abundantly expressed (Zlotnik, Burkhardt et al. 2011; Domanska, Kruizinga et al. 2013; Chatterjee, Behnam Azad et al. 2014). SDF-1 expressed at metastatic sites supports tumor cell migration and adhesion to these loci and thereby enhances their ability to propagate and form metastases. Several potential regulators of SDF-1/CXCR4-mediated cancer cell adhesion and migration include focal adhesion kinase (FAK), PKB/Akt, Erk1/2, etc. However, mechanisms regulating migratory properties of metastatic cells might be tumor type-specific (Ben-Baruch 2009). In addition, SDF-1 promotes tumor metastasis through increasing MMP-2 and MMP-9 secretion in breast cancer (Ben-Baruch 2008). It has been demonstrated that overexpression of CXCR4 in the B16 melanoma cell line was sufficient to enhance the *in vivo* metastatic potential (Murakami, Maki et al. 2002). SDF-1 signaling in metastatic lesion through CXCR4 can

stimulate the growth of metastatic cells as it has been demonstrated in glioblastoma (Zlotnik, Burkhardt et al. 2011).

6.1 Regulation of CXCR4 and SDF-1 functions in tumors

The expression of CXCR4 in tumors is regulated by epigenetic, transcriptional and posttranscriptional factors (Guo, Wang et al. 2015). For example, hypermethylation of the SDF-1 gene promoter and loss of methylation of the promoter of the CXCR4 gene contributes to an enhanced metastatic potential of various types of cancers including breast cancer. Another mechanism used by breast cancer cells to enhance CXCR4 expression and function is Her2/neu oncogene mediated inhibition of CXCR4 degradation (Burger and Kipps 2006). Interestingly, CXCR4 can upregulate the expression of Her2/neu suggesting a positive feedback loop (Sun, Cheng et al. 2010). Hypoxia-induced CXCR4 expression appears to be a mechanism commonly used by different tumor types (Burger and Kipps 2006). In normoxic conditions, pVHL (product of Hippel-Lindau tumor suppressor gene VHL) stimulates HIF-1 degradation, but, under hypoxic conditions, HIF-1 is accumulating and promotes expression of CXCR4. Upregulated expression of CXCR4 was demonstrated in renal carcinomas with a VHL gene inactivating mutation. This phenotype was associated with worse patients survival compared to that observed for patients with no VHL gene mutation. Moreover, CXCR4 was found to be upregulated in tumor tissue by various growth factors such as TGF-β1, bFGF, VEGF and EGF or by transcription factors like SOX9 and NRF (nuclear respiratory factor) (Ben-Baruch 2008; Guo, Wang et al. 2015). HIF-2 binds to the SDF-1 promoter under hypoxic conditions, thereby enhancing its expression, whereas p53 inhibits CXCR4 and SDF1 expression in cancers (Chatterjee, Behnam Azad et al. 2014; Guo, Wang et al. 2015).

Estradiol can enhance expression of both, SDF-1 and CXCR4. In addition, the expression of CXCR4 is also regulated by miR-mediated post-transcriptional modifications. The tumor-associated inflammatory mediator prostaglandin E regulates both, CXCR4 and SDF-1,

thereby inducing chemotaxis of myeloid-derived suppressor cells into the ascites of ovarian cancer.

7. SDF-1/CXCR4 axis in OS

Although, the role of CXCR4/SDF-1 axis was extensively investigated in different tumor types, its biological relevance in OS progression is largely unknown (Zhao, Guo et al. 2015). In our and other laboratories, CXCR4 has been identified as an independent prognostic biomarker for poor survival of OS patients (Laverdiere, Hoang et al. 2005; Brennecke, Arlt et al. 2014). Lin et al. demonstrated that co-expression of CXCR4 and VEGF in OS tumor tissue correlated with poor overall survival (Lin, Zheng et al. 2011). Baumhoer et al., on the other hand, showed that expression of SDF-1 alone or together with CXCR4 in OS is associated with favorable prognosis for OS patients (Baumhoer, Smida et al. 2012).

In *in vivo* studies in mice, the CXCR4 antagonists CTCE-9908 or AMD3100, interfering with the SDF-1/CXCR4 axis, decreased experimental lung metastasis in K7M2 (Kim, Lee et al. 2008) or F5M2 cell line-derived syngeneic OS mouse models (Guan, Zhang et al. 2015), respectively. In addition, Liao et al. demonstrated that AMD3100 treatment significantly reduced metastatic spread and primary tumor burden in an LM8 syngeneic OS mouse model (Liao, Fu et al. 2015). The CXCR4 antibody blocking principle in xenograft OS mouse model was first investigated by Brennecke et al. in our laboratory (Brennecke, Arlt et al. 2014). He showed that intravenous administration of CXCR4 12G5 blocking antibodies in SCID mice bearing intratibial, CXCR4 expressing human 143-B cell line-derived OS tumors, reduced the primary tumor size and decreased the number of pulmonary metastases in antibody compared to vehicle-treated animals.

Little is known about SDF-1/CXCR4 signaling and regulation in OS (Liao, Zhou et al. 2013; Guo, Cai et al. 2014). It has been shown that SDF-1 itself can enhance CXCR4 expression in

OS cells. Hypoxia was shown to stimulate *in vitro* the migration of human OS cells through HIF-1α-mediated upregulation of CXCR4 expression. The migration of human OS cells was demonstrated to be Erk-dependent. However, later it was shown that SDF-1 activates the JNK and PKB/Akt pathways upon binding to CXCR4 in mouse OS cells, thereby protecting the cells from apoptosis and mediating CXCR4-dependent chemotaxis (Liao, Fu et al. 2015). These effects were suppressed by the CXCR4 antagonist AMD3100.

8. Inhibition of the SDF-1/CXCR4 axis

Considering the important role of SDF-1/CXCR4 axis in various diseases including cancer, several CXCR4 antagonists have been developed (Kim, Lee et al. 2008). They include peptides, small-molecules and antibodies. For instance, CTCE-9908 is an SDF-1-based peptide that was shown to reduce growth, adhesion and migration of different tumor cells *in vivo*. Several other small peptide inhibitors of CXCR4 (e.g. T140 and its analogues) have been developed (Debnath, Xu et al. 2013). The common feature of these compounds is that they are able to bind the predominantly anionic extracellular domain of CXCR4. In addition, monoclonal antibodies against CXCR4 have been described (Muller, Homey et al. 2001; Peng, Damschroder et al. 2015; Scala 2015). In another approach, a NOX-A12 aptamer, which binds SDF-1, was used to block its function (Debnath, Xu et al. 2013). CXCR4-blocking compounds might be useful for both, the inhibition of SDF-1/CXCR4 signaling and for *in vivo* imaging of CXCR4. The low molecular weight CXCR4 antagonist, AMD3100 (plerixafor), is currently the only compound that has been approved by the FDA for the mobilization of hematopoietic stem cells (Debnath, Xu et al. 2013; Chatterjee, Behnam Azad et al. 2014). Recently, a new class of small SDF-1 neutralizing molecules, called chalcones, have been shown to potently interfere with the binding of SDF-1 to CXCR4 *in vitro* and to inhibit the recruitment of inflammatory cells to mouse lungs in an allergic asthma mouse

model *in vivo* (Daubeuf, Hachet-Haas et al. 2013). Chalcones are obtained by the Knoevenagel condensation of 3-methoxy-4-(methoxymethyloxy)benzaldehyde and parachlorobenzoylacetonitrile (Figure 5). Introduction of carbonitrile groups in chalcones significantly reduces their half-lives and make them perfect candidates for local inhibition of CXCR4 functions through neutralization of SDF-1.

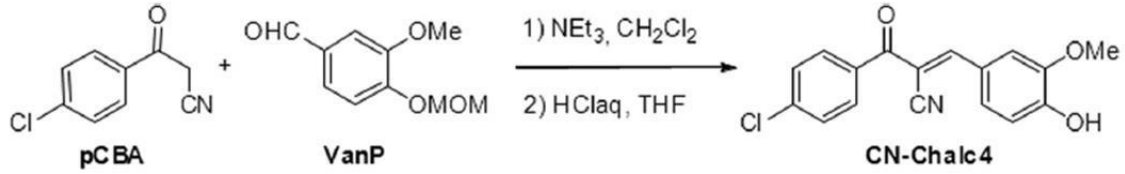

Figure 5. Synthesis of CN-chalcone 4 following Knoevenagel condensation of parachlorobenzoylacetonitrile (pCBA) and 3-methoxy-4-(methoxymethyloxy)benzaldehyde (VanP). Adopted from Daubeuf et al. (Daubeuf, Hachet-Haas et al. 2013).

8.1 Inhibition of SDF-1/CXCR4 functions via P2G and SDF-1-KDEL

Alternatively, CXCR4 functions can be inhibited via P2G and SDF-1-KDEL. P2G, a potent competitive antagonist of SDF-1, is a 67 amino acid analog of SDF-1 with a single proline to glycine substitution in position 2 at the N-terminus of the 21-amino acid cleaved signaling peptide that is shared by all SDF-1 isoforms (Crump, Gong et al. 1997). Importantly, this proline substitution in SDF-1 results in a complete loss of agonist function. However, the affinities of P2G and SDF-1 in CXCR4 binding are comparable and P2G is therefore a potent antagonist of SDF-1. P2G or its motif dimer corresponding to the first N-terminal 9 residues completely blocked SDF-1 binding to CXCR4 (Loetscher, Gong et al. 1998). Hodohara et al. showed that 1-9 amino acid motif of P2G inhibited megakaryocyte colony growth induced by combination of thrombopoietin and serum-derived SDF-1 (Hodohara, Fujii et al. 2000). An *in vivo* study in a mouse breast cancer model showed that overexpression of P2G in breast

cancer cells remarkably reduced their metastatic spread when compared to that of nonmanipulated control cells (Williams, Harata-Lee et al. 2010).

A second approach to inhibit SDF-1/CXCR4 interactions focused on the overexpression of the fusion peptide SDF-1-KDEL (Onai, Zhang et al. 2000; Zeelenberg, Ruuls-Van Stalle et al. 2001; Wheeler, Chen et al. 2003; Zeelenberg, Ruuls-Van Stalle et al. 2003). SDF-1-KDEL consists of SDF-1 with an extension at the C-terminus of the four amino acid peptide KDEL (Lys-Asp-Glu-Leu) acting as an endoplasmic reticulum (ER) retention signal. Since newly synthesized CXCR4 binds to SDF-1-KDEL inside the cell it is retained in the ER. Thus SDF1-KDEL prevents expression of functional CXCR4 at the cell surface. Accordingly, overexpression of SDF-1-KDEL in bone-marrow-derived hematopoietic progenitor cells impaired B-lymphopoiesis and myelopoiesis in mice, indicating that SDF-1-KDEL effectively interferes with CXCR4 and SDF-1 functions *in vivo* (Onai, Zhang et al. 2000). Similarly, SDF-1-KDEL was shown to reduce CXCR4-dependent outgrowth of micrometastases in colon carcinoma (Zeelenberg, Ruuls-Van Stalle et al. 2003).

8.2. Aim of the thesis

The SDF-1/CXCR4 chemokine axis has been widely investigated in breast and other cancers, and its relevance in metastasis progression has been confirmed (Chatterjee, Behnam Azad et al. 2014). However, its role in OS primary tumor growth and metastasis development remains to be clarified (Liao, Zhou et al. 2013). Therefore, in this thesis we defined the following aim:

Investigation of the biological relevance of SDF-1/CXCR4 interaction in OS primary tumor growth and metastasis development via local interference using P2G and SDF-1KDEL.

9. Results

9.1 Manuscript

Altered CXCL12 expression reveals a dual role of CXCR4 in osteosarcoma primary tumor growth and metastasis

Olga Neklyudova,[1] Matthias JE Arlt,[1] Patrick Brennecke,[2] Marcus Thelen,[3] Ana Gvozdenovic,[1] Aleksandar Kuzmanov,[1] Bernhard Robl,[1] Sander M. Botter,[1] Walter Born,[1] Bruno Fuchs.[1]

[1]Balgrist University Hospital, Laboratory for Orthopedic Research, Department of Orthopedics, Zurich, Switzerland

[2]Alpinia Institute, Walenstadt, Switzerland

[3]Institute for Research in Biomedicine, Bellinzona, Switzerland

Address correspondence to: Bruno Fuchs, MD, PhD, Laboratory of Orthopedic Research, Balgrist University Hospital, Forchstrasse 340, CH-8008 Zurich, Switzerland. E-mail:

bfuchs@research.balgrist.ch

Disclosures

All the authors state that they have no conflicts of interest.

Abstract

Metastasis is the major cause of death in osteosarcoma (OS). Therefore, a better understanding of the molecular mechanisms of metastasis is a key for the development of more effective metastasis-suppressive therapy in OS. The CXCL12/CXCR4 chemokine axis is known to mediate the homing of tumor cells to metastatic sites. Its role in OS progression, however, remains largely undetermined. Here, we investigated in SCID mice the biological relevance of the CXCL12/CXCR4 axis in intratibial OS xenografts metastasizing to the lung. We interfered with CXCL12/CXCR4 signaling in CXCR4-expressing human 143-B OS cells through stable expression of CXCL12, of its competitive antagonist P2G or of CXCL12-KDEL, designed to retain CXCR4 within the cell. Constitutive expression of native CXCL12 in 143-B cells promoted lung metastasis without affecting intratibial tumor growth. Stable expression of P2G or CXCL12-KDEL in 143-B cells significantly accelerated intratibial tumor growth but diminished lung metastasis. Tumors grown from P2G or CXCL12-KDEL expressing 143-B cells contained higher levels of CXCR4-encoding mRNA going along with a higher percentage of CXCR4 expressing tumor cells. Higher abundance of CXCR4 possibly contributed to increased local retention of tumor cells by bone marrow-derived CXCL12, reflected in the faster primary tumor growth and the lower number of lung metastases in mice with P2G- or CXCL12-KDEL expressing tumors. Most interestingly, lung metastases in all mice analyzed in this study contained a much higher percentage of CXCR4-expressing tumor cells than corresponding primary tumors pointing to important functions of the CXCL12/CXCR4 axis in late steps of metastasis supporting survival and growth of the tumor cells in the lung microenvironment. In conclusion, based on the here reported results, local treatment of lung metastases with novel CXCR4-targeting therapeutics might be considered and favored over anti-CXCR4 systemic therapy.

Osteosarcoma, CXCR4, CXCL12/SDF-1, Metastasis, Mouse Model

Introduction

Osteosarcoma (OS) is the most common non-hematologic primary bone tumor that predominantly affects children and young adolescents.[1] The main cause of death of OS patients is the high propensity of primary tumors to establish pulmonary metastases. Despite remarkable improvements in the treatment of OS patients by combined chemotherapy and surgery, the five-year survival rate of patients with metastatic or recurrent disease remains at approximately 20%.[2] Consequently, there is a continuous need for a better understanding of the molecular mechanisms that control the metastatic process in order to find new targets for therapy and thereby improve the treatment efficacy in metastatic OS.

The CXCL12/CXCR4 chemokine axis has been shown to be involved in the pathogenesis of different types of tumor.[3] CXCL12, also described as SDF-1, is a secreted small protein that elicits its functions upon binding to the G-protein-coupled seven-transmembrane-domain chemokine receptor CXCR4.[4] CXCL12 is constitutively produced in a wide variety of tissues including bone marrow, spleen, liver, the lungs, and lymph nodes. Binding of CXCL12 to CXCR4 activates several downstream signaling pathways that control cell proliferation, survival and migration. The CXCL12/CXCR4 chemokine axis is essential for leukocyte trafficking, immune homeostasis in secondary lymphoid organs, and for the maintenance of the hematopoietic niche in the bone marrow,[4] which includes hematopoietic stem and progenitor cell homing, transendothelial migration, survival, adaptation to specific microenvironments and proliferation. The metastatic dissemination of cancer cells largely recapitulates these processes.[5] First evidence for a role of CXCL12/CXCR4 in the regulation of the migratory behavior of tumor cells has been reported for breast cancer cells metastasizing to the lung.[6] Expression of CXCR4 in tumor cells has later been reported in 23 different types of cancer.[3] This also included chondrosarcoma and Ewing's sarcoma, where CXCR4 expression was found to be associated with an unfavorable prognosis.[7,8] In OS, however, the role of CXCR4 is contradictorily discussed. Several studies demonstrated

upregulated expression of CXCR4 in lung metastases compared to primary tumors of OS patients and found CXCR4 expression associated with metastatic activity.[9-11] Other studies, however did not find evidence for a correlation between CXCR4 expression in primary tumor tissue and metastatic activity[12] or patient survival.[13]

In vivo studies in mice demonstrated that upregulated expression of CXCR4 in OS cells was associated with primary tumor [14] and lung metastasis progression,[15] and blocking of CXCR4 was found to inhibit primary tumor growth and metastatic spread.[16,17] A previous study in our laboratory in mice demonstrated that systemic administration of CXCR4-blocking antibodies inhibited the growth and metastasis of intratibial primary tumors grown from human 143-B OS cells.[18]

In the present study, we investigated the effects of local interference with CXCL12/CXCR4 interaction on intratibial tumor development and lung metastasis of 143-B OS cells in SCID mice. We employed an autocrine mechanism by making use of stable expression in 143-B OS cells of the CXCL12 antagonist P2G obtained by a single proline to glycine substitution in the second position of CXCL12. P2G has been shown to block the binding of CXCL12 to CXCR4 in human lymphocytes *in vitro* [19] and to inhibit breast cancer metastasis in mice.[20] In a second approach, we stably expressed CXCL12 with a C-terminal KDEL endoplasmic reticulum (ER) retention signal (CXCL12-KDEL) in 143-B cells. It has been demonstrated that CXCL12-KDEL, when overexpressed in bone-marrow-derived hematopoietic progenitor cells, impaired B-lymphopoiesis and myelopoiesis in mice,[21] suggesting that it effectively trapped newly synthesized CXCR4 inside the cells. To further elucidate the role of the CXCL12/CXCR4 axis in OS progression, we also generated 143-B cells stably expressing native CXCL12. The results of our study have shown that the CXCL12/CXCR4 axis might play a unique role in OS metastasis.

Materials and Methods

Cell lines

The human 143-B OS cell line (CRL-8303) was obtained from the European Collection of Cell Cultures (Salisbury, UK). pcDNA3.1 based plasmids containing CXCL12 and P2G coding sequences were kind gifts from Prof. Dr. M. Thelen (IRB Bellinzona, Switzerland). The primers 5'-CGC GAA TTC GCC ACC ATG GAC GCC AAG GTC GTC-3' and 5'-GAC GAA TTC TCA CTT GTT TAA AGC TTT CTC CAG-3' were used for amplification of DNA fragments encoding CXCL12 or P2G flanked by 5' and 3' EcoRI sites. A DNA fragment encoding CXCL12-KDEL flanked by 5' and 3' EcoRI sites was a kind gift from Dr. Ueda and Prof. T. Kitamura (University of Tokyo, Japan). The DNA fragments were ligated into the pMYs-IRES-EGFP retroviral vector. Retroviral transduction of 143-B *lacZ* cells[(18)] with empty vector (EV) or the respective constructs and subsequent EGFP-based fluorescent activated cell sorting revealed the 143-B *lacZ* EV, 143-B *lacZ* CXCL12, 143-B *lacZ* P2G and 143-B *lacZ* CXCL12-KDEL cell lines. Later in the manuscript we refer to the 143-B cell line derivatives expressing the *lacZ* gene as 143-B EV, 143-B CXCL12, 143-B P2G and 143-B CXCL12-KDEL cells. All 143-B cell line derivatives were cultured in DMEM/F12 medium (a 1:1 mixture of DMEM and Ham's F12 medium) supplemented with 10 % FBS (GIBCO, Basel, Switzerland) in a humidified atmosphere of 95 % air and 5 % CO2 at 37°C. All 143-B cell line derivatives were authenticated with polymorphic short tandem repeat loci profiling (Microsynth, Switzerland) less than six months before the animal experiments.

RNA isolation, reverse transcription, semiquantitative and real time PCR

Total RNA was purified from cell lysates or from primary tumor tissue homogenates with an RNA isolation spin technology kit (Qiagen, Germantown, MD, USA) and reverse transcribed with a High Capacity cDNA Reverse Transcription Kit (Applied Biosystems, Life Technologies, Carlsbad, CA 92008, USA). CXCL12, P2G, CXCL12-KDEL and CXCR4

encoding transcripts were quantified by semi-quantitative or real-time PCR (SYBR Green method, SYBR Select Master Mix, Applied Biosystems, USA), respectively, with the following primers: CXCL12 and P2G: forward 5'-ATGTGAGAACATGCCTAGATTTAC-CC-3', reverse 5'-GCTTCATGGCAAGATTCTGGCTTA-3'; CXCL12-KDEL: forward 5'-GATCCCAGTGTGGTGGTACGGGAAATC-3', reverse 5'-GAATCCTTACACCTCGTCC-TTCTCGCT-3', CXCR4: 5'-ACTTGTGGGTGGTTGTGTTCCAGTTTC-3', reverse 5'-AAGGAGTCGATGCTGATCCCAATGTAGT-3'. The nucleotide sequence homology between CXCL12 and P2G encoding sequences was too high for selective amplification. The step One Plus Real-Time PCR system was used. The results were calculated with the ΔΔCt method [(22)] and normalized to the expression levels of endogenous GAPDH transcripts. Amplification products were verified by DNA sequencing (Microsynth AG, Balgach, Switzerland).

CXCL12 immunocytochemistry

Cells were grown on glass microscope cover slips to 70-80% subconfluency. For intracellular staining of CXCL12, the cells were formalin-fixed and permeabilized with 0.1% saponin. CXCL12 was immunostained with goat polyclonal CXCL12 antibody (R&D Systems, Minneapolis, MN, USA) and visualized using secondary Alexa Fluor 546-conjugated anti-goat fluorescence antibodies (Invitrogen, Life Technologies, Carlsbad, CA, USA). Cell nuclei were stained with DAPI (Invitrogen, Life Technologies, USA). Staining was analyzed with a Nikon Eclipse E600 microscope (Nikon, Tokyo, Japan) with an appropriate filter block at 40-fold magnification and images were taken with Kappa Image Base Software for the Nikon camera (Kappa Optronics GmbH, Gleichen, Germany).

CXCL12 ELISA

Protein products expressed by the individual 143-B cell line derivatives were quantified with a CXCL12 ELISA (CXCL12/SDF-1 ELISA DuoSet® development kit, R&D Systems, USA) in conditioned medium 48 hours after cell seeding and in extracts of intratibial primary tumors collected from the mice at autopsy. Tumor tissue was extracted with ice-cold extraction buffer (Pierce by Thermo Scientific, Waltham, MA USA) supplemented with a protease inhibitor cocktail (Roche, Basel, Switzerland) and cleared by centrifugation at 10'000 g for 5 min. Tissue sediments were incubated with acidic buffer (Glycine, pH 2) for high yield extraction of the peptides and the resulting wash fractions were pooled with the corresponding tumor extracts. Dilution series of 1:10, 1:20 or 1:40 for conditioned medium or of 1:2, 1:4 or 1:8 for tumor extracts were analyzed with a Microplate Reader (Benchmark by Bio-Rad, Hercules, CA, USA). All measurements were done in duplicates in three independently collected medium samples or in extracts of three randomly selected tumors per experimental group of mice. The amount of peptides released by 106 cells into 1 ml of conditioned medium in 48 hours was then calculated. The amount of peptides in tumor extracts was normalized to total protein content measured with a Bradford assay (BioRad, USA) according to the manufacturer's instructions.

CXCL12 chemotaxis assay

CXCL12 dependent chemotaxis of the 143-B OS cell line derivatives was studied in a 48-well trans-membrane Boyden Chamber with polyvinylpyrrolidone-free polycarbonate membranes of 8 μm pore size (NeuroProbe, Gaithersburg, MD, USA) as previously described.[18] Migrated cells were counted under a Nikon Eclipse E600 microscope (Nikon, Japan) at 100-fold magnification in 15 randomly selected membrane areas of 0.015 mm^2 per condition (with three wells per condition and five randomly selected areas per well).

Animal experiments

All animal experiments were performed according to the institutional guidelines and approved by the Ethics Committee of the Veterinary Department, Canton of Zurich, Switzerland. Mice selected for the experiment were randomly divided into four groups of ten mice per group. Ten µl containing 105 cells were injected into the medullar cavity of the left tibia of individual mice as described previously.[23] The individual groups of mice were named according to the cell type injected. Tumor growth was monitored weekly by X-ray. The tumor volume was calculated from the caliper measurements as previously described.[18] All mice were sacrificed three weeks after tumor cell inoculation and primary tumors and organs were prepared as reported.[18] *lacZ* expressing metastatic cells in the lungs were visualized as described previously.[24] Metastases, visible as blue stained foci, were counted on the surface of whole-mounts of lungs.

Micro-Computed Tomography-derived mouse tibia morphometry *in vivo*

The SkyScan1176 µCT system (SkyScan/Bruker, Billerica, MA, USA) was used for high definition scanning of control and tumor-bearing mouse legs. Scans were performed in at least four randomly selected mice per group before sacrifice at a working source voltage of 50 kV and a source current of 500 µA with voxel size of 35 μm^3. The number of repeated measurements per one tomography projection (frame averaging) was 2 with an exposure time of 80 ms per projection. Each shot required a source rotation step of 0.8°. Duration of each scanning was approximately 6 min with 360° sample rotation. An aluminium (Al 0.5 mm) filter was used to reduce beam hardening effects. Post-acquisition three-dimensional image reconstitution was done in NRecon software v1.6.9.18 (Skyscan/Bruker, USA). Reconstituted images were segmented and bone volumes were calculated using Data Viewer v1.5.0 and CTAn v1.13.11.0 (Skyscan/Bruker, USA). Three-dimensional images of the mouse tibiae were made in Ctvox v.2.7.0 (Skyscan/Bruker, USA).

Ex vivo Flow Cytometry

The expression of CXCR4 at the surface of 143-B cell derivatives isolated from primary tumors and metastases-bearing lungs was analyzed *ex vivo* by flow cytometry. Tumor and lung tissue was digested in collagenase IV (2 mg/ml) solution (Gibco, Life Technologies, Carlsbad, CA, USA). The cells were aspirated through a 20 G needle and filtered through a 100 μm filter. Resuspended cells were incubated with monoclonal CXCR4 antibody (clone 12G5, IgG2, R&D Systems, USA) and visualized with an Alexa Fluor 647 anti-mouse IgG2 secondary antibody (Life Technology, Carlsbad, CA, USA). Dead cells were labelled in Fixable Viability Dye eFluor450 (Affymetrix by eBioscience, Santa Clara, CA, USA). The cells were fixed with 4% paraformaldehyde and analyzed by flow cytometry with a BD LRS Fortessa (Fortessa by BD Biosciences, Franklin Lakes, NJ, USA). EGFP fluorescence was used to identify tumor cells in whole cell isolates.

Data analysis

The results were analyzed with GraphPad PRISM v5.01 software (GraphPad Software, La Jolla, CA, USA) using one way variance analysis when measurements in three or more groups were compared. Two-way analysis of variance was used for the analysis of two independent variables, or a Student's t-test was used when two individual groups were compared. Correlation analysis was done using Pearson correlation. All *in vitro* experiments were repeated at least three times and the results are represented as mean values ± standard error of the mean (SEM). The results were considered significant when $p < 0.05$.

Results

Characterization of 143-B OS cells stably expressing CXCL12, P2G and CXCL12-KDEL

The highly metastatic 143-B OS cell line expressing endogenous CXCR4[18] and a *lacZ* reporter gene was retro-virally transduced with constructs for stable expression of native

CXCL12, or of P2G or of CXCL12-KDEL (Fig. 1*A*). 143-B cells transduced with empty vector (EV) were used as a control. The transduction efficiency, examined by fluorescence imaging of the bicistronically co-expressed reporter gene EGFP, was nearly 100% in all populations of transduced cells (Fig. 1*B*). Expression of the transgenes at the transcript level was confirmed by semi-quantitative PCR (Fig. 1*C*) and sequencing of reverse transcribed cDNA (data not shown). CXCL12 encoding transcripts remained undetectable in 143-B EV cells. Immunocytochemistry with polyclonal CXCL12 antibodies further confirmed robust expression of CXCL12, P2G or CXCL12-KDEL in the respective cell lines (Fig. 1*D*).

Analysis of conditioned medium by CXCL12-ELISA confirmed the release of CXCL12 (4.823 ± 0.938 ng/ml) and P2G (3.227 ± 0.938 ng/ml) into the medium by the corresponding cell lines (Fig. 1*E*). As expected, immunoreactivity of 0.015 ± 0.008 ng/ml detected in conditioned medium of 143-B CXCL12-KDEL cells was comparable to that detected in the medium of 143-B EV cells, confirming that CXCL12-KDEL was retained inside the cells.

Stable expression of CXCL12, P2G, or CXCL12-KDEL in 143-B cells suppressed CXCL12-provoked chemotaxis *in vitro*

CXCL12 dose-dependent chemotaxis exhibited by 143-B EV cells in a Boyden chamber transmembrane migration assay was not observed when 143-B CXCL12, 143-B P2G and 143B CXCL12-KDEL cells were examined (Fig. 1*F*). The chemotactic response of 143-B EV cells at 300 (28.32 ± 7.8 cells/well) and 1000 nM (25.05 ± 5.4 cells/well) concentrations of CXCL12 was significantly ($p < 0.001$) higher than the basal migratory activity in the absence of CXCL12 and peaked at 300 nM CXCL12. The results showed that stable expression of CXCL12, P2G or CXCL12-KDEL effectively blocked migration of 143-B cells towards CXCL12 *in vitro*.

Stable expression of P2G or CXCL12-KDEL in 143-B cells increased the growth and promoted osteolysis of corresponding intratibial tumors

To assess the effect of P2G and CXCL12-KDEL on 143-B OS growth, SCID mice were intratibially injected with 143-B P2G, - CXCL12-KDEL, -CXCL12 and -EV (control) cells accordingly. Expression of CXCL12, P2G and CXCL12-KDEL, in primary tumors grown from respective 143-B cell line derivatives in SCID mice was confirmed by ELISA. Concentrations of the individual components in 143-B CXCL12, -P2G and CXCL12-KDEL-derived tumor tissue extracts were 136.0 ± 41.5 ng/mg, 73.6 ± 25.2 ng/mg and 113.0 ± 30.8 ng/mg total protein, respectively (mean ± SEM). CXCL12 immunoreactivity of 3.0 ± 1.05 ng/mg total protein detected in extracts from 143-B EV cell derived tumors was considered as non-specific (Fig. 2*A*). The relative levels of expression of CXCL12 and P2G in tumor tissue extracts normalized to total protein concentrations were comparable to the relative amounts of the peptides released into conditioned medium by the corresponding cell lines.

Three weeks post injection 143-B P2G and -CXCL12-KDEL groups developed significantly ($p < 0.05$) larger primary tumors (170 ± 15 mm^3 and 134 ± 14 mm^3, respectively) compared to the control group (78 ± 10 mm^3) (Fig. 2*B* and *C*). In addition, we observed pronounced osteolysis in mice injected with 143-B P2G and 143-B CXCL12-KDEL cells (Fig. 2*D*). Tumors developing from 143-B CXCL12 cells showed comparable tumor growth to the control. Three-dimensional reconstruction and quantitative analysis of the bone lesions in tumor-bearing tibiae by μCT three weeks after tumor cell injection showed significantly less bone volume in 143-B P2G (9.5 ± 0.5 mm^3, p ± 0.001) and -CXCL12-KDEL (11.3 ± 0.9 mm^3, p ± 0.01) cell-derived tumors compared to the control tumors (16.0 ± 0.8 mm3) (Fig. 2*E* and *F*). The bone volume of 15.1 ± 0.6 mm^3 in tumors grown from 143-B CXCL12 cells was similar to that of control tumors. The tumor and bone volumes in affected legs of mice

randomly selected from all experimental groups were found to be inversely related ($p = 0.03$ r = 0.52) (Fig. 2*G*).

The significantly increased tumor growth in 143-B P2G and -CXCL12-KDEL groups prompted us to investigate the proliferative capacity of the tumors and the cells themselves. Ki67 immunostaining of primary tumor sections and *in vitro* proliferation assay did not reveal any significant difference between the groups (Supplemental Fig. S1*A*, *B* and *C*). Tumor angiogenesis, known to be affected by CXCL12 pathways,[3] was also considered as a parameter that might have an effect on primary tumor growth in the different experimental groups of mice. However, quantification of the micro-vessel density by CD31 immunostaining in sections of primary tumors did not reveal any significant differences (Supplemental Fig. S2*A* and *B*). These results were confirmed by ERG immunohistochemical staining [25] (data not shown).

Stable expression of P2G and CXCL12-KDEL in 143-B cells inhibits lung metastasis

The metastatic load in the lungs of SCID mice with intratibial 143-B EV, -CXCL12, -P2G or -CXCL12-KDEL cell-derived tumors was assessed by *ex vivo* X-gal staining of whole mounts of lungs collected at sacrifice of the mice (Fig. 3*A*). The quantification of metastatic loci show that overexpression of P2G or of CXCL12-KDEL in 143-B OS cells significantly ($p < 0.05$, $p < 0.01$, respectively) decreased the number of lung metastases by more than 60% or 66%, respectively, compared to the number observed in lungs of control mice (Fig. 3*B*). Unexpectedly, stable expression of CXCL12 in 143-B cells significantly ($p < 0.05$) increased the number of lung metastases more than 2-fold compared to the control group.

Transcripts encoding CXCR4 were found upregulated compared to control in intratibial tumors grown from 143-B CXCL12, - P2G or - CXCL12-KDEL OS cells

Our findings, showing that stable expression of P2G or CXCL12-KDEL in 143-B cells results in larger primary tumor size and decreased metastatic potential led us to investigate the levels of CXCR4 expression in primary tumors. CXCR4 gene transcripts were expressed at 2.2- (11.7 ± 3.7, $p < 0.01$), 7.4- (39.0 ± 12.0, $p < 0.001$) and 4.6- (24.0 ± 7.0, $p < 0.001$) fold higher levels in 143-B CXCL12, -P2G or -CXCL12-KDEL cell-derived tumors, respectively, than in tumors grown from control 143-B EV cells (4.9 ± 1.3) (Fig. 4*A*).

Tumor cells expressing CXCR4 at the cell surface were found significantly enriched in 143-B P2G and -CXCL12-KDEL intratibial tumors and uniformly predominant in lung metastases in all experimental groups

The expression of CXCR4 on the surface of tumor cells was examined in cell isolates obtained by enzymatic digestion of primary tumors and of lung tissue collected at sacrifice. To determine the total number of tumor cells, identifiable by EGFP fluorescence and among them the percentage of cells expressing cell surface CXCR4, the cell isolates were analyzed by flow cytometry. The mean percentage of tumor cells expressing CXCR4 at the cell surface was comparable and surprisingly low in tumors grown from 143-B EV or -CXCL12 cells (3.6 ± 0.6% and 2.9 ± 0.7%, respectively), but 2.7- and 1.9-fold higher in 143-B P2G or CXCL12-KDEL cell-derived tumors (9.7 ± 1.4%, $p < 0.01$ and 6.9 ± 1.1%, $p < 0.001$, respectively) when compared to control (Fig. 4*B*, left panel). A significant linear correlation ($p < 0.05$, r = 0.9) was observed between the mean primary tumor size in the different experimental groups and the mean percentage of tumor cells expressing CXCR4 at the cell surface in the corresponding groups (Fig. 4*C*). In addition, lung metastases in all four experimental groups of mice consisted of between 78.0 ± 9.7 and 91.0 ± 1.7 % of tumor cells expressing CXCR4

at the cell surface (Fig. 4*B*, right panel). These data suggest that the OS cell lines investigated here apparently adapted to the local lung tissue environment by the expression of CXCR4.

Discussion

The CXCL12/CXCR4 axis has been shown to play an important role in mediating lung directed metastasis through homing of CXCR4 expressing tumor cells along a gradient of CXCL12 expressed in the lung.[3] CXCL12/CXCR4 signaling has been extensively investigated in different types of tumors and the relevance in metastasis progression and poor patient outcome has been confirmed.[3] However the functional role of this axis in OS progression remains to be clarified.[26]

In the present study, we have investigated the effects of local interference with CXCL12/CXCR4 signaling in intratibial primary tumors derived from the human 143-B OS cell line on tumor progression and lung metastasis in SCID mice. Interestingly, auto-/ paracrine blocking of CXCL12/CXCR4 signaling by stable expression of the P2G antagonist or inhibition of CXCR4 cell surface expression by stable expression of CXCL12-KDEL in 143-B cells resulted in larger intratibial tumors than those grown from control 143-B EV cells or from 143-B cells stably expressing CXCL12. A detailed histological and immunohistochemical analysis of primary tumor tissue showed that the proliferative activity assessed by Ki67 staining and tumor tissue vascularization analyzed by CD31 immunostaining were indistinguishable in the primary tumors grown from the different 143-B cell line derivatives. The finding that constitutive expression of CXCL12 in 143-B cells did not affect tumor angiogenesis was in good agreement with those reported in a study in a breast cancer mouse model.[20] The findings of two other studies showing a direct correlation between CXCR4 expression and primary tumor growth,[14,18] prompted us to analyze the expression of CXCR4 in intratibial tumors derived from the four 143-B cell line derivatives. The results showed indeed higher mRNA and protein levels of CXCR4 in intratibial tumors

expressing P2G and CXCL12-KDEL, than in tumors grown from 143-B EV and -CXCL12 cells. This finding was consistent with the flow cytometry data, which showed an enrichment of tumor cells expressing CXCR4 at the cell surface in 143-B P2G and -CXCL12-KDEL compared to -EV and -CXCL12 cell line derived tumors. This was a somehow unexpected finding since P2G should prevent recognition of the receptor by 12G5 antibody [27] and CXCL12-KDEL is supposed to trap CXCR4 inside the cell. The results suggested that 143-B P2G and -CXCL12-KDEL cells in primary tumors compensated P2G or CXCL12-KDEL mediated inhibition of CXCR4 by an upregulation of receptor expression. The mean size of the primary tumors correlated with the percentage of CXCR4 expressing cells, which is in good agreement with the results of a previous study showing that the level of CXCR4 expression was related to the tumorigenic potential of OS cells *in vivo*.[14]

Since it has been shown that CXCR4 mediates site-specific metastasis in mice and that its expression in primary tumors correlates with the metastatic disease in cancer patients,[6,17,28] we expected in the present study a higher metastatic activity of tumor cells expressing CXCR4 than of those with low or non-detectable CXCR4 expression. However, P2G- and CXCL12-KDEL-expressing tumors, which contained a remarkably higher percentage of CXCR4 expressing cells than 143-B EV-derived tumors formed significantly lower numbers of lung metastases than those grown from 143-B EV cells. Thus, although, the CXCL12/CXCR4 axis has been shown to support the migration of metastatic cells from primary tumor site to the lung in breast [6] and several other cancers,[28,29] it might have a unique role in OS. OS occurs in bone, where CXCL12 is abundantly expressed by bone marrow cells and is well known to attract and retain CXCR4 expressing hematopoietic cells in this tissue.[4] This mechanism likely also applies to CXCR4 expressing tumor cells in the intratibial OS model used in this study. 143-B P2G and -CXCL12-KDEL cells in intratibial tumors expressed CXCR4 at the cell surface more frequently than 143-B EV cells and according to the described CXCL12-mediated mechanism they were likely retained at higher

incidence in the bone than 143-B EV cells and, consequently, formed larger tumors and fewer lung metastases.

According to the homing theory, stable expression of CXCL12 by tumor cells should have abrogated a normal CXCL12 gradient and thereby inhibited tumor cell dissemination like it has been observed with CXCL12 overexpressing murine breast cancer cells in a syngeneic model using immunocompetent mice.[20] In the present study, however, expression of CXCL12 in tumor cells significantly promoted lung metastasis while intratibial tumor growth was comparable to that of 143-B EV cells. Taking into account that only a small share of 143B CXCL12 cells in intratibial tumors expressed CXCR4 at the cell surface, they were probably less retained in the intratibial tumors as it has been already discussed for the 143-B EV group. Our findings suggest that CXCL12/CXCR4 signaling was not essential for tumor cell homing to the lung in the here used intratibial xenograft OS model, but it appeared to facilitate other biological processes that are essential for successful formation of metastatic lesions. For example, CXCL12 activates platelet aggregation,[30] which is known to support the survival of circulating tumor cells in the blood stream, to facilitate the arrest of circulating tumor cells in micro-vessels of a target organ and to protect them from attacks by immune cells.[31]

Strong evidence for an essential role of the CXCL12/CXCR4 axis in the development and growth of lung metastatic lesions from disseminating 143-B OS cells was obtained from the results of the flow cytometric analysis of metastases-containing lung tissue. These results showed that the percentage of CXCR4 expressing tumor cells in lung metastases, amounting to over 80% independent of the expressed transduced gene, was significantly higher than that observed in the primary tumors. These findings are in line with the results obtained from analyses of human OS primary tumor tissue and lung metastases that also showed higher expression of CXCR4 in lung metastases than in primary tumors.[10,11] These observations suggest that the expression of CXCR4 in OS cells settling in the lung is likely induced by

regulatory molecules released from the lung microenvironment as recently proposed in studies of colon [28] and lung cancer.[32]

In summary, the results of the present study provide evidence for important functions of the CXCL12/CXCR4 axis in OS progression, which is different from that reported for other types of tumor including breast cancer. The results suggest that CXCR4 expressed in intratibially injected 143-B OS cells mediates retention of the tumor cells in the developing tumor through interaction with CXCL12 of bone marrow origin. This was reflected by a significant correlation between the size of primary tumors and the percentage of CXCR4 expressing tumor cells. Moreover, it is likely that also the reduced dissemination from the primary tumor was due to the CXCR4-mediated retention of the tumor cells. In lung metastatic lesions, however, the percentage of CXCR4 expressing 143-B OS cells was found to be much higher than that in primary tumors, pointing to an important function of CXCR4 later in the metastatic process, for example in survival and growth of the tumor cells in the lung microenvironment and presumably even in self-seeding in lung parenchyma.[33] In conclusion, CXCR4 expressed in OS lung metastases should be considered as a potential attractive target for novel therapeutics strategies. Furthermore, the findings of the present study also indicate that a strategy for anti-CXCR4 local treatment of lung metastases might be favored over a systemic anti-CXCR4 therapeutic approach. The efficacy of a local anti-CXCR4 treatment of OS lung metastasis needs to be investigated in a therapy study. Local treatment of OS lung metastasis is particularly attractive since primary tumor control can be achieved by surgery whereas metastasis remains to be the major obstacle in effective OS treatment and the main cause of death in OS patients.

Acknowledgments

Our work is supported by the University of Zurich, the Schweizerischer Verein Balgrist (Zurich, Switzerland), the Walter L. & Johanna Wolf Foundation (Zurich, Switzerland), the

Highly Specialized Medicine for Musculoskeletal Oncology program of the Canton of Zurich, the Zurcher Krebsliga (Zurich, Switzerland), the "Kind und Krebs" fund (Zollikerberg, Switzerland), and the Swiss National Science Foundation SNF Nr.310030_149649. We thank Christopher Bühler for the excellent technical assistance and Dr. Malgorzata Kisielow and Dr. David Jarrossay for their help with flow cytometry analysis.

Authors' roles

Study design: ON, MJEA, MT and AG; Study conduct: ON and PB; Animal work: ON, MJEA, AK, BR and SB; Contributed material: MT; Data analysis and interpretation: ON, MJEA, MT, WB; Manuscript preparation: ON, MJEA, PB, WB, MT and BF.

References

1. Klein MJ, Siegal GP 2006 Osteosarcoma: anatomic and histologic variants. Am J Clin Pathol 125(4):555-581.
2. Mialou V, Philip T, Kalifa C, Perol D, Gentet JC, Marec-Berard P, Pacquement H, Chastagner P, Defaschelles AS, Hartmann O 2005 Metastatic osteosarcoma at diagnosis: prognostic factors and long-term outcome--the French pediatric experience. Cancer 104(5):1100-1109.
3. Chatterjee S, Behnam Azad B, Nimmagadda S 2014 The intricate role of CXCR4 in cancer. Adv Cancer Res 124:31-82.
4. Nagasawa T 2014 CXC chemokine ligand 12 (CXCL12) and its receptor CXCR4. J Mol Med (Berl) 92(5):433-439.
5. Valastyan S, Weinberg RA 2011 Tumor metastasis: molecular insights and evolving paradigms. Cell 147(2):275-292.

6. Muller A, Homey B, Soto H, Ge N, Catron D, Buchanan ME, McClanahan T, Murphy E, Yuan W, Wagner SN, Barrera JL, Mohar A, Verastegui E, Zlotnik A 2001 Involvement of chemokine receptors in breast cancer metastasis. Nature 410(6824):50-56.

7. Berghuis D, Schilham MW, Santos SJ, Savola S, Knowles HJ, Dirksen U, Schaefer KL, Vakkila J, Hogendoorn PC, Lankester AC 2012 The CXCR4-CXCL12 axis in Ewing sarcoma: promotion of tumor growth rather than metastatic disease. Clin Sarcoma Res 2(1):24.

8. Bai S, Wang D, Klein MJ, Siegal GP 2011 Characterization of CXCR4 expression in chondrosarcoma of bone. Arch Pathol Lab Med 135(6):753-758.

9. Lin F, Zheng SE, Shen Z, Tang LN, Chen P, Sun YJ, Zhao H, Yao Y 2011 Relationships between levels of CXCR4 and VEGF and blood-borne metastasis and survival in patients with osteosarcoma. Medical oncology 28(2):649-653.

10. Oda Y, Yamamoto H, Tamiya S, Matsuda S, Tanaka K, Yokoyama R, Iwamoto Y, Tsuneyoshi M 2006 CXCR4 and VEGF expression in the primary site and the metastatic site of human osteosarcoma: analysis within a group of patients, all of whom developed lung metastasis. Mod Pathol 19(5):738-745.

11. Namlos HM, Kresse SH, Muller CR, Henriksen J, Holdhus R, Saeter G, Bruland OS, Bjerkehagen B, Steen VM, Myklebost O 2012 Global gene expression profiling of human osteosarcomas reveals metastasis-associated chemokine pattern. Sarcoma 2012:639038.

12. Ma Q, Zhou Y, Ma B, Chen X, Wen Y, Liu Y, Fan Q, Qiu X 2012 The clinical value of CXCR4, HER2 and CD44 in human osteosarcoma: A pilot study. Oncol Lett 3(4):797-801.

13. Baumhoer D, Smida J, Zillmer S, Rosemann M, Atkinson MJ, Nelson PJ, Jundt G, von Luettichau I, Nathrath M 2012 Strong expression of CXCL12 is associated with a favorable outcome in osteosarcoma. Mod Pathol 25(4):522-528.

14. Miura K, Uniyal S, Leabu M, Oravecz T, Chakrabarti S, Morris VL, Chan BM 2005 Chemokine receptor CXCR4-beta1 integrin axis mediates tumorigenesis of osteosarcoma HOS cells. Biochem Cell Biol 83(1):36-48.

15. de Nigris F, Rossiello R, Schiano C, Arra C, Williams-Ignarro S, Barbieri A, Lanza A, Balestrieri A, Giuliano MT, Ignarro LJ, Napoli C 2008 Deletion of Yin Yang 1 protein in osteosarcoma cells on cell invasion and CXCR4/angiogenesis and metastasis. Cancer research 68(6):1797-1808.

16. Kim SY, Lee CH, Midura BV, Yeung C, Mendoza A, Hong SH, Ren L, Wong D, Korz W, Merzouk A, Salari H, Zhang H, Hwang ST, Khanna C, Helman LJ 2008 Inhibition of the CXCR4/CXCL12 chemokine pathway reduces the development of murine pulmonary metastases. Clin Exp Metastasis 25(3):201-211.

17. Portella L, Vitale R, De Luca S, D'Alterio C, Ierano C, Napolitano M, Riccio A, Polimeno MN, Monfregola L, Barbieri A, Luciano A, Ciarmiello A, Arra C, Castello G, Amodeo P, Scala S 2013 Preclinical development of a novel class of CXCR4 antagonist impairing solid tumors growth and metastases. PloS one 8(9):e74548.

18. Brennecke P, Arlt MJ, Campanile C, Husmann K, Gvozdenovic A, Apuzzo T, Thelen M, Born W, Fuchs B 2014 CXCR4 antibody treatment suppresses metastatic spread to the lung of intratibial human osteosarcoma xenografts in mice. Clin Exp Metastasis 31(3):339349.

19. Loetscher P, Gong JH, Dewald B, Baggiolini M, Clark-Lewis I 1998 N-terminal peptides of stromal cell-derived factor-1 with CXC chemokine receptor 4 agonist and antagonist activities. J Biol Chem 273(35):22279-22283.

20. Williams SA, Harata-Lee Y, Comerford I, Anderson RL, Smyth MJ, McColl SR 2010 Multiple functions of CXCL12 in a syngeneic model of breast cancer. Mol Cancer 9:250.

21. Onai N, Zhang Y, Yoneyama H, Kitamura T, Ishikawa S, Matsushima K 2000 Impairment of lymphopoiesis and myelopoiesis in mice reconstituted with bone marrowhematopoietic progenitor cells expressing SDF-1-intrakine. Blood 96(6):2074-2080.

22. Livak KJ, Schmittgen TD 2001 Analysis of relative gene expression data using realtime quantitative PCR and the 2(-Delta Delta C(T)) Method. Methods 25(4):402-408.

23. Sabile AA, Arlt MJ, Muff R, Bode B, Langsam B, Bertz J, Jentzsch T, Puskas GJ, Born W, Fuchs B 2012 Cyr61 expression in osteosarcoma indicates poor prognosis and promotes intratibial growth and lung metastasis in mice. J Bone Miner Res 27(1):58-67.

24. Arlt MJ, Banke IJ, Walters DK, Puskas GJ, Steinmann P, Muff R, Born W, Fuchs B 2011 LacZ transgene expression in the subcutaneous Dunn/LM8 osteosarcoma mouse model allows for the identification of micrometastasis. J Orthop Res 29(6):938-946.

25. Miettinen M, Wang ZF, Paetau A, Tan SH, Dobi A, Srivastava S, Sesterhenn I 2011 ERG transcription factor as an immunohistochemical marker for vascular endothelial tumors and prostatic carcinoma. Am J Surg Pathol 35(3):432-441.

26. Liao YX, Zhou CH, Zeng H, Zuo DQ, Wang ZY, Yin F, Hua YQ, Cai ZD 2013 The role of the CXCL12-CXCR4/CXCR7 axis in the progression and metastasis of bone sarcomas (Review). Int J Mol Med 32(6):1239-1246.

27. Tan Y, Li Y, Xiao J, Shao H, Ding C, Arteel GE, Webster KA, Yan J, Yu H, Cai L, Li X 2009 A novel CXCR4 antagonist derived from human SDF-1beta enhances angiogenesis in ischaemic mice. Cardiovasc Res 82(3):513-521.

28. Zeelenberg IS, Ruuls-Van Stalle L, Roos E 2003 The chemokine receptor CXCR4 is required for outgrowth of colon carcinoma micrometastases. Cancer research 63(13):38333839.

29. Murakami T, Maki W, Cardones AR, Fang H, Tun Kyi A, Nestle FO, Hwang ST 2002 Expression of CXC chemokine receptor-4 enhances the pulmonary metastatic potential of murine B16 melanoma cells. Cancer research 62(24):7328-7334.

30. Abi-Younes S, Sauty A, Mach F, Sukhova GK, Libby P, Luster AD 2000 The stromal cell-derived factor-1 chemokine is a potent platelet agonist highly expressed in atherosclerotic plaques. Circ Res 86(2):131-138.

31. Tsuruo T, Fujita N 2008 Platelet aggregation in the formation of tumor metastasis. Proc Jpn Acad Ser B Phys Biol Sci 84(6):189-198.

32. Bertolini G, D'Amico L, Moro M, Landoni E, Perego P, Miceli R, Gatti L, Andriani F, Wong D, Caserini R, Tortoreto M, Milione M, Ferracini R, Mariani L, Pastorino U, Roato I, Sozzi G, Roz L 2015 Microenvironment-Modulated Metastatic CD133+/CXCR4+/EpCAM- Lung Cancer-Initiating Cells Sustain Tumor Dissemination and Correlate with Poor Prognosis. Cancer research 75(17):3636-3649.

33. Norton L, Massague J 2006 Is cancer a disease of self-seeding? Nat Med 12(8):875878.

34. Campanile C, Arlt MJ, Kramer SD, Honer M, Gvozdenovic A, Brennecke P, Fischer CR, Sabile AA, Muller A, Ametamey SM, Born W, Schibli R, Fuchs B 2013 Characterization of different osteosarcoma phenotypes by PET imaging in preclinical animal models. J Nucl Med 54(8):1362-1368.

35. Berndt K, Campanile C, Muff R, Strehler E, Born W, Fuchs B 2013 Evaluation of quercetin as a potential drug in osteosarcoma treatment. Anticancer Res 33(4):1297-1306.

Figure legends

Fig. 1. Characterization of the genetically modified 143-B OS cell line derivatives. *(A)* Partial amino acid sequences of indicated protein products overexpressed in the 143-B cell line derivatives. Mutations introduced into the native CXCL12 sequence are indicated in red. *(B)* Efficiency of retroviral transduction of the indicated 143-B cell line derivatives visualized by fluorescence imaging of EGFP expressed as a reporter protein from the retroviral vectors. Bars = 50 μm. *(C)* Semi-quantitative RT-PCR analysis of the expression of indicated transcripts derived from the corresponding retrovirally transduced transgenes (EV: empty vector control) in indicated 143-B cell line derivatives. GAPDH was used as a control for RNA input. *(D)* Expression of transgene products in indicated cell lines visualized by fluorescence immunocytochemistry with antibodies recognizing native CXCL12 and the mutated derivatives. 143-B CXCL12 cells incubated with the secondary Alexa Fluor 547 antibody alone (NC) served as controls for non-specific staining. Bars = 50 μm. *(E)* Concentrations of transgene products accumulating in the tissue culture medium of indicated cell lines cultured for 48 hours. The results indicate the mean (± SEM) concentrations measured by ELISA in three independent experiments normalized to 106 cells. *(F)* CXCL12 concentration-dependent chemotaxis of the indicated cell lines was measured in a Boyden Chamber assay. Bars indicate the mean (± SEM; three independent experiments) number of cells per well (three wells per condition) migrating across the membrane at 37°C during 4 hours, # $p < 0.01$ compared to the number of migrating 143-B EV cells at the other CXCL12 concentrations; * $p < 0.01$ compared to the number of migrating cells of the other 143-B cell line derivatives at 300 nM and 1000 nM CXCL12, respectively.

Fig. 2. 143-B OS cells stably expressing P2G or CXCL12-KDEL grow to larger intratibial osteolytic primary tumors in SCID mice than 143-B CXCL12 and control 143-B EV cells. *(A)* Concentrations of transgene products in tissue extracts of primary intratibial tumors grown

from indicated cell lines. The results show the mean (± SEM) concentrations per mg of total protein measured in extracts of three randomly selected tumors per experimental group. ** $p < 0.01$). *(B)* Primary tumor growth of indicated 143-B OS cell derivatives over time. The values indicate mean (± SEM) primary tumor volumes calculated from caliper measurements in ten mice per experimental group at indicated time points. *(C)* Primary tumor volumes observed three weeks after injection of the indicated 143-B cell line derivatives. The results are the mean (± SEM) volumes measured with a caliper in ten mice per group normalized to the mean volume observed in 143-B EV cell injected mice (78 ± 10 mm^3) set to 100 %, * $p < 0.05$; ** $p < 0.01$; *** $p < 0.001$. *(D)* Representative X-ray images of tumor-bearing legs (right) and corresponding healthy legs (left) taken three weeks after intratibial injection of indicated 143-B OS cell line derivatives. *(E)* Bone volume in tumor-bearing legs determined by μCT analysis three weeks after intratibial injection of indicated 143-B OS cell line derivatives. The results indicate the mean (± SEM) bone volumes in the ROI (region of interest) measured in at least four mice per experimental group, * $p < 0.05$; ** $p < 0.01$; *** $p < 0.001$. *(F)* Representative μCT images of tumor-bearing legs of mice intratibially injected with the indicated 143-B OS cell line derivatives. White arrows point to osteolytic lesions in tumor legs of mice injected with 143-B EV or 143-B CXCL12 cells. *(G)* Inverse correlation of tumor and bone volume in tumor-bearing legs of at least four animals randomly selected from the four experimental groups of mice.

Fig. 3. Stable expression of P2G or of CXCL12-KDEL significantly inhibited while stable expression of CXCL12 promoted pulmonary metastasis. *(A)* Representative images of X-gal stained metastatic nodules (blue) in lung lobes collected at autopsy from mice injected with indicated 143-B cell line derivatives. Selected rectangular areas enlarged in the bottom panels show close-ups with multiple small metastases such as those marked by arrows. Bars = 250

μm. *(B)* Quantitative analysis of X-gal stained metastatic nodules on the surface of lung whole mounts. Data show the mean (± SEM) numbers of metastases per lung counted in ten mice per group and normalized to metastases observed in the EV group set to 100 %. * $p < 0.05$; ** $p < 0.01$; *** $p < 0.001$

Fig. 4. Intratibial tumors grown from 143-B P2G or -CXCL12-KDEL cells contained higher percentage of CXCR4 expressing tumor cells and lung metastases in all experimental groups were enriched with CXCR4 expressing tumor cells. *(A)* Expression of CXCR4 encoding mRNA in primary tumors grown from the indicated cell lines. The results show the mean (± SEM) transcript levels in three randomly selected tumors of indicated cell lines normalized to GAPDH encoding transcripts in individual tumors and to the mean levels detected in 143-B EV cell line-derived tumors set to 100% (** $p < 0.01$; *** $p < 0.001$). *(B)* Mean percentage (± SEM) of primary tumor-derived (left) or lung metastasis-derived (right) CXCR4 cell surface immunostained tumor cells normalized to the total number of EGFP fluorescent tumor cells. Tumor cells in primary tumor and lung cell isolates obtained from five randomly selected mice per experimental group at sacrifice were analyzed by fluorescence cytometry. * $p < 0.05$; ** $p < 0.01$; *** $p < 0.001$ *(C)* The average sizes of intratibial tumors (n=10) measured at sacrifice in the mice of the individual experimental groups (143-B EV, 143-B CXCL12, 143-B P2G or 143-B CXCL12-KDEL) correlated linearly with the average percentage of tumor cells expressing CXCR4 on the cell surface in the respective intratibial tumors. CXCR4-immunostained tumor cells were estimated by flow cytometry in cell isolates of at least five tumors per experimental group.

Supplemental data

Histology and immunostaining

Immunohistological stainings were performed as previously described.[34] Six micrometre tumor cross-sections were probed with either anti-CD31 or anti-Ki67 primary antibody (Abcam, UK). CD31 immunostainings were visualized with anti-rabbit Alexa Fluor 547 fluorescence secondary antibodies (Thermo Scientific, Waltham, MA USA) under a Zeiss microscope and pictures were taken at 20X magnification using an AxioCam MRm camera attached to Zeiss observer (Observer Z1, Zeiss Microscopy, Jena, Germany). Cell nuclei were stained with DAPI (Invitrogen, Life Technologies, USA). CD31 staining-based micro-vessel density was estimated in three randomly selected areas of 0.14 mm^2 per tissue section and calculated as the ratio between the area occupied by blood vessels and the total area of viable tissue imaged with a custom-made program (ETH, Zurich) for Image J software (NIH, Bethesda, MD, USA). Three representative tissue sections of three randomly selected tumors per experimental group of mice were analyzed. Ki67 immunostained tumor sections were visualized with peroxidase-conjugated anti-rabbit secondary antibodies (Vector Laboratories Inc., Burlingame, CA, USA), Vectastain Elite ABC (Vector Laboratories Inc., USA) and a substrate-chromogen system (Dako, Glostrup, Denmark). Images of Ki67 immunostained tissue sections were taken with a Nikon Eclipse E600 camera (Nikon, Japan) at 20X magnification. Ki67 immunostained cells were counted in at least two randomly selected areas of 0.37 mm^2 per primary tumor tissue section. Three representative sections of three randomly selected tumors per experimental group of mice were analyzed. The proliferation index was calculated with Image J software (NIH, USA) as the ratio between the number Ki67-immunostianed cells and the total number of tumor cells.

Cell proliferation assay

Doubling times of the 143-B cell line derivatives were determined as previously described.[35] Briefly, 5x105 cells were seeded in 12.5-cm^2 flasks and let to adhere overnight. The cells were counted with a hemocytometer at 24, 48, 72, and 96 hours after seeding. The experiment was repeated three times using five flasks per cell line at each time point. The doubling time was calculated using the following formula: $t1/2=\ln 2/\gamma$, where t1/2 is the doubling time and γ is the slope of the linear regression curve.

Supplemental Fig. 1. Stable expression of P2G, of CXCL12-KDEL or of native CXCL12 in 143-B cells did not affect proliferation *in vivo* and *in vitro*. *(A)* Representative Ki67-immunostained paraffin-sections of primary tumors grown from the indicated cell lines. Bars = 50 μm. *(B)* Percentage of Ki67-immunostained cells in sections of primary tumors of indicated cell lines. The results are mean values (± SEM) calculated from the numbers of cells counted as outlined in Supplemental Material in primary tumors of three randomly selected mice per experimental group. *(C)* Doubling times of the indicated 143-B cell line derivatives *in vitro*. The results are the mean (± SEM) values calculated as outlined in Supplemental Material from cell numbers counted over time in five flasks per cell line and per time point in three independent experiments.

Supplemental Fig. 2. Stable expression of P2G, of CXCL12-KDEL or of native CXCL12 in 143-B cells did not affect blood vessel formation in primary tumors. *(A)* Representative images of paraffin sections of tumors derived from indicated cell lines immunostained for CD31 (top panels) and with DAPI (bottom panels). Control tumor sections (NC) were incubated with the secondary antibody alone. Bars = 50 μm. *(B)* Micro-vessel density in primary tumors grown from indicated cell lines in percent of the density observed in 143-B EV cell-derived control tumors. The results are the mean values (± SEM) calculated from the

numbers determined as described in Supplemental Material in tumors of three randomly selected mice per experimental group.

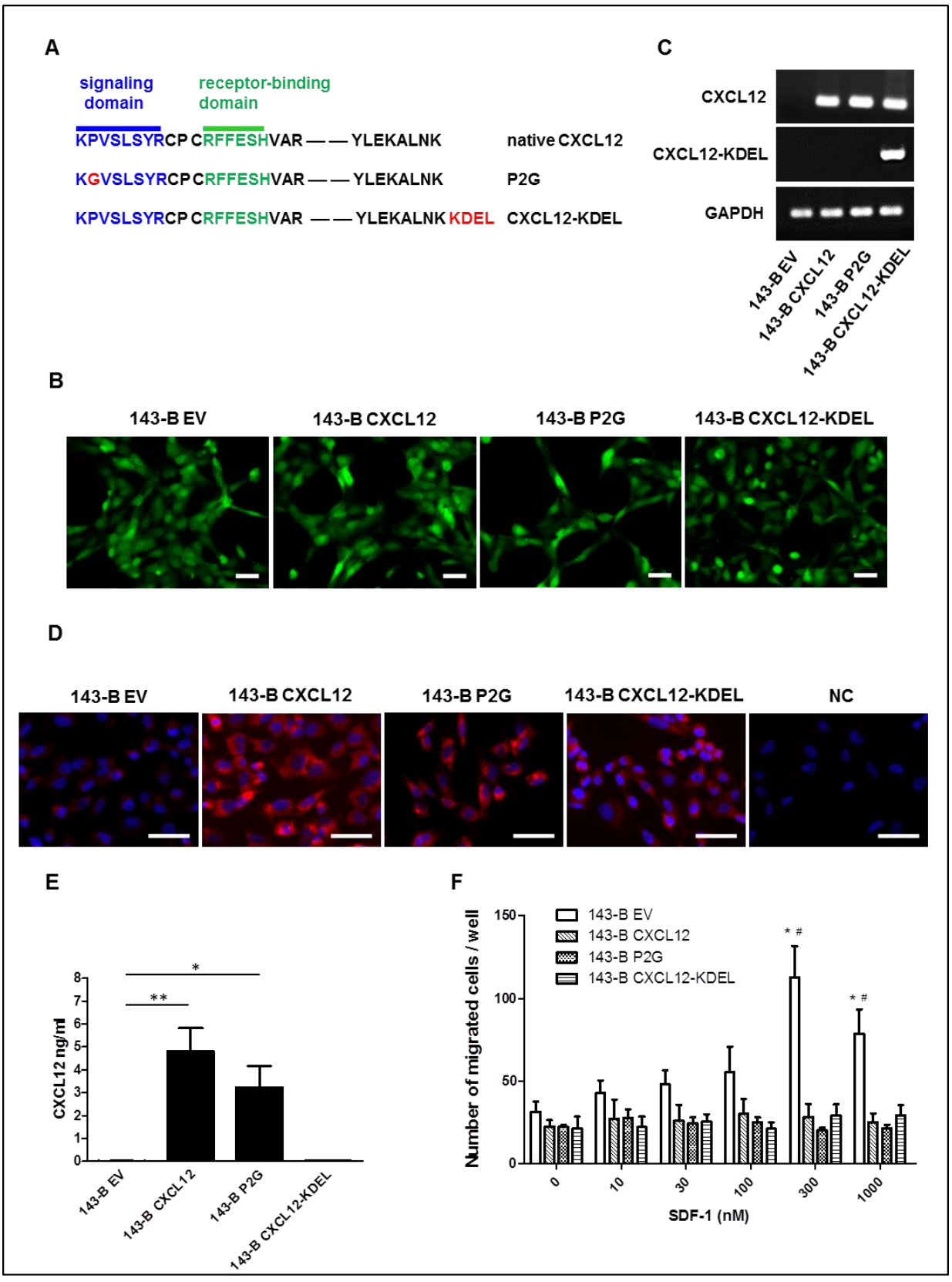
A
signaling domain
receptor-binding domain
KPVSLSYRCP CRFFESHVAR — — YLEKALNK native CXCL12
KGVSLSYRCP CRFFESHVAR — — YLEKALNK P2G
KPVSLSYRCP CRFFESHVAR — — YLEKALNK KDEL CXCL12-KDEL
C
CXCL12
CXCL12-KDEL
GAPDH
143-B EV
143-B CXCL12
143-B P2G
143-B CXCL12-KDEL
B
143-B EV
143-B CXCL12
143-B P2G
143-B CXCL12-KDEL
D
143-B EV
143-B CXCL12
143-B P2G
143-B CXCL12-KDEL
NC
E
CXCL12 ng/ml
*
**
143-B EV
143-B CXCL12
143-B P2G
143-B CXCL12-KDEL
F
Number of migrated cells / well
143-B EV
143-B CXCL12
143-B P2G
143-B CXCL12-KDEL
* #
* #
SDF-1 (nM)

Fig. 1

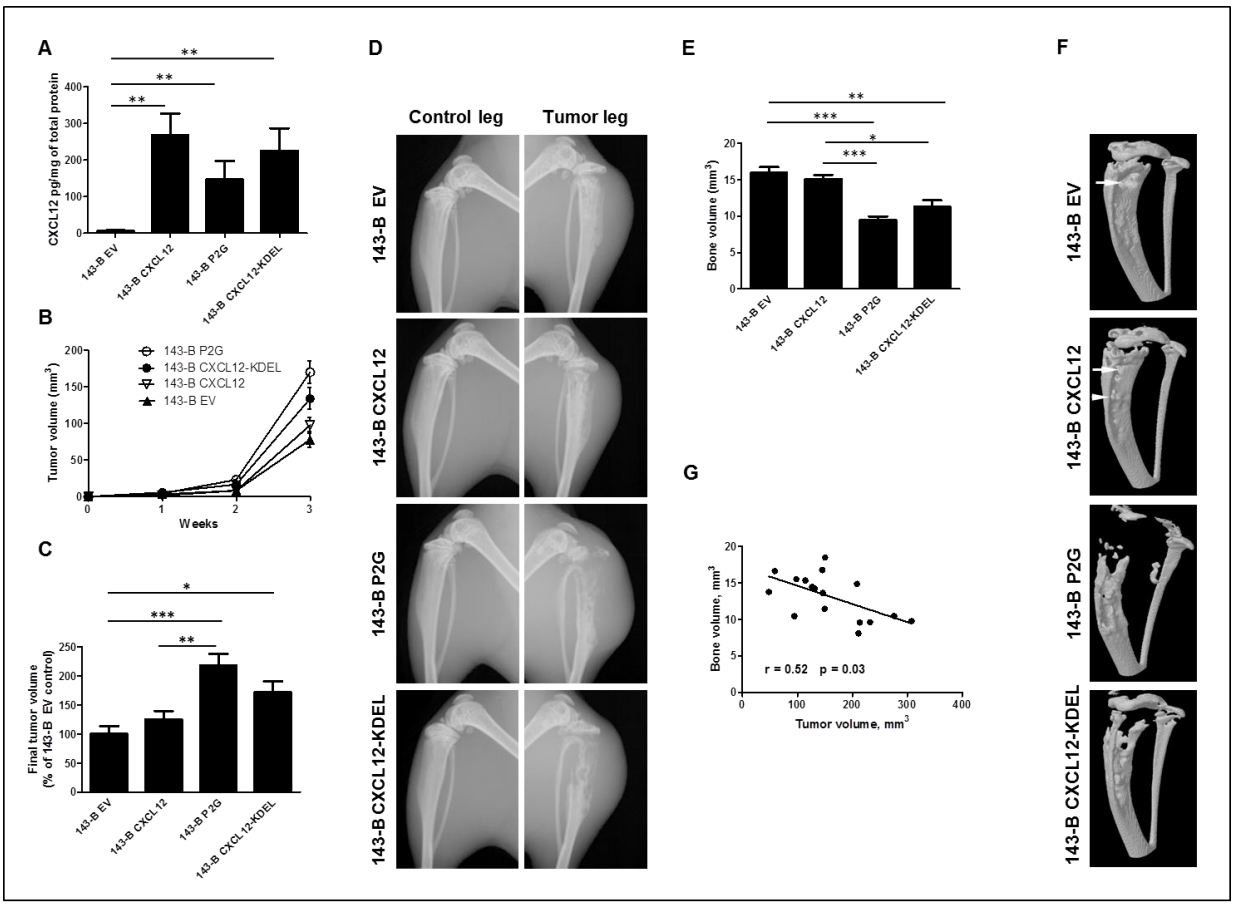
A
CXCL12 pg/mg of total protein
143-B EV
143-B CXCL12
143-B P2G
143-B CXCL12-KDEL
B
Tumor volume (mm3)
Weeks
143-B P2G
143-B CXCL12-KDEL
143-B CXCL12
143-B EV
C
Final tumor volume (% of 143-B EV control)
D
Control leg
Tumor leg
E
Bone volume (mm3)
F
G
Bone volume, mm3
Tumor volume, mm3
r = 0.52 p = 0.03

Fig. 2

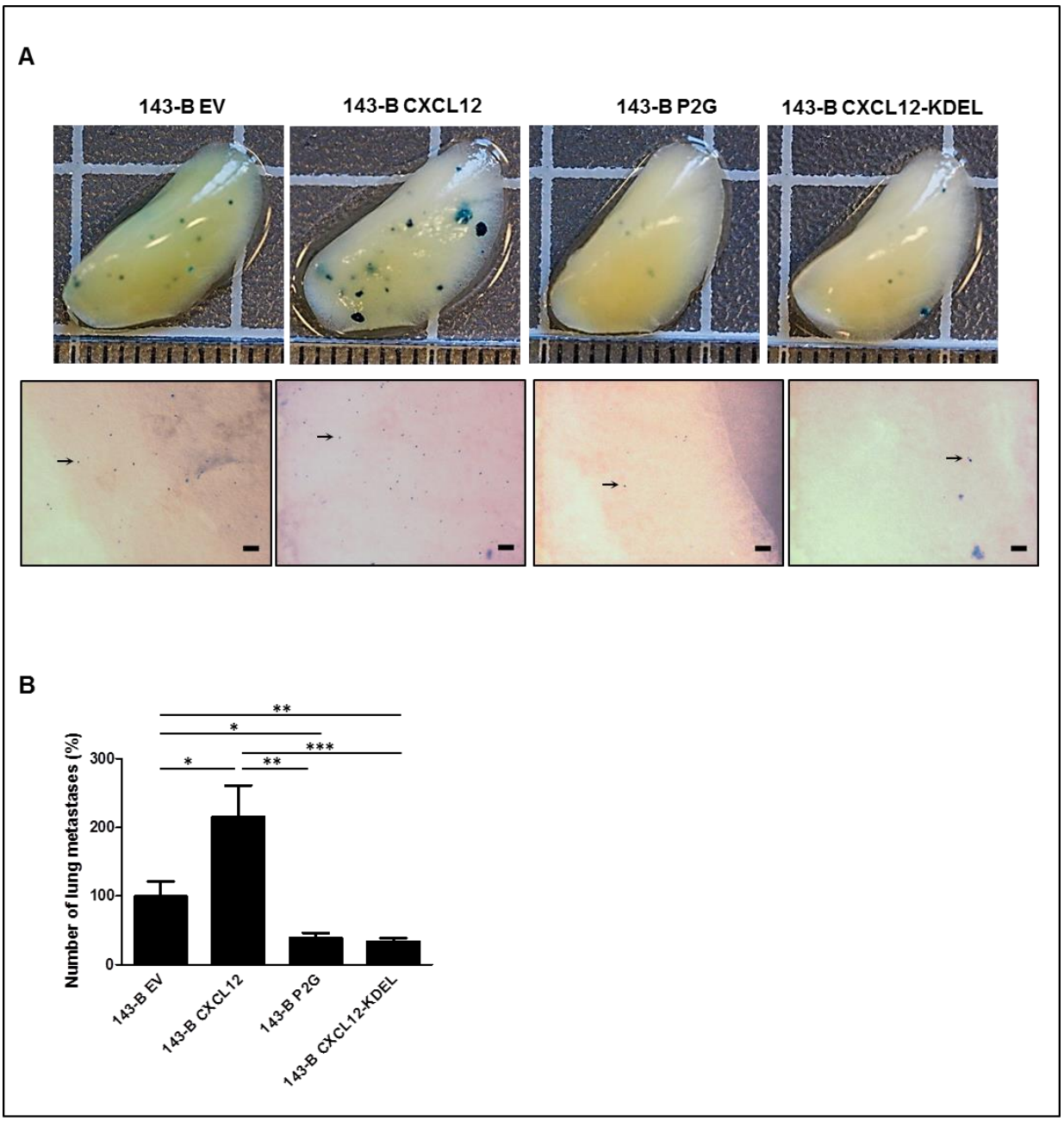
A
143-B EV
143-B CXCL12
143-B P2G
143-B CXCL12-KDEL
B
Number of lung metastases (%)
300
200
100
0
*
**
*
**
***
143-B EV
143-B CXCL12
143-B P2G
143-B CXCL12-KDEL

Fig. 3

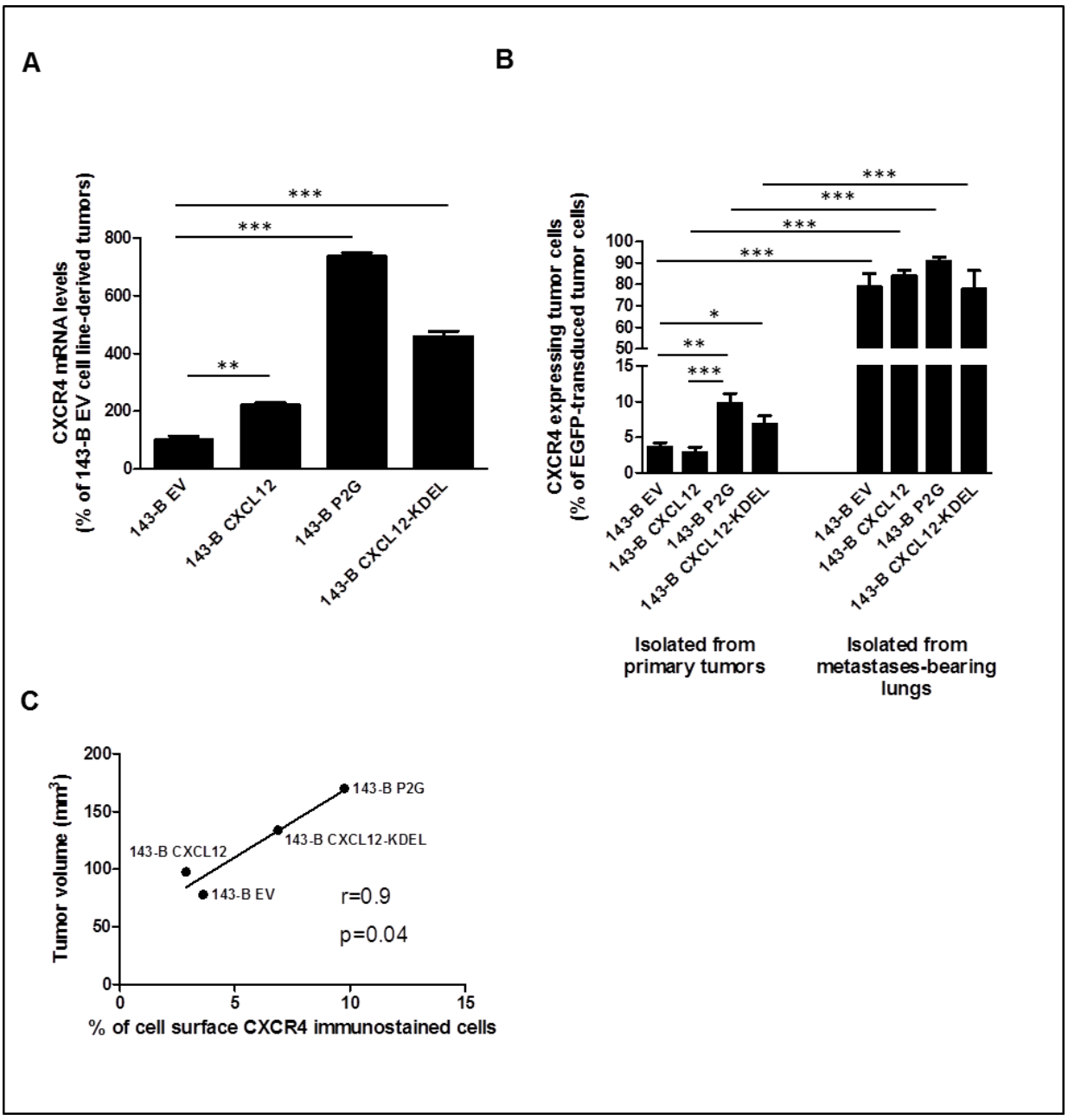
A
CXCR4 mRNA levels
(% of 143-B EV cell line-derived tumors)
800
600
400
200
0
***
***
**
143-B EV
143-B CXCL12
143-B P2G
143-B CXCL12-KDEL
B
CXCR4 expressing tumor cells
(% of EGFP-transduced tumor cells)
100
90
80
70
60
50
15
10
5
0
***
***
***
***
*
**
***
143-B EV
143-B CXCL12
143-B P2G
143-B CXCL12-KDEL
143-B EV
143-B CXCL12
143-B P2G
143-B CXCL12-KDEL
Isolated from primary tumors
Isolated from metastases-bearing lungs
C
Tumor volume (mm3)
200
150
100
50
0
143-B P2G
143-B CXCL12-KDEL
143-B CXCL12
143-B EV
r=0.9
p=0.04
0
5
10
15
% of cell surface CXCR4 immunostained cells

Fig. 4

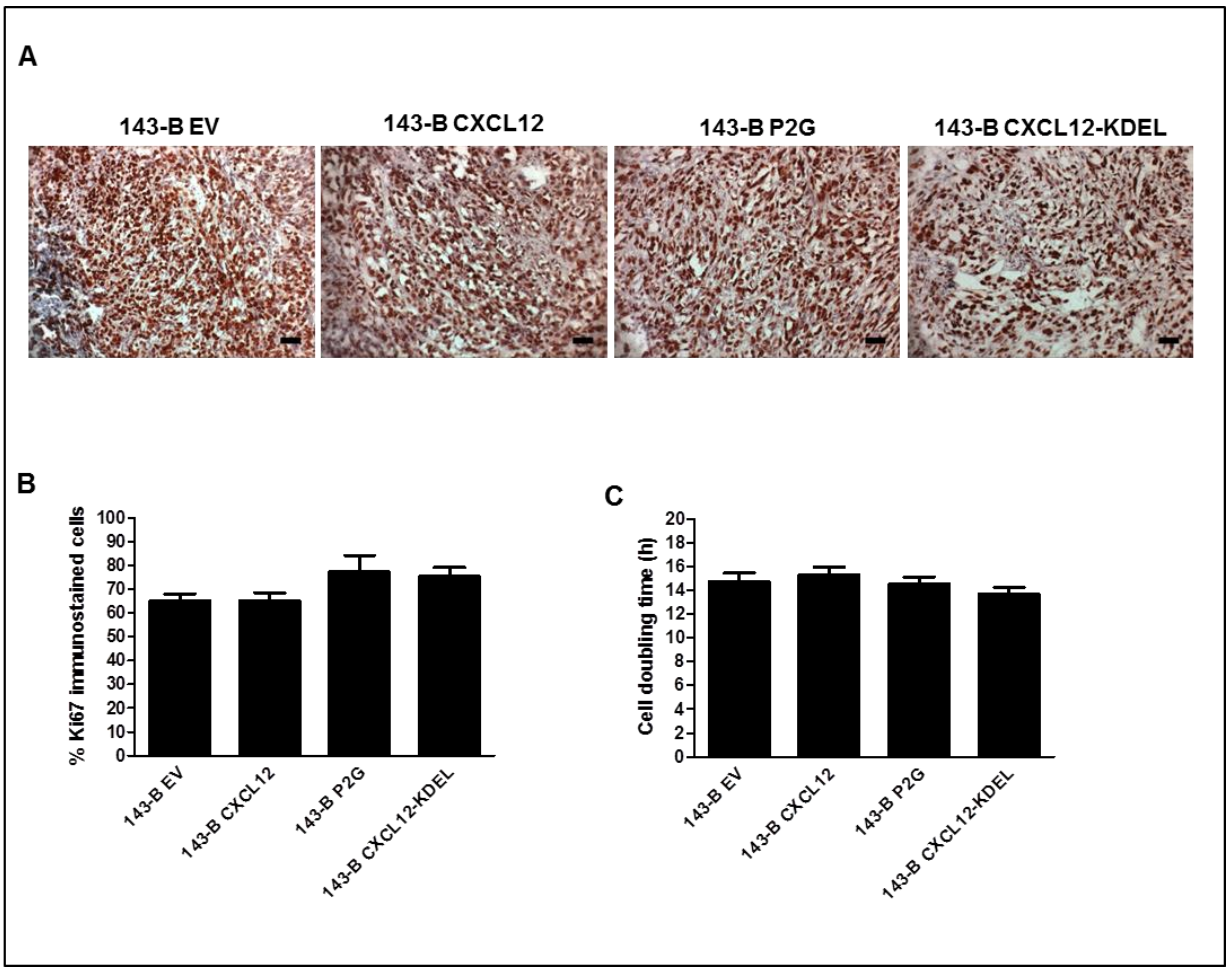

Supplemental Fig. 1

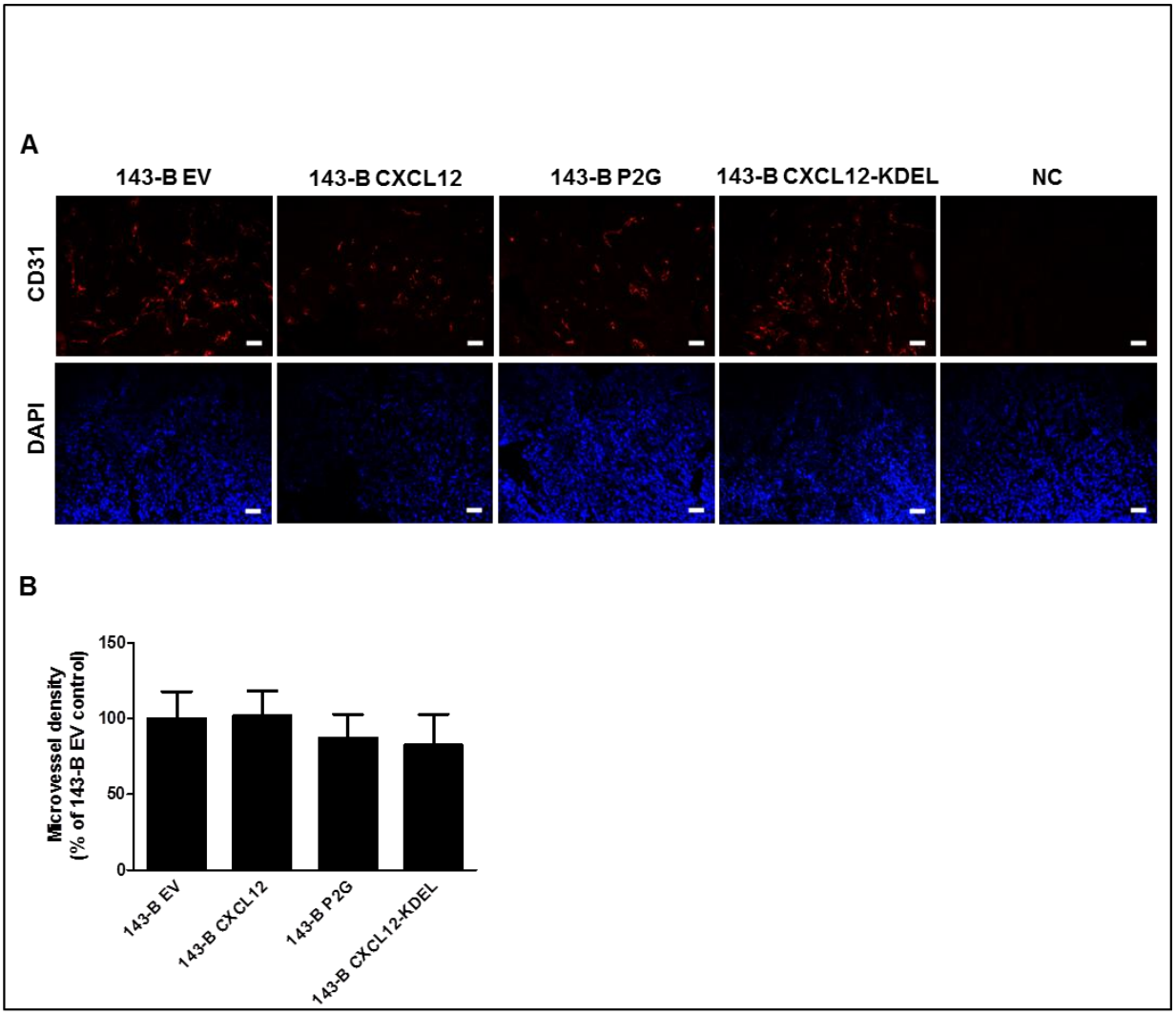

Supplemental Fig. 2

9.2 Additional studies and results

9.2.1 Role of the SDF-1/CXCR4 axis in OS metastasis

The expression of CXCR4 in OS 143-B EV, SDF-1/P2G and SDF-1-KDEL expressing cells at the mRNA level was quantified by real time PCR (Figure 1). Stable expression of SDF-1 in 143-B cells resulted in a non-significant increase of CXCR4 encoding transcripts to 137% of that measured in control 143-B EV cells. Stable expression of P2G or SDF-1-KDEL, on the other hand, resulted in a non-significant decrease of CXCR4 transcript levels by 61.3% or 58.1%, respectively, compared to control.

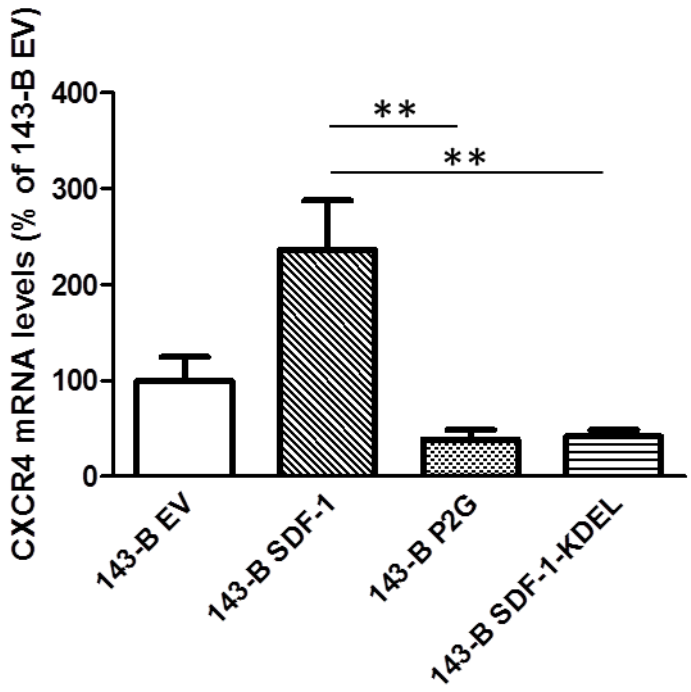

Figure 1. Expression of CXCR4 encoding mRNA in the 143-B cell line derivatives 143-B EV, SDF-1, P2G and SDF-1-KDEL. The results show the mean (±SEM) transcript levels measured in 3 independent mRNA extracts per cell line normalized to GAPDH and to the mean level detected in the control 143-B EV cell line set to 100%. $p<0.05$

We verified CXCR4 protein expression in our 143-B manipulated cell lines by immunocytochemical stainings (Figure 2). The results showed membrane expression of CXCR4 in 143-B EV, 143-B SDF-1 and 143-B P2G cells. As expected, only moderate

expression of membrane-located CXCR4 was observed in 143-B SDF-1-KDEL cells indicating efficient retention of CXCR4 inside the cells.

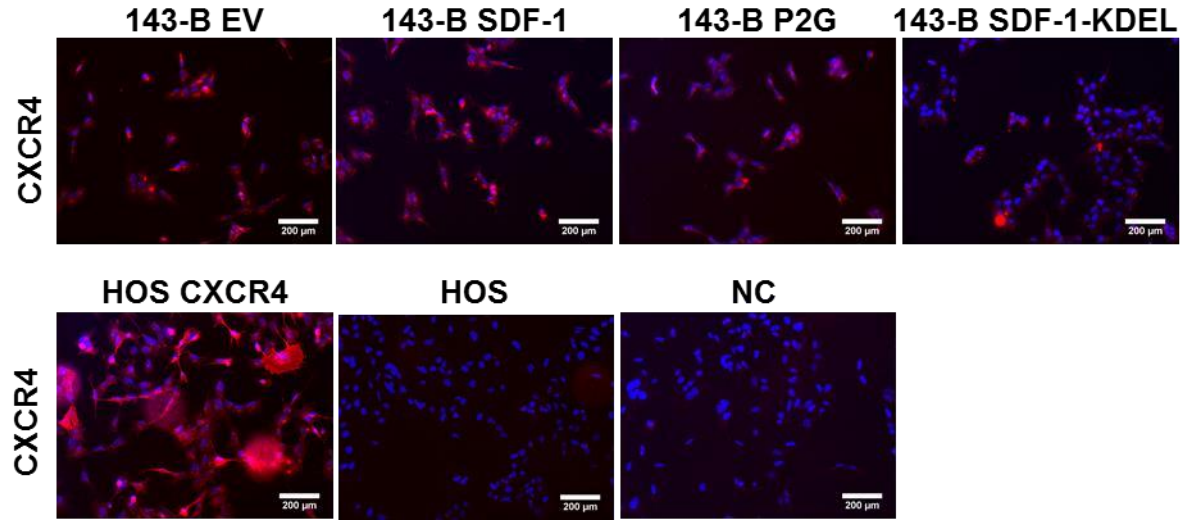

Figure 2. Expression of CXCR4 on the cell surface in indicated cell lines visualized by fluorescence immunocytochemistry with antibodies recognizing CXCR4. Cell nuclei are stained with DAPI. HOS cells manipulated to stably express CXCR4 were used as a positive control. HOS cells lacking endogenous CXCR4 were used as an additional negative control to verify the specificity of the CXCR4 antibody (antibody clone 12G5). HOS cells stably expressing CXCR4 and incubated with the secondary Alexa Fluor 547 antibody alone (NC) served as an additional control to exclude non-specific staining.

In order to further verify CXCR4 protein expression, we repeated immunocytochemical staining on permeabilized cells with a CXCR4 antibody (clone UMB-2) that selectively binds to the C-terminus of non-phosphorylated CXCR4 located in the cytoplasm or in the cell membrane. Surprisingly, only a small fraction of 143-B EV cells expressed CXCR4 (Figure 3, upper panel). 143-B SDF-1 cells showed only a moderate CXCR4 immunostaining, indicating that constitutive expression of SDF-1 might lead to receptor activation and phosphorylation, taking into account that the CXCR4 antibody UMB-2 does not recognize phosphorylated CXCR4. 143-B P2G and 143-B SDF-1-KDEL cells also showed low levels of CXCR4

expression. Although, the antibodies might not efficiently bind SDF-1-KDEL, they should recognize P2G.

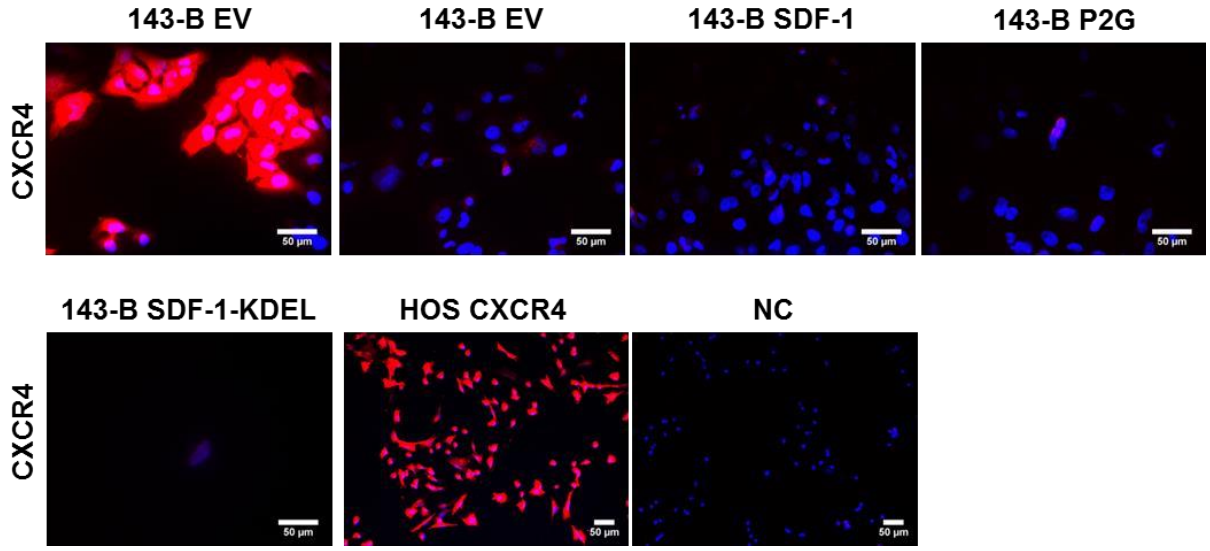

Figure 3. Expression of membrane and cytoplasmic CXCR4 in indicated cell lines visualized by fluorescence immunocytochemistry with UMB-2 antibody recognizing non-phosphorylated C-terminus of CXCR4. Cell nuclei are stained with DAPI. HOS cells manipulated to overexpress CXCR4 were used as a positive control. HOS cells overexpressing CXCR4 were incubated with the secondary Alexa Fluor 547 antibody alone (NC) served as controls for non-specific staining. Microscopic analysis of UMB-2-stained 143-B cells revealed subpopulations of CXCR4-expressing cells (upper panel, the first image from the left), whereas the majority of the cells stayed CXCR4-negative (upper panel, the second image from the left).

In our study we could detect membrane CXCR4 at least by immunocytochemical staining using anti-CXCR4 12G5 antibody and showed that SDF-1-KDEL remarkably reduced CXCR4 cell surface level in 143-B cells compared to 143-B EV cells. The results of the immunocytochemical stainings, however, indicated that the expression of CXCR4 at the protein level in 143-B cells is not stable. Intracellular examination of CXCR4 expression using UMB-2 antibody did not detect any CXCR4 in the 143-B cell line derivatives, with the exception of 143-B EV, where several cell subpopulations were shown to highly express the receptor. Importantly, UMB-2 antibody recognizes only non-phosphorylated C-terminus of the receptor. Stable expression of SDF-1 from 143-B cells may lead to the receptor activation and phosphorylation, leaving it undetectable by the antibody.

In order to investigate whether CXCR4 expression depends on cell confluency, we grew 143-B EV cells to 50-60%, 60-70% or to 95-100% confluency and reexamined cell surface expression of CXCR4 by flow cytometry (Figure 4). HOS cells manipulated to overexpress CXCR4 (HOS-CXCR4) were used as a positive control and HOS cells lacking endogenous CXCR4 were used as a negative control The results revealed that 143-B EV cells express CXCR4 at the cell surface at minimal levels largely independent of cell confluency. High CXCR4 expression was detected at the cells surface of the control HOS CXCR4 cells. No CXCR4 expression was detected on the surface of HOS cells (negative control).

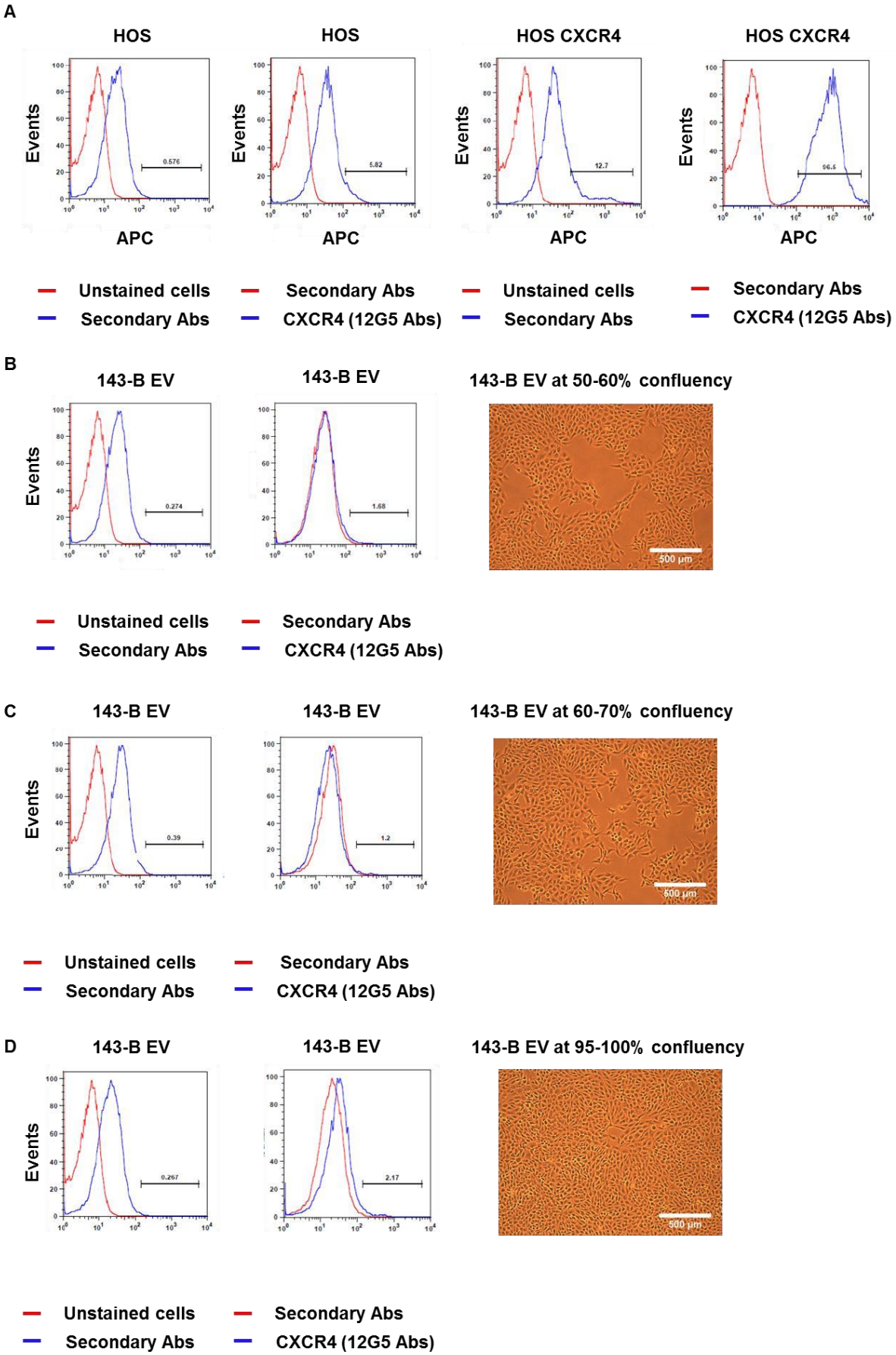

Figure 4. Cell surface expression of CXCR4 on 143-B EV cells at different confluent levels measured by flow cytometry. *(A)* Membrane expression of CXCR4 on HOS cells shown to be negative for CXCR4. These cells

were used as control for non-specific antibody binding (left panels). Cell surface expression of CXCR4 in HOS cells manipulated for stable CXCR4 expression (right panels). These cells were used as a positive control. *(B)* Cell surface expression of CXCR4 in 143-B EV cells grown to 50-60%, *(C)* 60-70% or *(D)* 95-100% confluency.

Finally, we decided to compare the levels of membrane-located and cytoplasmic CXCR4 in the individual manipulated cell lines. 143-B EV, -SDF-1, -P2G and -SDF-1-KDEL cells were grown to 60-70% confluency. The expression of membrane-located CXCR4 in intact cells (Figure 5 A) or of cytoplasmic CXCR4 in membrane-permeabilized cells (Figure 5 B) CXCR4 was measured by flow cytometry using the mouse monoclonal CXCR4 antibody 6H8. The results confirmed minimal levels of CXCR4 expression at the cell surface of intact cells, but robust intracellular expression of CXCR4 in membrane-permeabilized cells.

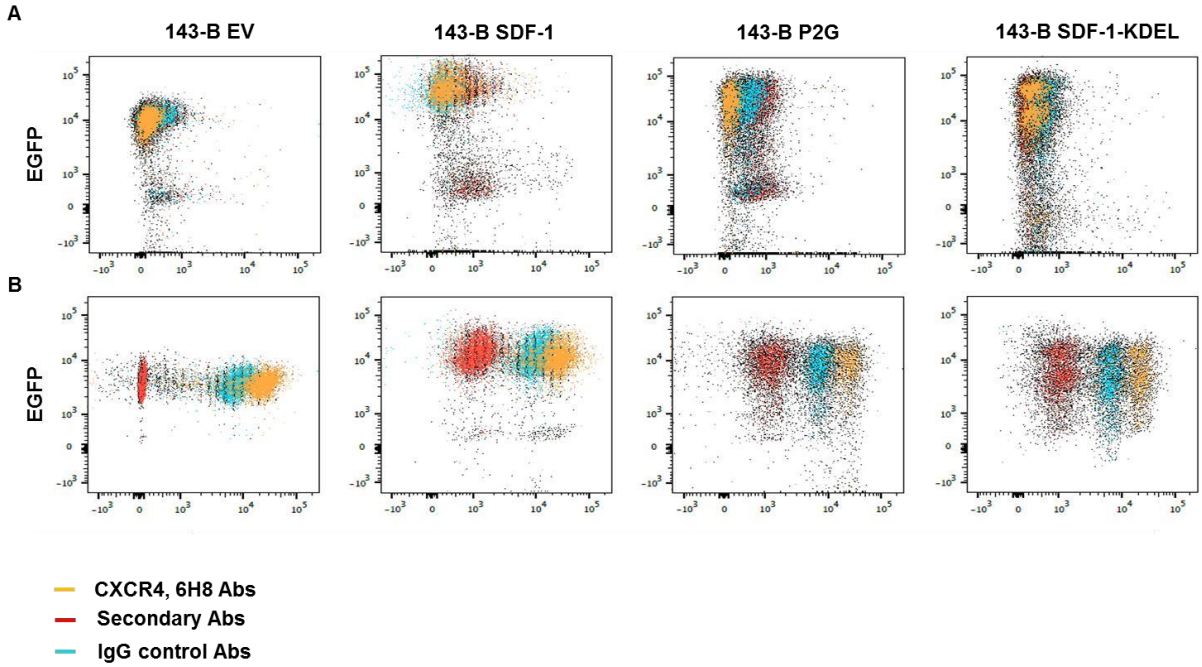

Figure 5. CXCR4 expression in indicated 143-B cell line derivatives examined by flow cytometry. *(A)* Membrane-located and *(B)* intracellular CXCR4 immunostaining in indicated cell lines. Isotype control mouse IgG were used as a control for non-specific binding.

Taken together, our results indicate that CXCR4 expression in human OS 143-B cells *in vitro* is variable. Moreover, a large fraction of CXCR4 expressed in the differently manipulated 143-B cells remains intracellular. These findings are consistent with results reported for

human CD34^{+} hematopoietic progenitor cells (Zhang, Foudi et al. 2004). Interestingly, Zeelenberg et al. reported that the expression of CXCR4 in colon and mammary carcinoma cells *in vitro* assessed by flow cytometry was low, but was remarkably upregulated *in vivo* presumably by stromal cell-derived factors (Zeelenberg, Ruuls-Van Stalle et al. 2003).

CXCR4 expression in OS cells appears to be also affected by cell culture conditions (Liao, Zhou et al. 2013). For example, Laverdiere et al. detected robust expression of CXCR4 encoding mRNA, measured by quantitative real-time PCR in 63% of OS primary tumor tissue specimens, but the levels in OS cell lines (HOS, SaOS-2, U2OS) in tissue culture were low (Laverdiere, Hoang et al. 2005).

It has been proposed that CXCL14 is also a ligand for CXCR4 (Tanegashima, Suzuki et al. 2013). In order to exclude that endogenous CXCL14 might interfere with our manipulations in the described 143-B cell line derivatives, we examined, by semi-quantitative RT-PCR, the expression of CXCL14 encoding mRNA in 143-B EV, -SDF-1, -P2G and-SDF-1-KDEL cells (Figure 8). Unlike in the human U2OS OS cell line, used as a positive control, CXCL14 mRNA remained undetectable in all the 143-B cell line derivatives investigated here.

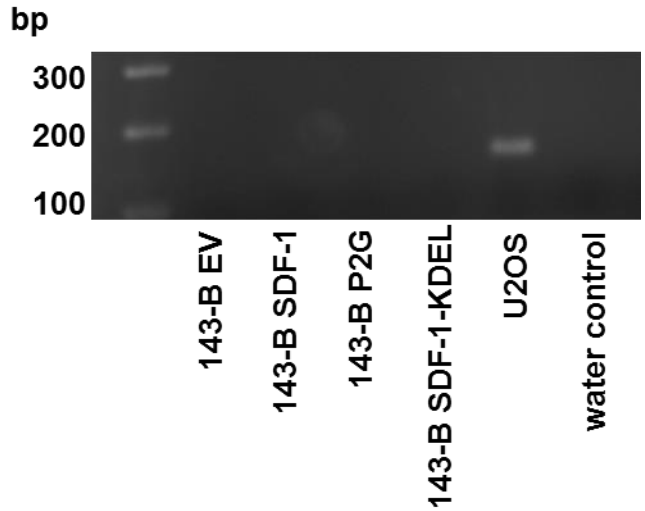

Figure 8. Semi-quantitative RT-PCR analysis of CXCL14 mRNA expression in indicated 143-B cell line derivatives. Human U2OS OS cells were used as a positive control for CXCL14 expression. GAPDH was used as a control for RNA input.

An important aspect in the analysis of primary tumors was tumor angiogenesis. Consequently, we performed in addition to CD31 immunohistochemistry shown in the manuscript (chapter 9.1), ERG immunostaining of paraffin-embedded primary tumor sections (Figure 9 A). Confirming the results of CD31 immunostaining, ERG staining did not reveal any significant differences in micro-vascularization of tumors grown from the indicated cell lines (Figure 9 B).

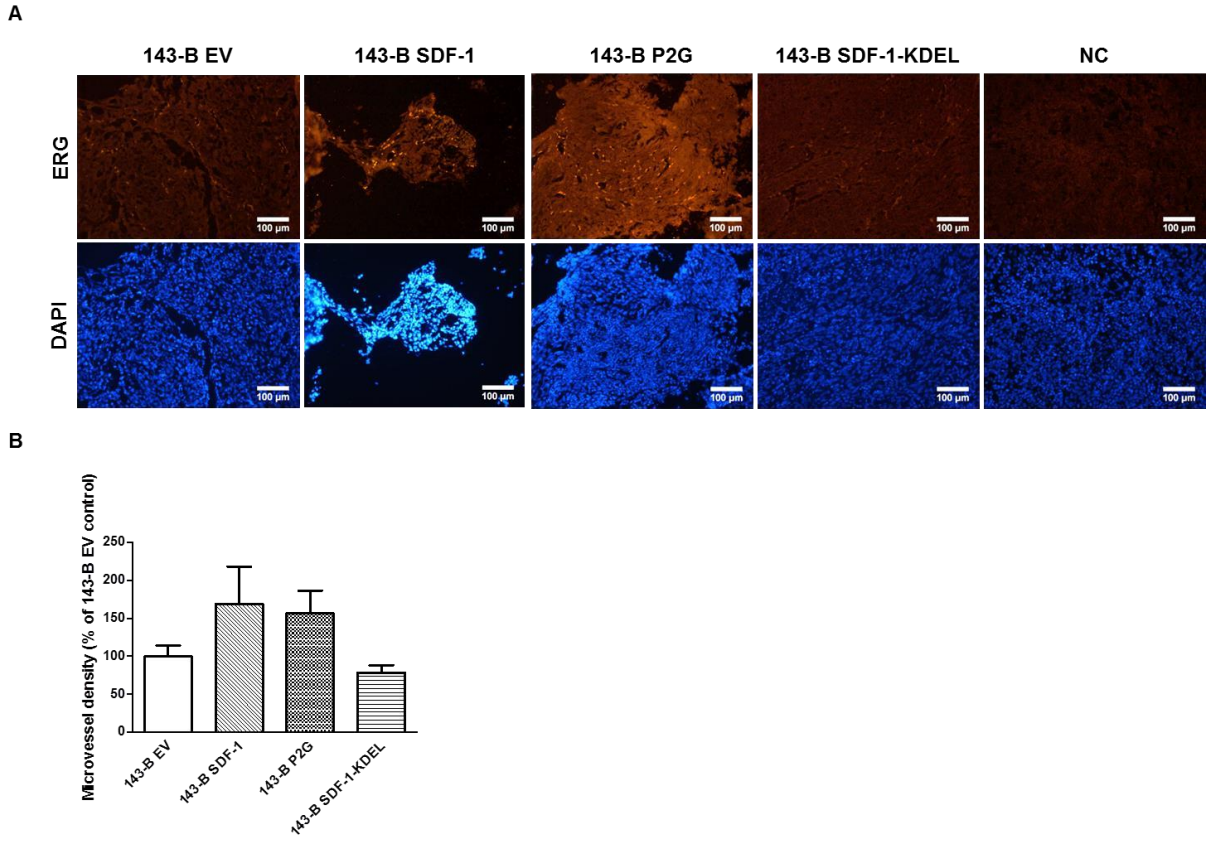

Figure 9. Estimation of micro-vessel density in tumors grown from 143-B cell line derivatives measured by ERG immunohistochemical staining of paraffin embedded primary tumor sections. (A) Representative images of paraffin sections of tumors grown from indicated cell lines immunostained for ERG (top panels) and stained with DAPI (bottom panels). Control tumor sections (NC) were incubated with the secondary antibody alone. *(B)* Micro-vessel density (determined as described in Materials and Methods) in primary tumors of indicated cell lines in percent of the density observed in 143-B EV control tumors. The results are shown as mean values (±SEM) calculated from 5 randomly selected areas of 0.14 mm^2 per tumor tissue section. Three randomly selected sections of tumors, collected from mice of the four indicated groups of experimental animals, were

immunostained and analyzed. The differences between the experimental groups shown in *(B)* were not significant.

9.2.2 Pulmonary administration of an SDF-1 neutralizing ligand for targeted treatment of lung metastasis in an intratibial metastasizing OS mouse model: a pilot study

Despite improvements in the treatment of OS, metastasis remains the main cause of death of OS patients (Koshkina and Kleinerman 2005; Whelan, Jinks et al. 2012). Many systemically applied drugs cause toxicity and undesirable side effects. Local administration of an antimetastatic drug to the site of secondary lesions will allow delivering drugs at concentrations higher than those used in systemic treatment and simultaneously reduce undesirable side effects.

The aim of this study is to develop a therapeutic strategy for targeting lung metastasis in OS by local delivery of an SDF-1 neutralizing compound. As reported in the enclosed manuscript, the expression of CXCR4 was found upregulated in OS cells growing to metastases in the lung as compared to the tumor cells in intratibial primary tumors. SDF-1 expressed by lung endothelial cells is supposed to support tumor cell survival, proliferation and metastasis self-seeding mediated by CXCR4 expressed by tumor cells. Along these lines, it has been demonstrated that targeting of CXCR4 by tail-vein administration of CXCR4-blocking antibody in mice with intratibial metastasizing OS reduced the number of lung metastatic nodules significantly in antibody-treated compared vehicle-treated animals (Brennecke, Arlt et al. 2014). Here, we propose to inhibit CXCR4 functions in tumor cells of OS lung metastases by pulmonary administration of chalcone 4 that, though interaction with SDF-1, blocks its binding to CXCR4 (Daubeuf, Hachet-Haas et al. 2013). An important advantage of chalcone over the antibody treatment is the feasibility of a local administration of the compound to the lung and a short half-life of CN-chalcone 4, which allows us to rather selectively investigate physiological and pathophysiological roles of SDF-1 in the lung

separate from potential effects in many other tissues where SDF-1 is expressed. Thus local administration of CN-chalcone 4 to the lung will also reduce undesirable side effects expected from systemic administration.

In a pilot study we evaluated and compared two different methods of drug delivery to the lung: direct intratracheal intubation and intranasal application. We applied a solution of 0.5% Evans blue in order to reproduce and visualize the tissue distribution of drugs upon pulmonary administration. Separate groups of healthy mice were intranasally treated with either 25 µl or 50 µl of Evans blue solution. A third group of mice, 25 µl of Evans blue solution were administered intratracheally upon intubation. Intranasal administration of 25 µl Evans blue solution resulted in minimal staining of lung tissue (Figure 1A), whereas administration of the larger volume of 50 µl resulted in a wider distribution of the dye in both lung lobes (Figure 1 B, C, D). Similarly, intratracheal administration of 25 µl of Evans blue also revealed a remarkable penetration of the dye into lung tissue (Figure 2) and a rather uniform distribution in lung parenchyma.

The results of the pilot study with Evans blue showed that intranasal drug administration was less efficient because the mice swallowed a largely non-predictable amount of the applied drug volume. Another disadvantage of using this application route is the risk that the compound might also pass the blood/brain barrier and end up in the central nervous system resulting in non-desirable side effects and a reduced drug concentration in the target organ (Hanson and Frey 2008). However, intranasal drug application is safe, minimally invasive and easy to perform.

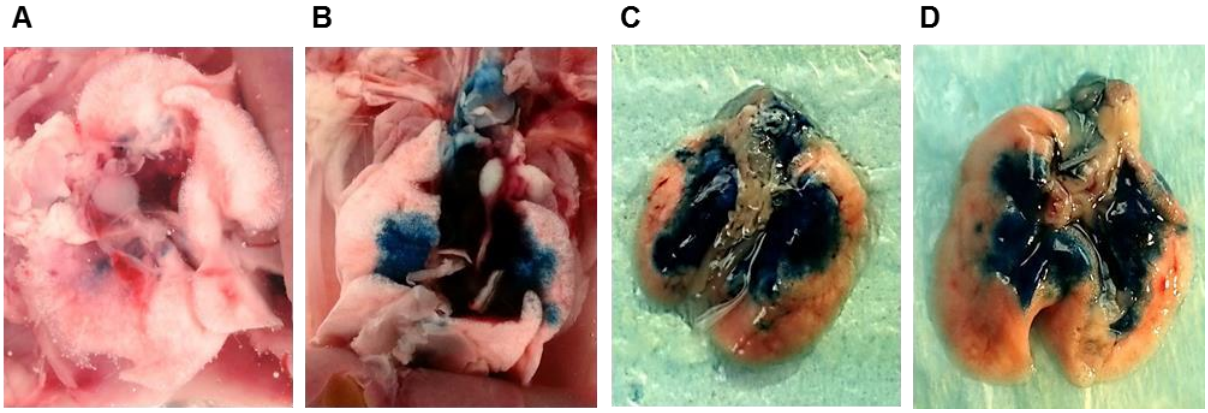

Figure 1. Tissue distribution of 0.5% Evans blue in mouse lungs upon intranasal administration. (A) Representative image of a lung of a mouse treated with 25 µl Evans blue solution. (B, C, D) Lungs of mice treated with 50 µl of 0.5% Evans blue solution.

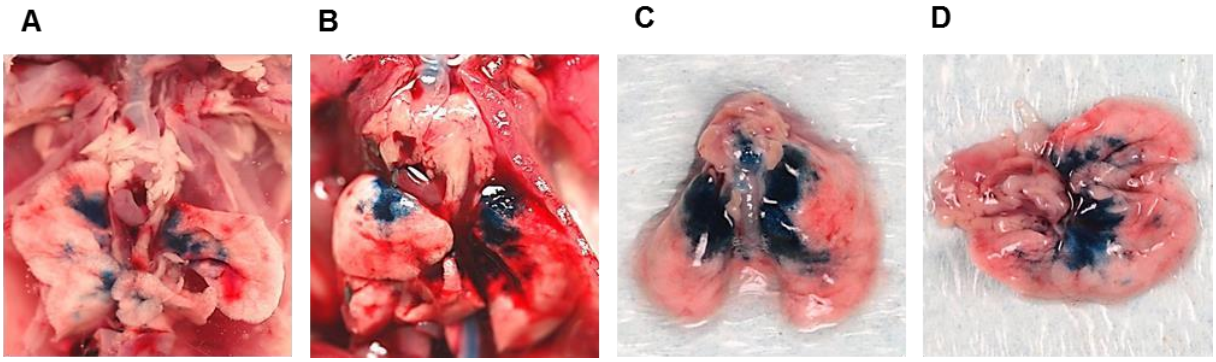

Figure 2. Tissue distribution of 0.5% Evans blue in mouse lungs upon intratracheal administration. (A, B, C and D) Representative images of lungs of mice treated with 25 µl of 0.5% Evans blue solution.

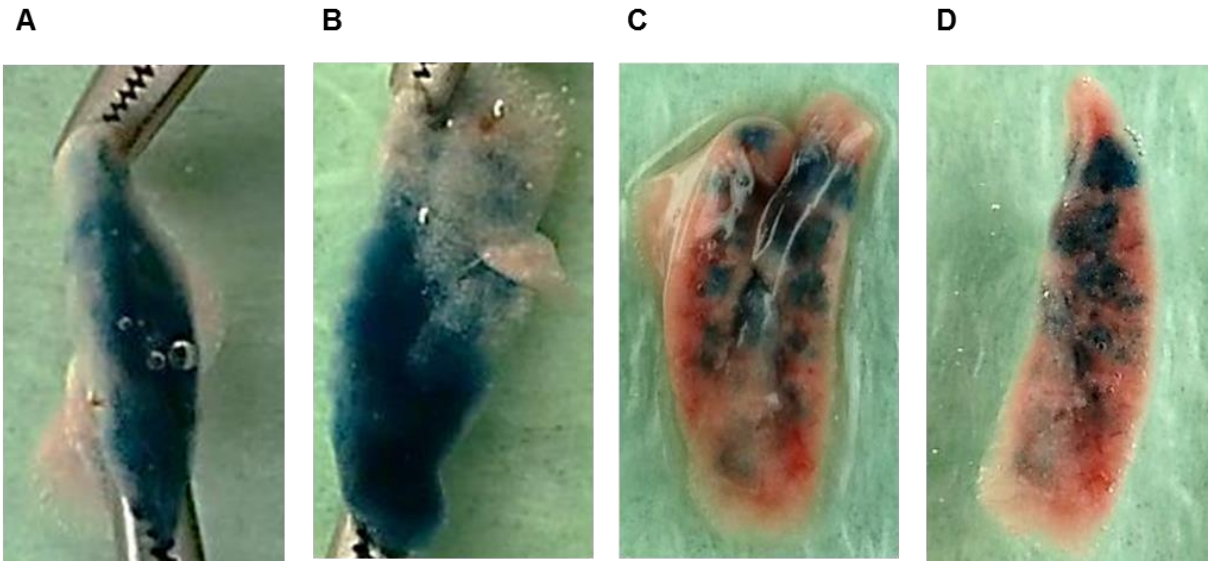

Figure 3. (A, B, C and D) Representative images of lateral cuts of lungs of mice upon intratracheal administration of 0.5% Evans blue solution.

We next started to evaluate the biodistribution of chalcone 4 and its derivate CN-chalcone 4 in tissues of healthy mice after intranasal or intratracheal administration. In order to improve the solubility of chalcone 4 in aqueous solutions, a phosphate-group was introduced, giving rise to phospo-chalcone 4 (P-chalcone 4) (Gasparik, Daubeuf et al. 2012). Importantly, the phosphate group of P-chalcone 4 (prodrug) is rapidly cleaved by cellular enzymes *in vivo* converting it to chalcone 4 (drug). Mice treated with P-chalcone 4 or CN-chalcone 4 through intranasal and intratracheal routes in the same manner described above were sacrificed at 15 min, 30 min, 1 h, 4 h, and 24 h after administration. The lungs, brain, the kidneys and liver from treated mice were collected and snap frozen in liquid nitrogen for further analysis. All the collected organs will be analyzed for the presence of chalcone 4 or CN-chalcone 4 or their degradation products, 3-methoxy-4-(methoxymethyloxy)benzaldehyde and para-chlorobenzoylacetonitrile. It is known that chalcones not only block the binding of SDF-1 to CXCR4, but also binding to GAGs (glycosaminoglycans) on cell surfaces, which resulted in removal of SDF-1 from the target organ. Therefore, we will also measure SDF-1 concentrations in mouse lungs treated with P-chalcone or CN-chalcone and compare the results with SDF-1 concentrations measured in lungs of mice treated with a vehicle (control).

Based on the results of the biodistribution study, we plan a future study in order to investigate the potential of the chalcones for local lung metastasis suppressive treatment in the intratibial OS mouse model.

9.2.3 *In vivo* characterization of K12 *lacZ*, K7M2 *lacZ*, and MOS-J *lacZ* OS models

The cell lines K7 and K12 have been isolated from an OS tumor that spontaneously occurred in a BALB/c mouse (Schmidt, Strauss et al. 1988). The K7M2 cell line has been established from lung metastatic nodules of a BALB/c mouse orthotopically injected with K7 cells into the proximal tibia after the second round of *in vivo* cell selection (Khanna, Prehn et al. 2000).

The metastatic potential of the K12 and K7M2 cell lines was assessed after orthotopic injection of cell suspensions or after implantation of intra-muscle-derived K12 and K7M2 tumor fragments into the mouse tibial muscle or a bone flap (Khanna, Prehn et al. 2000). The percentage of mice that developed primary tumors was higher after tumor tissue implantation than after orthotopic tumor cell injections. However, in order to be able to monitor metastasis, amputation of the primary tumor-bearing leg was required. The tumorigenic and metastatic potential of the K7M2 cell line was higher than that of the K7 cell line.

MOS-J cell line was derived from a spontaneously occurring OS in a C57Bl/6J mouse (Joliat, Umeda et al. 2002) and characterized as chondroblastic osteosarcoma. MOS-J cells formed fast growing primary tumors in immunocompromised and syngeneic hosts when injected intra-muscularly, however metastasis to lungs or other organs was not observed.

Consequently, the development of a mouse model which reproduces the main features of human OS, including lung metastasis, in non-immune compromised mice may be highly beneficial for future OS research. Specifically, the development of a highly tumorigenic and metastatic orthotopic MOS-J OS model is of a particular interest since many strains of mice engineered to carry different genetic mutations are maintained in the C57BL/6J genetic background. Highly tumorigenic and metastatic MOS-J cells would allow to study in manipulated C57BL/6J mice host genes that are involved in the pathogenesis of OS. Moreover, K12 and K7M2 represent an osteolytic subtype of OS, whereas MOS-J cells have an osteoblastic phenotype. The development of mouse models of OS with different histological phenotypes would significantly improve the options in preclinical OS research to study pathophysiological mechanisms and the efficacy of novel drugs in experimental animals with an intact immune system.

In our experiments we first reinvestigated the tumorigenic and metastatic potential of the K12, K7M2 and MOS-J cell lines upon intratibial injection into syngeneic mice and took advantage

of *ex vivo* monitoring of metastasis down to the single cell level by X-gal staining of *lacZ* transduced tumor cells in affected tissues, a technique that has been well established in our laboratory. Accordingly, mouse K12, K7M2, and MOS-J OS cells were stably transduced with a retroviral vector containing a *lacZ* and a neomycin resistance gene. After selection for antibiotic-resistant cells *in vitro*, X-gal staining showed that up to 100% of the *lacZ* gene transduced K12, K7M2, and MOS-J cells (Figure 1).

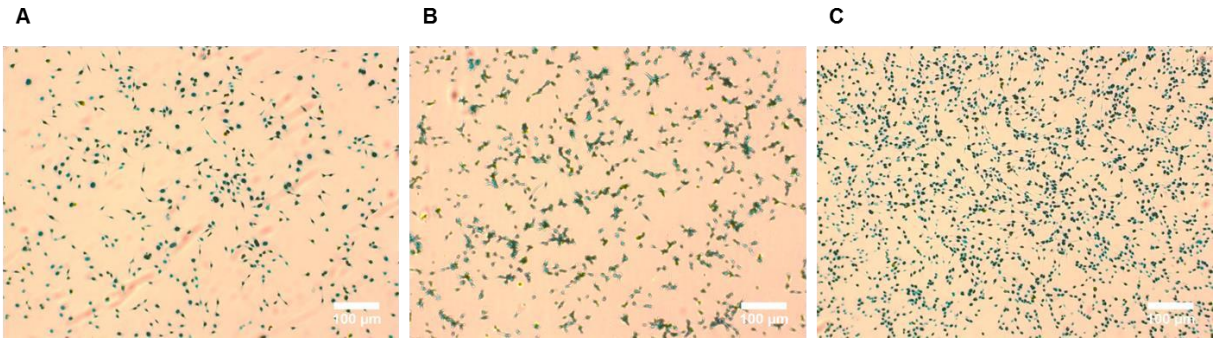

Figure 1. *In vitro* X-gal staining of *(A)* K12 *lacZ*, *(B)* K7M2 *lacZ*, *(C)* MOS-J *lacZ* cells. *lacZ* expressing cells are stained in indigo-blue color.

Before the *lacZ*-transduced cells were used in animal experiments, they were checked for mycoplasma contamination by PCR analysis. The results confirmed that none of the cell lines was contaminated with mycoplasma (not shown). In order to estimate tumorigenic and metastatic potential of the K12 *lacZ*, K7M2 *lacZ* or MOS-J *lacZ* cell line, we injected different numbers of cells orthotopically into the tibia of BALB/c or C57Bl/6J mice, respectively. The primary tumor growth was carefully measured with a caliper and visualized by conventional 2D X-ray imaging. None of the mice injected with $3x10^5$ or $1x10^5$ K12 *lacZ* cells developed primary tumors or bone lesions during 90 days of follow-up after tumor cell injection (TCI). *Ex vivo* X-gal staining of the lungs or other organs did also not show any metastases (not shown). On the contrary, most of the mice injected with K7M2 *lacZ* cells developed intratibial primary tumors. Interestingly, the size of intratibial tumors developing

from $1x10^5$ or from $3x10^5$ injected cells was indistinguishable over the entire experimental period of 90 days after TCI (Figure 2).

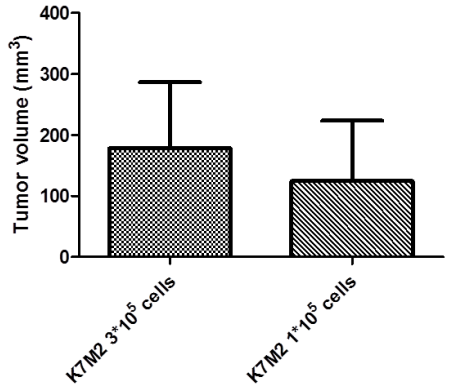

Figure 2. Tumor volumes measured BALB/c mice 90 days after intratibial injection of $3*10^5$ or $1*10^5$ K7M2 *lacZ* cells. The bars indicate the mean ± SEM tumor volumes in indicated experimental groups of 6 mice.

Although, X-ray imaging revealed moderate bone lesions in almost all mice injected with K7M2 *lacZ* cells, only three out of 12 mice (25%) developed tumors larger than 50 mm^3 (Figure 3A). The tumors in these three mice remained undetectable until day 27 after tumor cell injection. After day 27 they started to grow exponentially until the mice were sacrificed (Figure 3B and C).

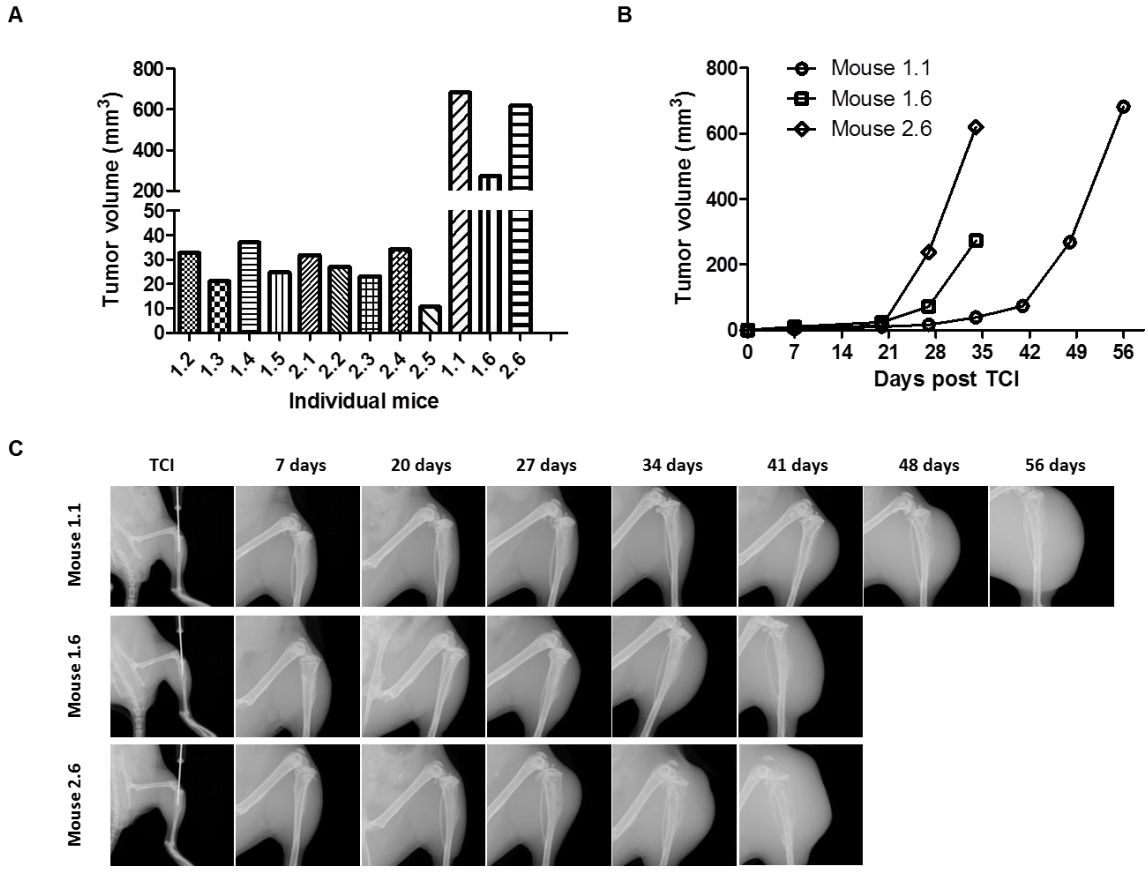

Figure 3. Primary tumor growth in mice injected with K7M2 *lacZ* cells. *(A)* The bar graph shows primary tumor volumes in individual mice before sacrifice. *(B)* Time course of primary tumor growth in the three indicated mice between the day of TCI and the day of sacrifice. *(C)* X-ray images of tumor-bearing legs of indicated mice taken on indicated days after TCI.

The three mice developed massive primary tumors of irregular shape. X-ray imaging showed osteolytic lesions in tumor-bearing tibiae and confirmed the osteolytic phenotype of the K7M2 cell line. Histological examination of K7M2 *lacZ*-derived primary tumors also confirmed bone osteolysis observed by X–ray imaging (Figure 4). The tumor cells invaded, in addition to the bone, surrounding muscles and connective tissues. The tumors in the three mice were histologically indistinguishable.

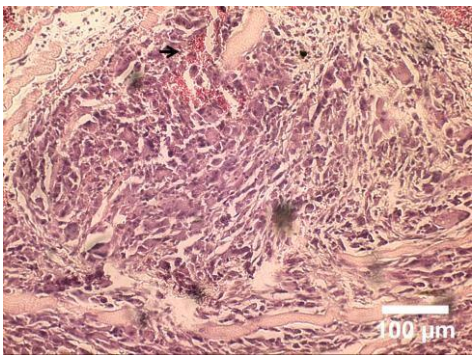

Figure 4. Representative hematoxylin and eosin (H&E) staining of a six µm section of a paraffin-embedded primary tumor. Primary tumor was derived from the mouse 1.6 injected with K7M2 *lacZ* cells. H&E staining demonstrates viable tumor cells (in pink color). The black arrow points at an area with infiltrating neutrophils.

The metastatic potential of K7M2 *lacZ* cells was investigated by analyzing lungs, spleens, livers and kidneys of tumor cell injected mice for X-gal stained micro- and macrometastatic nodules. Mice with intratibial primary tumors smaller than 50 mm^3 were also included. None of the investigated mice developed metastases in spleen, liver, kidney or distant bone tissue. Lung metastases were observed in mice with primary intratibial tumors larger than 200 mm^3, but remained undetectable in mice with primary tumors smaller than 50 mm^3 (Figure 5).

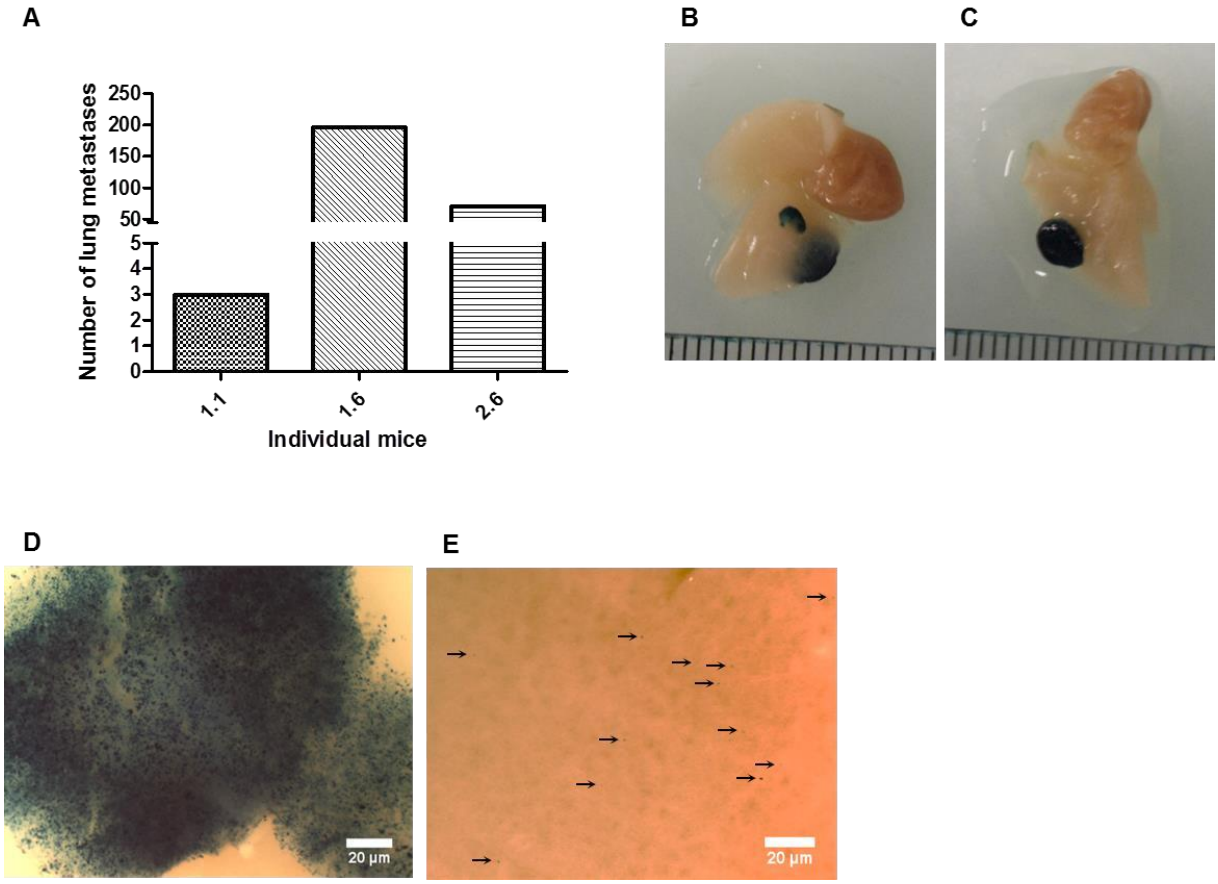

Figure 5. Analysis of lung metastases in mice injected with K7M2 *lacZ* cells. *(A)* The bars indicate the total number of metastases on lung whole mounts in indicated mice. Metastases were detected by *ex vivo* X-gal staining. *(B)* Macrometastases (in indigo-blue color) detected on the top or *(C)* on the bottom surface of the lung dissected from the 1.6 mouse. *(D)* Microscopic image of a macrometastasis or *(E)* micrometastases (in indigoblue color) in the lung of the 1.6 mouse. Black arrows point at micrometastases. Microscopic images were taken at 4X magnification.

K7M2 *lacZ* cells were isolated from primary tumors and grown in tissue culture under 800 µg/ml neomycin selection. Neomycin resistant K7M2 *lacZ* cells were checked again for *lacZ* expression (Figure 6) and collected for further reinjection. The cells showed a heterogeneous morphology with spindle-like and spherical cells in the population. All cells were mononuclear.

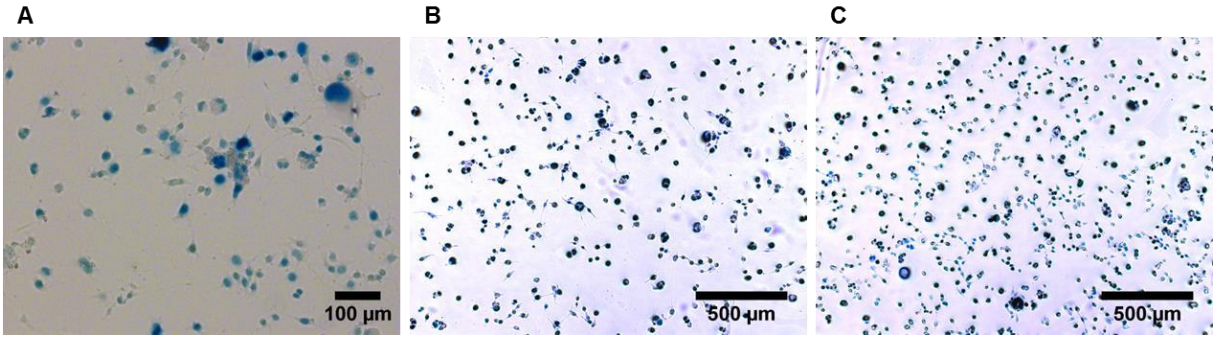

Figure 6. *In vitro* X-gal staining of K7M2 cells isolated from primary tumors of the *(A)* 1.1, *(B)* 1.6, and *(C)* 2.6 K7M2 *lacZ* tumor-bearing mice. *lacZ* expressing cells are stained in indigo-blue color.

Analysis of tumorigenicity of MOS-J *lacZ* cells revealed that all C57Bl/6J mice except one mouse developed primary tumors. One mouse did not show any sign of a primary tumor and was further excluded from the analysis (Figure 7 A). Two mice developed big primary tumor with a size larger than 50 mm^3. However, tumor growth was very slow and remained undetectable until the day 50 post TCI. After day 50, tumors grew exponentially, and the mice were sacrificed on day 85 (Figure 7 B and C).

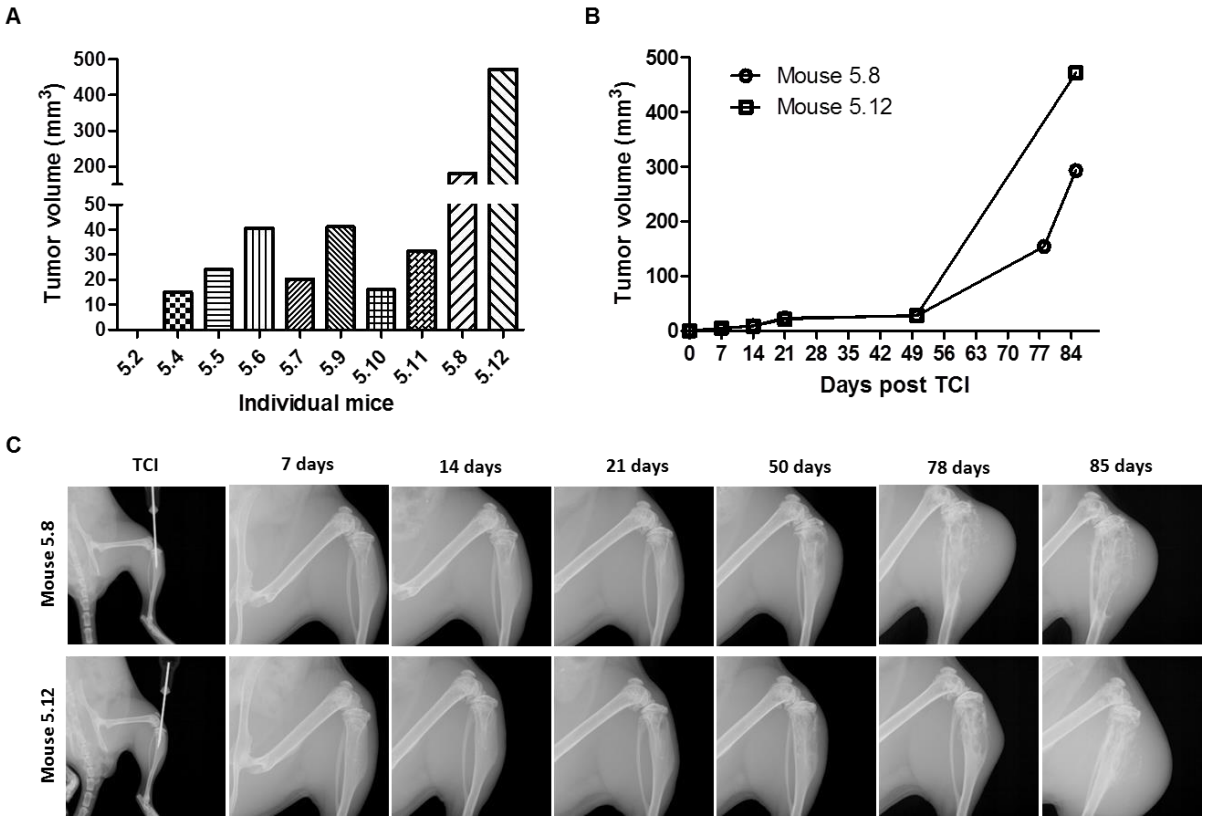

Figure 7. Primary tumor growth in mice injected with $5*10^5$ MOS-J *lacZ* cells. *(A)* The bars represent terminate tumor volumes measure in individual mice. All mice except one mouse developed primary tumors to the bone. Size of primary tumors exceeded 50 mm^3 in two mice. *(B)* The graph represents tumor growth in two mice, 5.8 and 5.12. *(C)* X-ray images of tumor-bearing legs of two mice (top-down: 5.8 and 5.12). The images were taken regularly starting with the day of TCI (on the left) until the day when the mice were sacrificed (on the right). X-ray revealed mixed phenotype of MOS-J *lacZ* tumors with osteolytic and osteoblastic features.

None of the mice injected with MOS-J *lacZ* cells formed distant metastasis to liver, kidneys, spleen, or tumor-free tibia. However, all mice developed metastasis to the lungs (Figure 8 A). Three mice developed large lung metastases visible with the naked eye (Figure 8 B, C, and D).

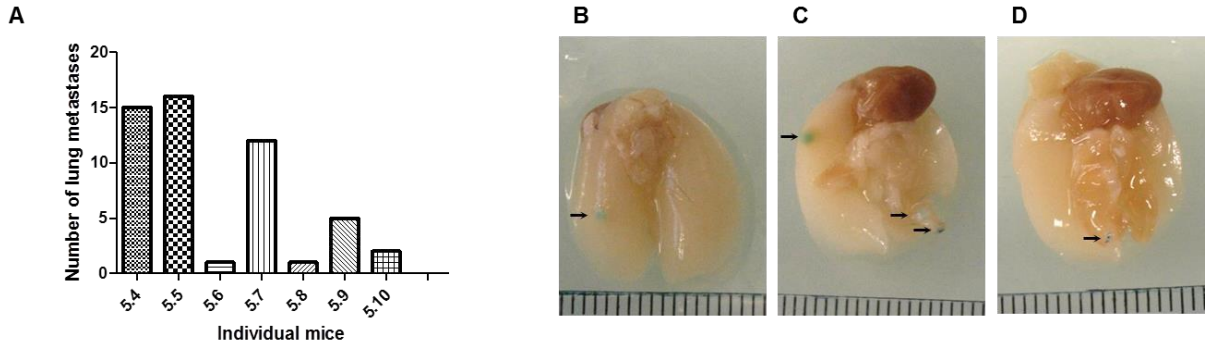

Figure 8. Analysis of lung metastasis injected with $5*10^5$ MOS-J *lacZ* cells. *(A)* The bars represent total number of metastases in individual mice. *(B)* Visualization of macrometastastic nodules with *ex vivo* X-gal staining in 5.5, *(C)* 5.9, and *(D)* 5.10 mice injected with MOS-J *lacZ* cells. Arrows point at metastases colored in blue.

MOS-J *lacZ* cells were isolated from primary tumors and lung metastatic nodules and further selected for neomycin-resistant cells *in vitro*. Antibiotic-resistant cells were checked for *lacZ* expression, and collected for *in vivo* selection (Figure 9).

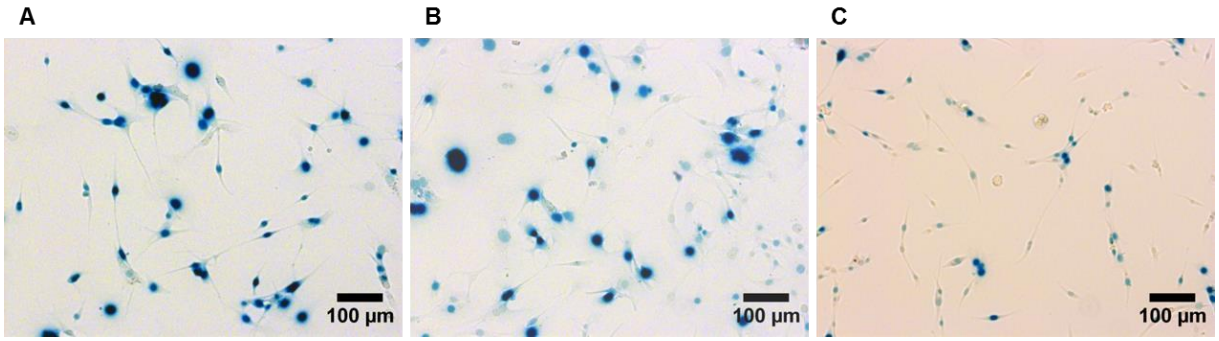

Figure 9. *In vitro* X-gal staining of MOS-J cells isolated from *(A)* primary tumors of 5.8, *(B)* 5.12, and *(C)* lung metastasis of 5.5 MOS-J *lacZ* tumor-bearing mice. *lacZ* positive cells are stained in indigo-blue color.

The results of this study demonstrated that although our K7M2 *lacZ* and MOS-J *lacZ* cell lines had a relatively low tumorigenic and metastatic potential, these models represent the metastatic pattern seen in human OS patients. Similar to the situation in clinics, our two OS models showed site-specific metastasis to lung, indicating that the molecular mechanisms that underlie site-specific spread of K7M2 *lacZ* and MOS-J *lacZ* cells are similar to those in OS

patients. However, the low incidence of metastatic disease and long delay until the tumor and metastasis detection make these models not suitable for studying the metastatic process of OS *in vivo*. In order to overcome this problem, we decided to increase tumorigenic and metastatic potential of K7M2 *lacZ* and MOS-J *lacZ* models via *in vivo* selection. K12 *lacZ* model was excluded from the further experiments, because no K12 *lacZ*-derived primary tumors did develop.

9.2.4 Establishment of highly metastatic mouse K7M2 *lacZ* and MOS-J *lacZ* OS models

*The second and the third rounds of the K7M2 *lacZ* and MOS-J *lacZ* cell lines *in vivo* selection were performed together with Bernhard Robl.

In order to select sublines of K7M2 *lacZ* and MOS-J *lacZ* cells with high tumorigenic and metastatic capacity, the cells were harvested from primary and metastatic sites followed by their expansion in cell culture and orthotopic reinjection into a mouse tibia of a syngeneic host. Primary tumors and metastases were allowed to occur and the cycles of selection were repeated.

This approach of *in vivo* selection was proposed by Fidler (Fidler 1990) and it suggests that tumor cells with metastatic gene expression signature can be selected from a heterogeneous population of poorly metastatic tumor cells. Therefore, the metastatic potential of bulk tumor cells is lower than that of disseminated cells.

The selection process for K7M2 *lacZ* and MOS-J *lacZ* cell lines is summarized in Figure 10. Primary tumor-derived OS cells were subsequently used for the selection of highly tumorigenic cell lines expressing gene products that support growth and survival of primary tumors, whereas metastatic-derived OS cells were subsequently selected to further enhance

their metastatic potential. Interestingly, our results revealed that selection of highly metastatic OS cells also altered the growth properties of a primary tumor indicating that gene products responsible for metastatic spread can also have a pro-tumorigenic effect.

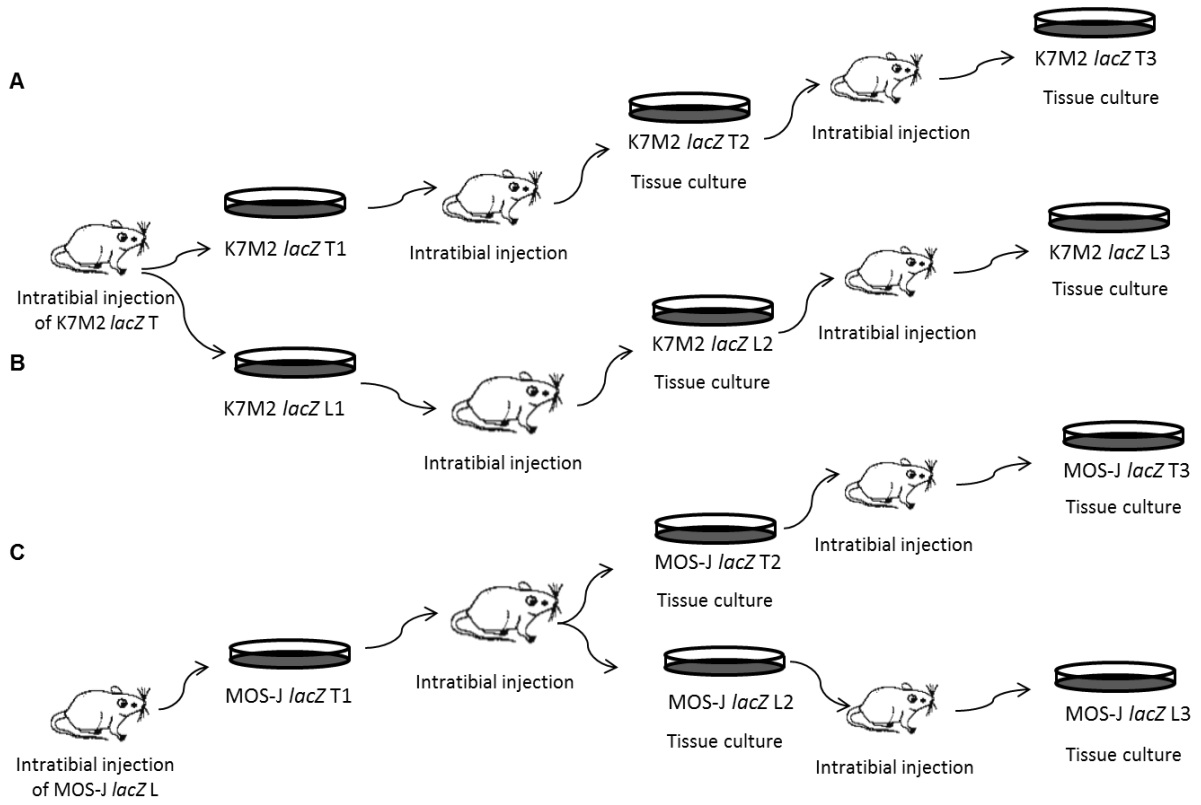

Figure 10. *In vivo* selection schemes for (A) K7M2 *lacZ* tumor-derived cells, (B) K7M2 *lacZ* lung metastasis-derived cells, and (C) for MOS-J *lacZ* tumor (MOS-J *lacZ* T2 and MOS-J *lacZ* T3) and lung metastasis-derived (MOS-J *lacZ* L2 and MOS-J *lacZ* L3) cells.

In the first round of our *in vivo* selection BALB/c mice were orthotopically injected with $3*10^5$ K7M2 *lacZ* primary tumor-derived cells (named K7M2 *lacZ* T). The results revealed that 11 out of 14 mice (78.5%) developed primary tumors larger than 50 mm^3 and extensive bone lesions (Figure 11 A and B). Primary tumors grew rapidly. Time until primary tumor detection was 14 days for K7M2 *lacZ* T cells vs 27 days for the parental K7M2 *lacZ* cell line.

Ex vivo X-gal staining of mouse lungs revealed macrometastatic nodules (Figure 11 C). K7M2 *lacZ* T cells were harvested from the primary tumor and metastatic sites and called K7M2 *lacZ* T1 and K7M2 *lacZ* L1 respectively (Figure 11 C and D).

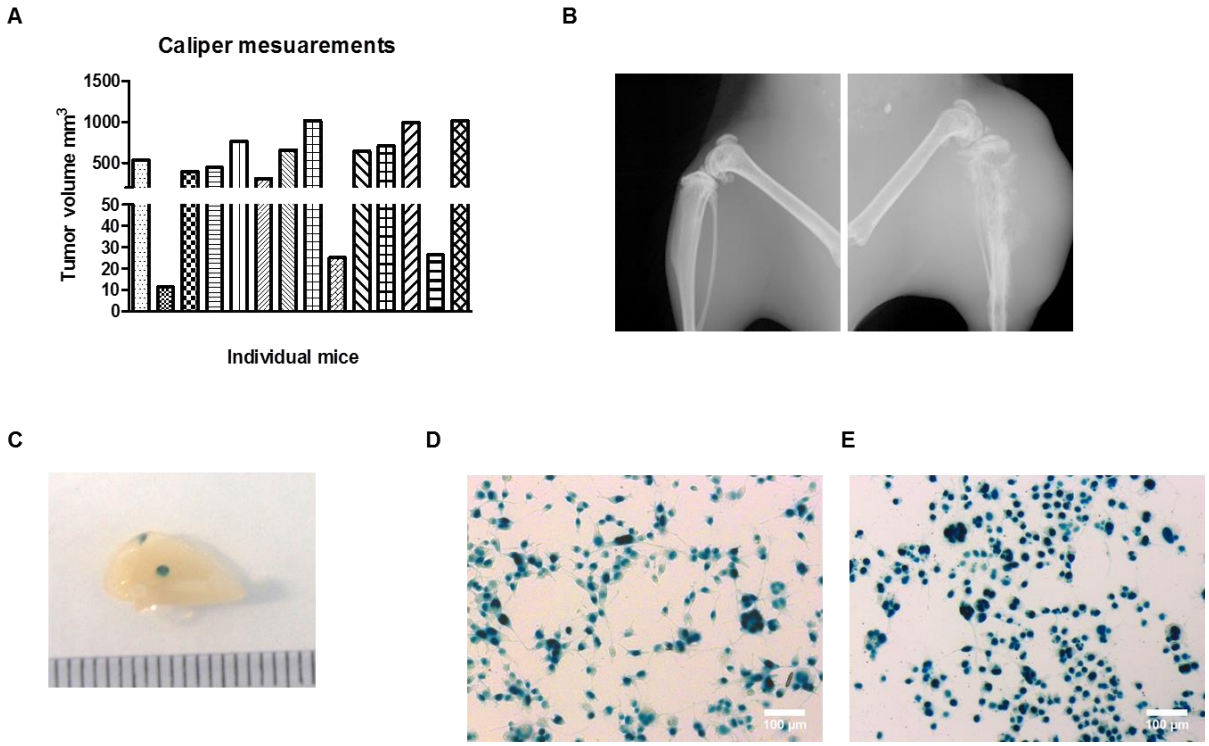

Figure 11. The first round of *in vivo* selection and isolation K7M2 *lacZ* T1 and K7M2 *lacZ* L1 cell lines. *(A)* The bars represent terminate tumor volumes in individual mice injected with $3*10^5$ K7M2 *lacZ* T cells. *(B)* Representative X-ray images of control (left) and tumor-bearing leg (right) of a mouse injected with K7M2 *lacZ* T cells. *(C)* X-gal stained lung macrometastatic nodules (stained in indigo-blue) of a mouse injected with K7M2 *lacZ* T cells. *(D) In vitro* X-gal staining of *lacZ* positive cells (in indigo-blue color) derived from primary tumor and (E) metastatic sites.

C57BL/6J mice were injected with $5*10^5$ MOS-J *lacZ* primary tumor (MOS-J *lacZ* T) and metastasis-derived cells (MOS-J *lacZ* L). To our surprise, none of the mice injected with MOS-J *lacZ* T cells developed primary tumors 90 days after TCI. However, eight out 16 mice injected with MOS-J *lacZ* L cells developed primary tumors larger than 50 mm^3 (Figure 12 A). The first tumors were detectable at day 49 post TCI and at day 90 tumors were prominent and appeared radiologically as "sunburst" (Figure 12 B). We could not visualize any lung

metastasis with *ex vivo* X-gal staining. The cell line isolated from the primary tumors was called MOS-J *lacZ* T1 (Figure 12 C). Notably, whereas maintaining antibiotic resistance properties, some MOS-J T1 lost their *lacZ* gene expression.

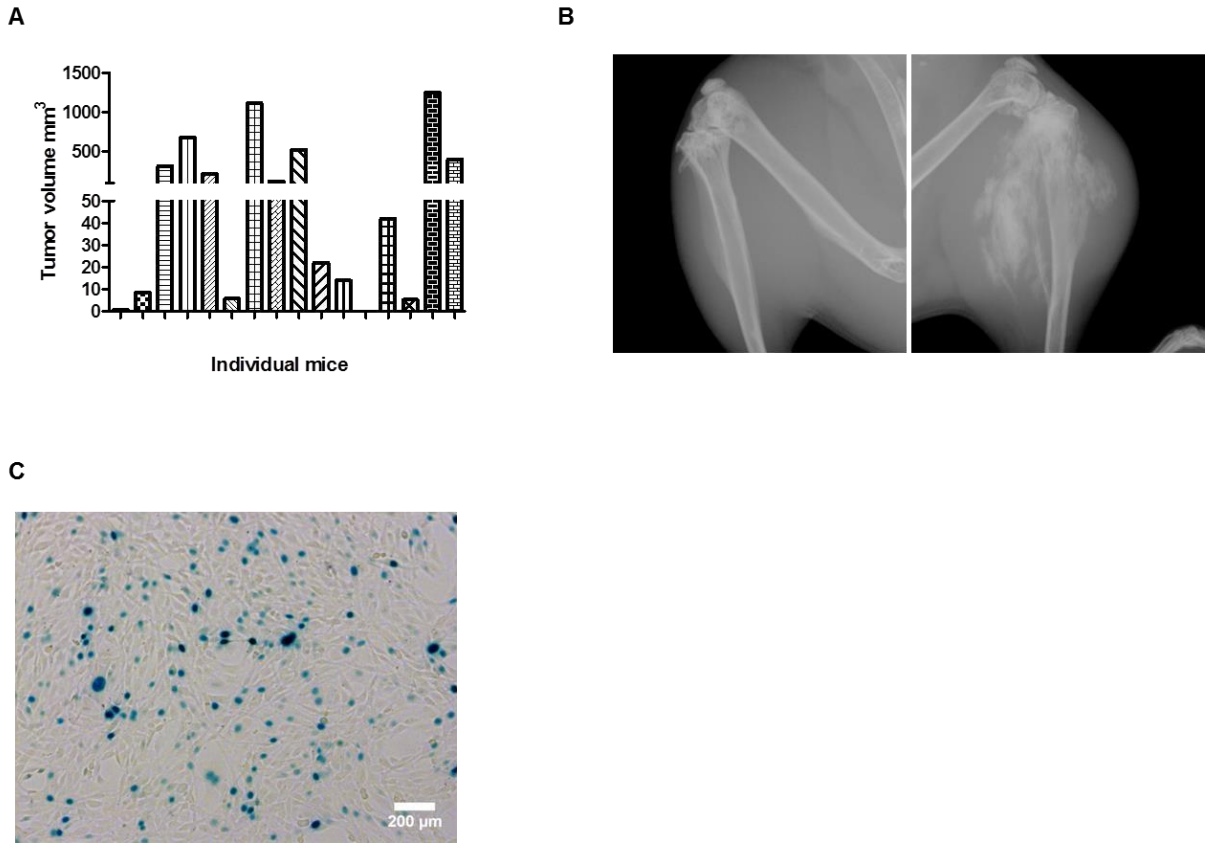

Figure 12. The first round of *in vivo* selection and isolation MOS-J *lacZ* T1 cell line. *(A)* The bars represent terminate tumor volumes in individual mice injected with $5*10^5$ MOS-J *lacZ* T cells. *(B)* Representative X-ray images of control (left) and tumor-bearing leg (right) of a mouse injected with MOS-J *lacZ* T cells. *(C) In vitro* X-gal staining of *lacZ* positive cells (in indigo-blue color) derived from primary tumor site.

In the second round of *in vivo* selection, cells isolated from the primary tumors and lung metastasis of BALB/c mice, K7M2 *lacZ* T1 and K7M2 *lacZ* L1 cell lines, respectively, were orthotopically reinjected into the syngeneic host, giving rise to K7M2 *lacZ* T2 and K7M2 *lacZ* L2 cell lines, respectively. Cell isolated from the primary tumor of C57BL/6J mice, MOS-J *lacZ* T1, were also orthotopically reinjected in the syngeneic host.

The results of the second round of *in vivo* selection revealed that K7M2 *lacZ* L1 cells grew rapidly and the time until the first tumor detection was 21 days. Incidence of tumor development was high and comparable to K7M2 *lacZ* T cells (75% vs 78.5%). However, tumor growth of K7M2 *lacZ* T1 cells was slow and the first tumors were detected only on day 41 post TCI. Only 1 out of 8 mice developed a primary tumor which was larger than 50 mm^3 (Figure 13 A and B). MOS-J *lacZ* T1 tumor growth was rapid and the first primary tumors could be detected already after 28 days compared to the previous round of MOS-J *lacZ* T cell injection, when the tumors were detectable only on the day 49. More than 50% of the mice developed tumors larger than 50 mm^3 (Figure 13 C).

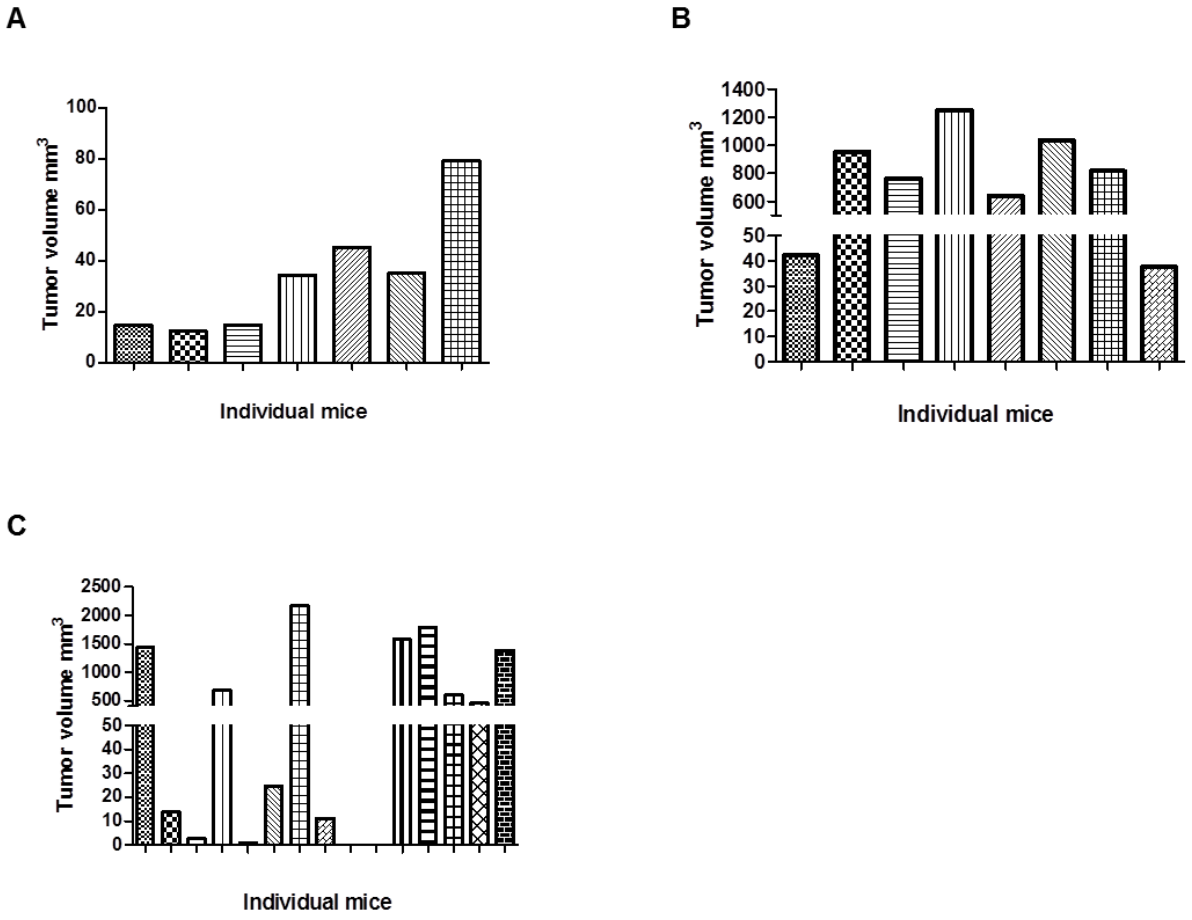

Figure 13. The second round of *in vivo* selection. *(A)* The bars represent terminate tumor volumes in individual mice injected with $3*10^5$ K7M2 *lacZ* T1 cells, *(B)* K7M2 *lacZ* L1 cells, and *(C)* with $5*10^5$ MOS-J *lacZ* T1 cells.

Ex vivo X-gal staining showed metastasis to the lung of mice injected with K7M2 *lacZ* T1, K7M2 *lacZ* L1 and MOS-J *lacZ* T1 cells (Figure 14). Interestingly, K7M2 *lacZ* L1 cells had remarkably higher metastatic potential compared to the clonally related K7M2 *lacZ* T1 cell line, supporting the theory that only a small population of cells within the primary tumor can establish distant metastasis.

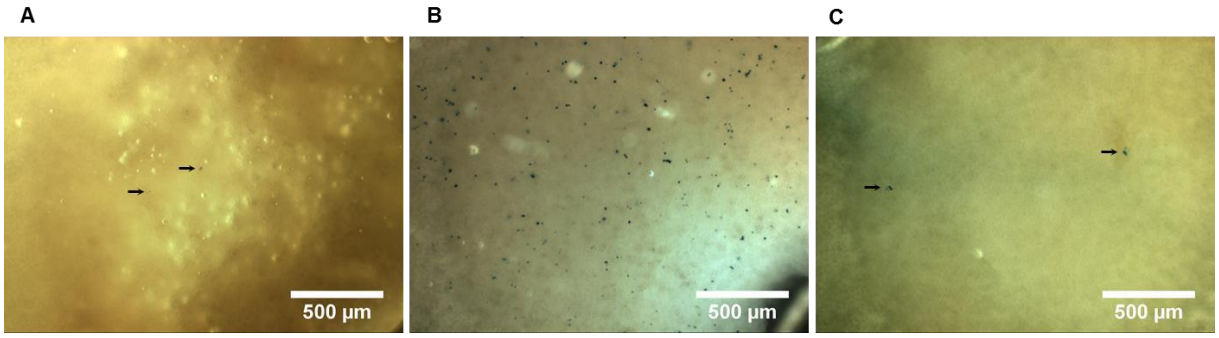

Figure 14. X-gal stained lung metastatic nodules (stained in indigo-blue) of a mouse injected with *(A)* K7M2 *lacZ* T1 cells, *(B)* K7M2 *lacZ* L1 cells, and *(C)* with MOS-J *lacZ* T1 cells. Arrows point at soma metastatic nodules as an example.

In the third round of *in vivo* selection we could significantly improve the speed of tumor growth for K7M2 *lacZ* cell lines. The first K7M2 *lacZ* T2 tumors were detected after 27 days (vs 41 days of K7M2 *lacZ* T1), and the first K7M2 *lacZ* L2 tumors were detected after 14 days (vs 21 days of K7M2 *lacZ* L1). Time until the first tumors were detected in both MOS-J *lacZ* T2 and MOS-J *lacZ* L2 models was the same as that for MOS-J *lacZ* T1 (28 days). 62.5% of mice injected with K7M2 *lacZ* T2 and 87.5% of mice injected with K7M2 *lacZ* L2 cells developed primary tumors larger than 50 mm^3 (Figure 15 A and B). All mice injected with MOS-J *lacZ* T2 and MOS-J *lacZ* L2 cells developed primary tumors larger than 50 mm^3 (Figure 15 C and D).

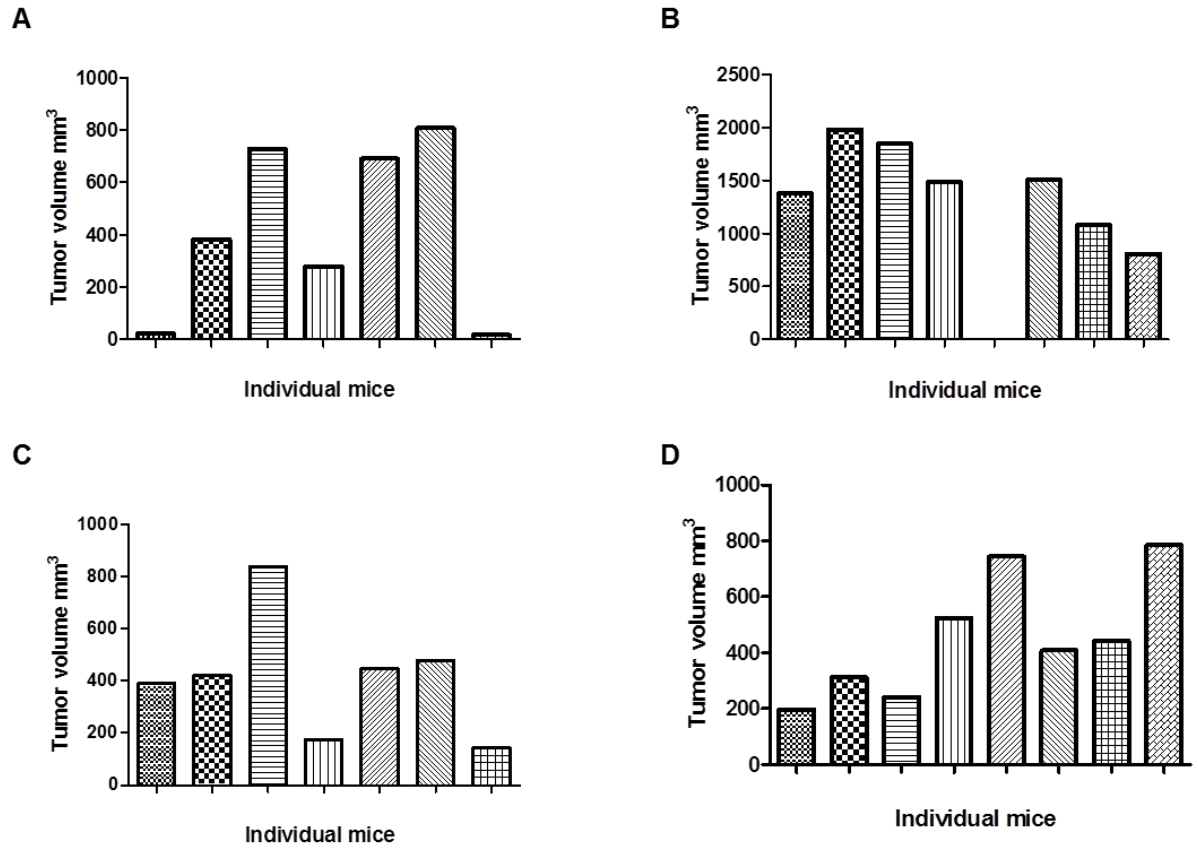

Figure 15. The third round of *in vivo* selection. *(A)* The bars represent terminate tumor volumes in individual mice injected with $3*10^5$ K7M2 *lacZ* T2 cells, *(B)* K7M2 *lacZ* L2 cells, *(C)* with $5*10^5$ MOS-J *lacZ* T2 cells, and *(D)* MOS-J *lacZ* L2 cells.

Metastatic nodules were detected in lungs of mice bearing K7M2 *lacZ* T2, K7M2 *lacZ* L2, MOS-J *lacZ* T2 and MOS-J *lacZ* L2 tumors (Figure 16). However metastatic potential of K7M2 *lacZ* L2 cell line was higher when compared to K7M2 *lacZ* T2 cell line.

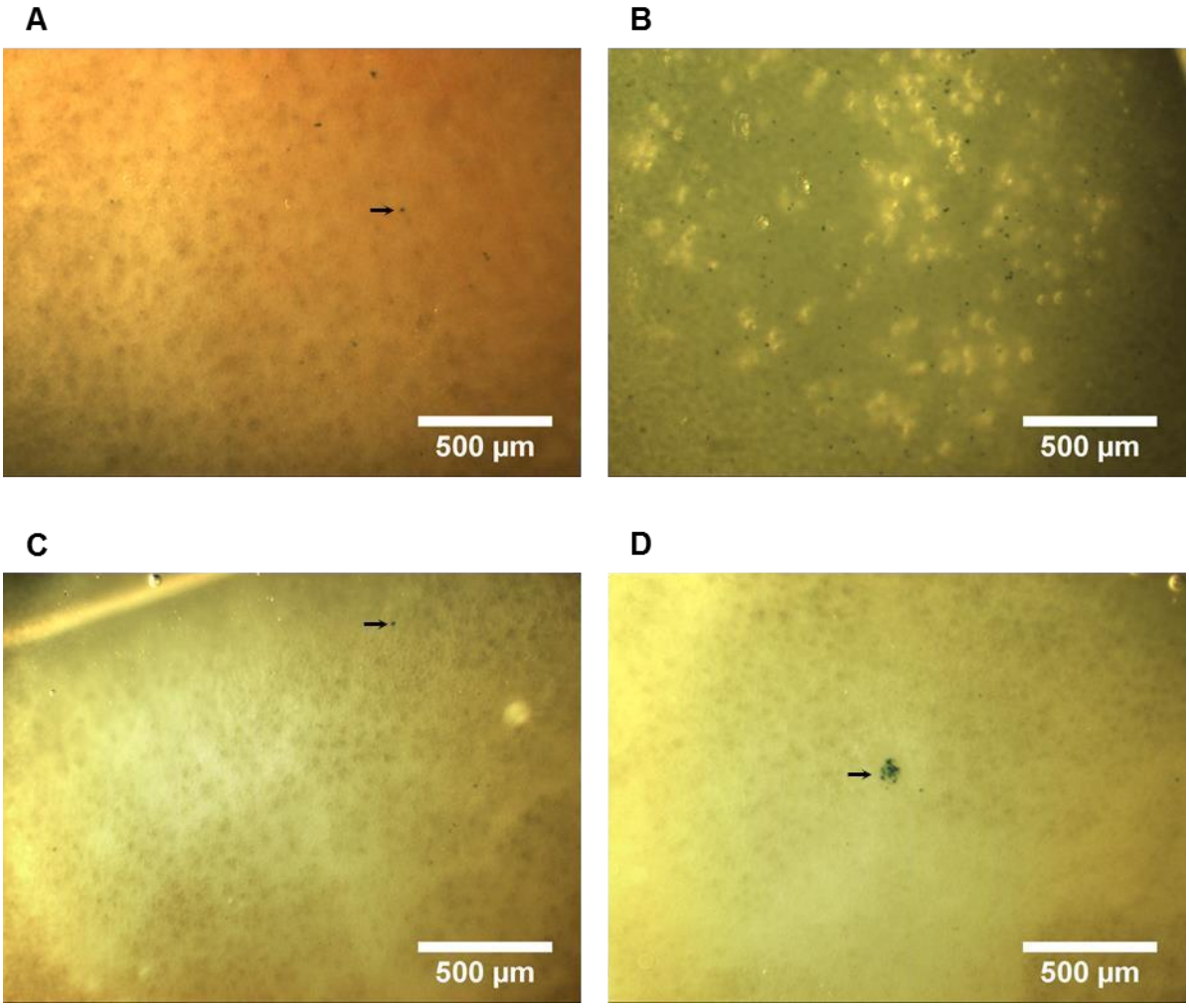

Figure 16. X-gal stained lung metastatic nodules (stained in indigo-blue) of a mouse injected with K7M2 *lacZ* T2 cells, *(B)* K7M2 *lacZ* L2 cells, *(C)* with MOS-J *lacZ* T2 cells, and *(D)* MOS-J *lacZ* L2 cells. Arrows point at some metastatic nodules as an example.

Following the third round of *in vivo* selection K7M2 *lacZ* T3, K7M2 *lacZ* L3, MOS-J *lacZ* T3, and MOS-J *lacZ* L3 cells were isolated and checked for expression of the *lacZ* gene by *in vitro* X-gal staining (Figure 17).

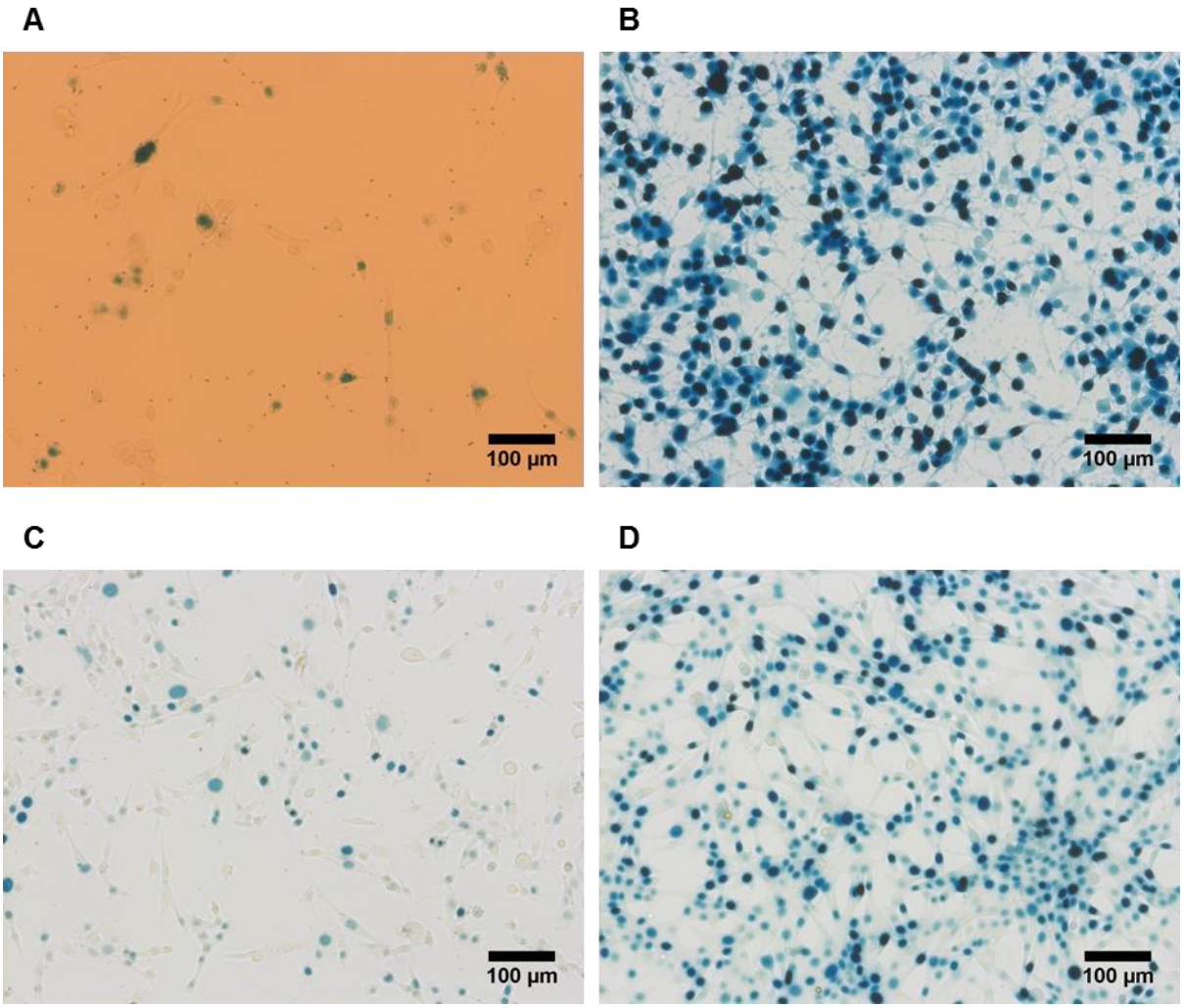

Figure 17. *In vitro* X-gal staining of *lacZ* positive cells (in indigo-blue color) derived from (A) primary tumor and (B) metastatic sites of mice injected with K7M2 *lacZ* T2 and K7M2 *lacZ* L2, respectively. The newly derived cell lines were called K7M2 *lacZ* T3 and K7M2 *lacZ* L3, respectively. (C) X-gal stained MOS-J *lacZ* T3 and (D) MOS-J *lacZ* L3 cells derived from primary tumors and lung metastasis of mice injected with MOS-J *lacZ* T2 and MOS-J *lacZ* L2 cell lines, respectively.

Results of the three *in vivo* selection round for K7M2 *lacZ* and MOS-J *lacZ* cells lines are summarized in the Table 1.

Table 1. Summary of the *in vivo* selection of K7M2 *lacZ* (A) and MOS-J *lacZ* (B) cell lines: from the first, the second and the third rounds. A.

Injected cell line	**Time until the first primary tumor detection**	**% of primary tumors larger than 50 mm^3**	***Ex vivo* X-gal visualized metastatic nodules**	**Isolated cell lines**
K7M2 *lacZ* T	14 days	78.5	yes	K7M2 *lacZ* T1 K7M2 *lacZ* L1
K7M2 *lacZ* T1	41 days	12.5	yes	K7M2 *lacZ* T2
K7M2 *lacZ* T2	27 days	62.5	yes	K7M2 *lacZ* T3
K7M2 *lacZ* L1	21 days	75	yes	K7M2 *lacZ* L2
K7M2 *lacZ* L2	14 days	87.5	yes	K7M2 *lacZ* L3

B.

Injected cell line	**Time until the first primary tumor detection**	**% of primary tumors larger than 50 mm^3**	***Ex vivo* X-gal visualized metastatic nodules**	**Isolated cell lines**
MOS-J *lacZ* T	N/A	N/A	N/A	N/A
MOS-J *lacZ* L	49 days	50	no	MOS-J *lacZ* T1
MOS-J *lacZ* T1	28 days	53.3	yes	MOS-J *lacZ* T2 MOS-J *lacZ* L2
MOS-J *lacZ* T2	28 days	100	yes	MOS-J *lacZ* T3
MOS-J *lacZ* L2	28 days	100	yes	MOS-J *lacZ* L3

In the here presented study, we characterized K12 *lacZ*, K7M2 *lacZ*, and MOS-J *lacZ* OS mouse models *in vivo* and performed three rounds of the *in vivo* selection for K7M2 *lacZ* and MOS-J *lacZ* cell lines according to the Fidler method. For improved metastasis visualization, we employed our *lacZ* gene system that allows for the detection of metastasis with a higher efficacy than before on the level down to a single cell.

Through the three rounds of the selection we could increase tumorigenic and metastatic potential of K7M2 *lacZ* and MOS-J *lacZ* cell lines. More than 60% and more than 80% of mice injected with K7M2 *lacZ* T2 and K7M2 *lacZ* L2 cell lines developed large primary tumors. It is worth mentioning that in our K7M2 *lacZ* mouse model, a mouse leg amputation was not necessary and lung metastasis could be detected through *ex vivo* X-gal staining.

All of the mice injected with MOS-J *lacZ* T2 and MOS-J *lacZ* L2 cells developed large primary tumors. Importantly, although MOS-J cells were originally shown to be nonmetastatic, we could detect metastasis to the lung and isolated metastatic cells.

10. Discussion

Please find a detailed discussion of the study **"Altered CXCL12 expression reveals a dual role of CXCR4 in OS tumor growth and metastasis"** in the enclosed manuscript (paragraph 9.1). A summary of the major findings of this study is included in the section Conclusion/Synthesis of the Discussion chapter.

The study **"Pulmonary administration of an SDF-1 neutralizing ligand for targeted treatment of lung metastasis in an intratibial metastasizing OS mouse model: a pilot study"** is not yet completed and therefore no conclusions can be drawn at the moment. However, the results of the pilot study and the perspectives of future investigations are discussed in the subchapter Outlook/Future direction.

Here I focus on the results obtained from the additional studies **"*In vivo* characterization of K12 *lacZ*, K7M2 *lacZ*, and MOS-J *lacZ* OS models"** and **"Establishment of highly metastatic mouse K7M2 *lacZ* and MOS-J *lacZ* OS models"**.

10.1 *In vivo* characterization of K12 *lacZ*, K7M2 *lacZ*, and MOS-J *lacZ* OS models and Establishment of highly metastatic mouse K7M2 *lacZ* and MOS-J *lacZ* OS models

Several OS mouse models have been described however, none of them fulfills all the requirements of an ideal OS model that would recapitulate all the aspects of the human disease. For our study, we selected the two mouse OS cell lines K7M2 and MOS-J, which, in mice, develop histologically different tumors. The K12 OS cell line was excluded from the study, since in our experiments, these cells exhibited a very low tumorigenic potential.

A particular advantage of MOS-J and K7M2 cells over other established mouse OS cell lines, for example LM8, is their ability to metastasize to the lungs, a predominant metastatic site in human OS, without affecting other tissues. They therefore provide a better model than the LM8 cell line for recapitulating human metastatic OS. Although the mouse OS MOS-J cell line was previously shown to be non-metastatic (Joliat, Umeda et al. 2002), we were able to detect micro- and macrometastases to the lung, but did not find, by X-gal staining, *lacZ* gene expressing tumor cells in other tissues.

Following three rounds of *in vivo* selection according to the Fidler method (Fidler 1990), we were able to remarkably increase the tumorigenic and metastatic potential of the two mouse OS cell lines. Importantly, unlike the orthotopic implantation of K7M2-derived primary tumors in mice, which led to rapid tumor growth prior to the development of lung metastasis (Khanna, Prehn et al. 2000), the here performed orthotopic injection of a K7M2 *lacZ* cell suspension slowed down intratibial tumor growth considerably and therefore allowed to study lung metastasis without amputation of the primary tumor bearing leg.

Interestingly, our results showed that the selection for highly metastatic cells also enhanced tumorigenic properties of these cells. An analysis of gene expression by RNA sequencing or

microarray in K7M2 and MOS-J cell lines obtained in different rounds of *in vivo* selection for higher malignancy may shed light on genes involved in acceleration of OS tumorigenesis as well as identification of new metastatic signature genes in two different histological types of OS. Moreover, MOS-J OS cell line provides a unique opportunity to study roles of single host genes in the pathogenesis of OS by using syngeneic C57BL/6J knockout mice with corresponding defective genes.

Both, the K7M2 and MOS-J cell lines, perfectly reproduce lung metastasis seen in OS patients. The metastatic properties of the K7M2 and MOS-J cell lines need to be further improved through additional rounds of *in vivo* selection in order to also achieve the development of macrometastasis. This will allow the identification and study of genes (metastatic virulence genes) and cellular processes in later steps of the development of lung macrometastasis.

10.2 Conclusions/Synthesis

In more than 90% of cancer patients, metastatic disease is the ultimate cause of death (Christofori 2006; Gupta and Massague 2006; Valastyan and Weinberg 2011). This also applies to OS patients with metastatic disease (Meyers, Heller et al. 1993; Marina, Gebhardt et al. 2004).

Although, SDF-1/CXCR4 signaling was shown to be associated with metastasis promoting mechanisms in more than 23 different cancer types (Chatterjee, Behnam Azad et al. 2014), its role in pathophysiological mechanisms of OS lung metastasis remains poorly defined, mainly due to the fact that OS is a rare disease, which limits the number of studies needed for faster progress. However, authors of a few studies found elevated levels of CXCR4 expression at lung metastatic sites compared to those detected in primary tumor tissue collected from OS patients. Based on these findings, they concluded that SDF-1/CXCR4 signaling might have a crucial function in OS metastasis (Oda, Yamamoto et al. 2006; Namlos, Kresse et al. 2012).

This conclusion was supported by findings of Lin et al, who reported that OS patients with detectable CXCR4 immunostaining in their primary tumor tissue more likely developed recurrent lung metastasis and, consequently, died more rapidly than patients with nondetectable CXCR4 in their primary tumor (Lin, Zheng et al. 2011). Although, Laverdiere et al. did not find any significant correlation between CXCR4 expression in OS primary tumor and metastatic sites, they also were able to show that the expression of CXCR4 in primary OS tumor patient samples inversely correlated with lung metastasis and patient survival (Laverdiere, Hoang et al. 2005). Meanwhile, other groups reported no correlation between CXCR4 expression and the development of lung metastasis (Ma, Zhou et al. 2012) or patient survival in OS (Baumhoer, Smida et al. 2012).

Although, it is generally accepted that SDF-1/CXCR4 signaling is involved in cancer cell homing to metastatic sites, thereby contributing to site-specific metastasis, we showed in the studies of this thesis that SDF-1/CXCR4 signaling might indeed have different roles at the primary tumor site and in lung metastasis.

For our *in vivo* study we used an orthotopic (intratibial) xenograft OS mouse model. About 50% of all OSs in humans occur around the knee (Marina, Gebhardt et al. 2004; Klein and Siegal 2006). Unlike subcutaneous OS mouse models, our intratibial model well represents the location of human OS primary tumor and represents the microenvironment in which OS occurs and develops, mimicking the interaction between the tumor and stromal cells. Moreover, our model allows the development of lung-specific spontaneous metastasis, again well representing the clinical situation. In addition, we tagged our 143-B OS cell line derivatives with the *lacZ* gene, which enabled us to visualize not only macro-, but also micrometastasis in the affected tissue on the level down to a single cell, which would not be possible to do with untagged cells. It is important to be able to assess micro-metastases as most of all OS patients eventually develop metastasis, indicating that those patients had undetectable micro-metastases (Marina, Gebhardt et al. 2004).

Our results showed that stable expression of P2G and SDF-1-KDEL in OS cells led to the formation of significantly larger primary tumors, but a lower number of lung metastases than found in animals with tumors grown from 143-B EV cells. On the contrary, stable expression of SDF-1 in OS cells did not affect primary tumor growth, but remarkably enhanced metastatic potential of 143-B OS cells. The size of primary tumors was found to significantly correlate with the number of cells in the tumor expressing CXCR4 at the cell surface as revealed by flow cytometry. These results are consistent with those of a previous report of Miura et al. demonstrating a direct correlation between the level of CXCR4 expression in OS cells and their ability to form primary tumors (Miura, Uniyal et al. 2005).

Giving the fact that the SDF-1/CXCR4 axis was reported to be involved in homing of metastatic cells from primary tumors to organs of the secondary lesion in different tumor types, our observations indicating that P2G and SDF-1-KDEL expressing tumors which contained higher percentage of CXCR4 positive cells, showed a significantly lower metastatic potential compared to EV control cells, were rather unexpected. Apparently, the here observed behavior of intratibially injected 143-B OS cells is more closely related to the homing and retention of hematopoietic stem and progenitor cells within the bone marrow than to the metastatic behavior of CXCR4 expressing tumor cells of epithelial origin, for example breast cancer cells. Unlike breast cancer, OS arises in the bone, where SDF-1 is abundantly expressed by bone marrow. Thus, whereas CXCR4 expressing breast cancer cells migrate towards a concentration gradient of SDF-1 in the lungs and the bone (Hung, Su et al. 2014; Masuda, Endo et al. 2015; Xu, Zhao et al. 2015), OS cells are located close to bone marrow, where SDF-1 is produced by marrow cells (Tashiro, Tada et al. 1993). Thus, we conclude that bone marrow derived SDF-1 detains CXCR4 expressing 143-B OS cells from systemic spread and consequently from the development of distant metastases. This explains the observed

larger volume of tumors derived from CXCR4 expressing OS cells and the lower number of metastases that these cells form when compared to cells with low CXCR4 expression.

However, it needs further verification whether the conclusions in this study can be applied to all histologically defined OS subtypes in patients. One has to consider that, in our animal model, OS were been injected directly into the medullar cavity of mouse tibiae, where they were allowed to grow and develop tumors in close proximity to the bone marrow that constitutively expresses SDF-1. In patients, however, 3-6% of all OSs arise in the periphery of a bone with minimum or no involvement of the medullary cavity (Klein and Siegal 2006; Kumar, Barwar et al. 2014)(Klein and Siegal 2006; Kumar, Barwar et al. 2014). In case of OSs at the bone surface and outside of the bone cortex, CXCR4 expressing cells might not be retained within primary tumors by bone marrow-derived SDF-1. Therefore, our findings might not apply to this particular type of OS, and the role of the SDF-1/CXCR4 axis in the metastatic process of surface OS awaits further investigation.

Interestingly, SDF-1 expressing 143-B OS cells exhibited significantly higher metastatic potential compared to control EV-transduced cells. The ability of SDF-1 to facilitate additional steps in the metastatic process may account for these observations. For example, SDF-1-mediated platelet aggregation (Abi-Younes, Sauty et al. 2000) may support and thereby enhance the survival of circulating cells and improve their chances to establish distant metastases (Valastyan and Weinberg 2011). In comparison to our results, Williams et al. reported that SDF-1 overexpression in breast cancer cells led to the inhibition of primary tumor development and a reduction in the number of lung metastases in mice (Williams, Harata-Lee et al. 2010). However, these observations were ascribed to the tumor-suppressor effect of the immune system. Taken together, these results indicate that mechanisms by which SDF-1 regulates metastasis might depend on the tumor type and immune system. Later, Baumhoer et al. reported that SDF-1 expression correlates with an increased 10-years survival

rate and lower prevalence of metastasis in OS patients (Baumhoer, Smida et al. 2012). These results contrast with our findings. However, OS tumors are rich in stromal cells which can be an additional source for SDF-1. Furthermore, it has not been investigated whether SDF-1 induces the recruitment of cytotoxic immune cells to primary tumors and thereby promoted anti-tumor immune response. Therefore, it cannot be excluded that SDF-1 had an effect on the host rather than on the tumor itself.

Another important result of our study was the observation that CXCR4 was found significantly enriched in OS cells infiltrating the lung (ranging between 78.0 ± 9.7 and 91.0 ± 1.7 % of CXCR4 expressing cells) compared to the primary tumor cells. This finding is in perfect agreement with observations made by Oda et al. and Namlos et al., who demonstrated that CXCR4 expression in lung metastases was remarkably higher than that found in primary tumors of OS patients (Oda, Yamamoto et al. 2006; Namlos, Kresse et al. 2012). The higher percentage of CXCR4 expressing cells in metastases on our mouse model was likely not the result of a selection of cells derived from a small subpopulation of CXCR4 expressing primary tumor cells, since P2G- and SDF-1-KDEL-expressing tumors that contained significantly higher numbers of CXCR4-expressing cells, formed remarkably lower numbers of lung metastases than tumors developing from 143-B EV and - SDF-1 cells, in which the number of CXCR4 expressing cells was low. Therefore, we suggest that in our study lung infiltrating cells upregulated the expression of CXCR4. A similar observation was made by Zeelenberg et al., who showed that intravenous injection of CXCR4 negative colon carcinoma cells in mice resulted in the formation of lung metastases with a strongly upregulated expression of CXCR4 shown by flow cytometry. This indicated de novo expression of CXCR4 in cells of lung metastases (Zeelenberg, Ruuls-Van Stalle et al. 2003). Apparently, in the here investigated intratibial OS mouse model, lung infiltrating OS cells adapted to the new lung microenvironment by fine-tuning of gene expression resulting in an upregulation of CXCR4, which promoted survival and inhibited apoptosis that likely contributes to an early

loss of metastatic cells in a distant organ (Chambers, Groom et al. 2002)(Chambers, Groom et al. 2002). This upregulation of CXCR4 expression is likely triggered by lung tissue-derived factors. It has previously been shown that the lung tissue microenvironment influences gene expression in metastasizing cells of different tumor models in a paracrine manner (Fidler 2002; Bertolini, D'Amico et al. 2015).

In summary, our results suggest that CXCR4 plays a dual role in OS progression and the regulation of metastasis. When expressed by OS cells within a primary tumor site, CXCR4 may act as a tumor-promoting and metastasis-suppressor gene by decreasing tumor cell shedding. By definition, metastasis-suppressor genes inhibit metastasis without compromising primary tumor growth (Stafford, Vaidya et al. 2008). CXCR4 would comply with this definition in the case of our OS mouse model. When expressed by lung infiltrating cells, CXCR4 likely supports OS metastatic disease. However, the role of CXCR4 in established OS metastases needs to be further investigated. Interestingly, it has previously been reported that CXCR7 might also promote tumor growth, but suppress lung metastases in a breast cancer mouse model (Hernandez, Magalhaes et al. 2011).

The results of our study confirm a pathophysiological role of CXCR4 in OS metastasis and provide new insights into the process by which the SDF-1/CXCR4 axis regulates OS metastasis. The present report extends previous findings of OS metastasis inhibition by systemic administration of anti-CXCR4 agents, and gives a rational for the development of future new therapeutic strategies aiming at local inhibition of the interaction of SDF-1 with CXCR4 in tumor cells in the lung, which might potentially be more efficient than systemic treatment in targeting OS metastatic spread.

11. Outlook/Future directions

The identification of CXCR4 as an important prognostic biomarker of tumor progression in different types of cancer made it an attractive target for the development of new therapeutic strategies and pharmaceutical agents. Recent advances in preclinical research emphasizing the utility of CXCR4 antagonists as anti-cancer drugs led to initiation of several clinical trials. For example, BMS-936564, an anti-CXCR4 agent, is currently being tested in a phase I clinical trials in relapsed or refractory multiple myeloma as monotherapy or in a combination with Lenalidomide/Dexamethasone or Bortezomib/Dexamethasone (NCT01359657, as listed on https://clinicaltrials.gov). However, as of today, only one CXCR4 antagonist, plerixafor, also known as AMD3100, has been approved by FDA as a mobilizer of hematopoietic stem cells from bone marrow for patients with non-Hodgkin's lymphoma and multiple myeloma (Steinberg and Silva 2010). Another drug, Zydelig, shown to block CXCR4 signaling via inhibition of PI3K, has recently been approved by FDA for the treatment of relapsed chronic lymphoblastic leukemia, in a combination with rituximab (Shah and Mangaonkar 2015). For the treatment of OS no anti-CXCR4 agents have been approved by the FDA. Although, FDA, in July 2005, assigned an orphan drug status to CTCE9908, a peptide analogue of SDF-1, for the treatment of OS, there is no further information available on advanced clinical trials (Zhao, Guo et al. 2015).

An ideal anti-cancer agent should fulfill several criteria. It should be effective in eliminating the disease or improving the survival and/or quality of life of cancer patients, cause minimal side effects, and be easily applicable. Although, chalcone-4 and CN-chalcone-4, recently identified as neutralizing ligands for SDF-1, have not been used so far for anti-cancer therapy, they were shown to effectively reduce the number of CXCR4-expressing macrophages recruited to the lungs in an experimental allergic asthma mouse model (Daubeuf, Hachet-Haas et al. 2013). By analogy to the effect on inflammatory cells, chalcone-4 and CN-

chaclone-4 would be expected to reduce the number of lung infiltrating tumor cells, which either use the SDF-1/CXCR4 axis to home to the lungs or which need CXCR4 signaling for survival and/or proliferation in the lung tissue microenvironment. Importantly, both chalcone-4 and CN-chalcone-4 were shown to not cause any cytotoxicity and to be safe for local administration in mice. Moreover, CN-chalcone-4 is rapidly degraded in mouse serum and lung homogenates, which makes it a very attractive agent for the development of a local lung anti-metastatic therapy in OS. It is very important to achieve a local effect of CN-chalcone-4 in lung tissue, especially if the drug needs to be administered over a longer period of time. Considering the wide tissue distribution of CXCR4, interfering with SDF-1/CXCR4 interaction in tissues other than the lung might cause undesirable side effects. Moreover, the results of our study indicate that systemic treatment with anti-CXCR4 agents might not be optimal in OS and therefore a local therapy needs to be pursued. A previous study in the laboratory, using the same intratibial OS mouse model as in here, demonstrated that intravenous injections of CXCR4-blocking antibodies significantly reduced both primary tumor burden and the number of lung metastases in treated compared to mock-treated control mice (Brennecke, Arlt et al. 2014). The findings of the present study, however, suggest that the observations of the previous report might be explained through enhanced primary tumor cell shedding triggered by antibody mediated blocking of CXCR4 functions in the primary tumor along with the inhibition of the survival and/or outgrowth of established metastasis in the lung by local inhibition of SDF-1/CXCR4 signaling by the antibodies. Therefore, systemic treatment with anti-CXCR4 agents could potentially lead to shrinkage of the primary tumor, but it could also stimulate tumor cells to leave the primary tumor site and to eventually establish distant metastases. For the development of future treatment regimens, the focus needs to be on local lung metastasis suppressive treatment, since surgical removal of the primary tumor has been proven to be an effective therapeutic strategy in the treatment of OS patients with localized disease.

In our pilot study, we demonstrated that intratracheal intubation in mice is an effective noninvasive method for local administration of drugs to the lungs. Alternatively, the intranasal route of application can be considered. In order to study the biodistribution of the chalcones upon administration through either one of the two routes, the mice were treated with either P-chalcone-4 (a prodrug of chalcone-4) or CN-chalcone-4. Based on the result of this biodistribution study, a proof of concept treatment study may be performed to estimate and compare anti-metastatic effects of the two chalcone derivatives in the orthotopic OS mouse model using the 143-B OS cell line.

Based on the findings of our pilot biodistribution study a treatment study according to the following protocol can be envisaged:

1. Analysis of the biodistribution of the compounds (chalcone-4, CN-chalcone-4 and the degradation products, 3-methoxy-4-(methoxymethyloxy)benzaldehyde and parachlorobenzoylacetonitrile) in lungs, brain, kidneys, and liver by HPLC/massspectrometry
2. Orthotopic injection of 143-B *lacZ* OS cells into the mouse tibiae
3. Daily administration of the chalcones (P-chalcone-4 or CN-chalcone 4) or a vehicle control solution (PBS or hydroxypropyl-β-cyclodextrin, respectively) to the mice (starting with the first day after tumor cell injection)
4. Estimation of potential undesirable side effects (body weight loss, respiratory or cardiovascular abnormalities, liver cell cytotoxicity, kidney damage, mobilization of the hematopoietic cells into the circulation, etc)
5. Assessment of the effect of the chalcones on
    a) primary tumor growth
    b) number of lung macro- and micrometastases
    c) metastasis to other organs rich in SDF-1, such as the bone, lymph nodes, spleen.

12. Materials and Methods

12.1 Cell lines

The human 143-B OS cell line was purchased from the European Collection of Cell Cultures (Salisbury, UK). The mouse K12 and K7M2 OS cell lines were kind gifts of Dr. Chand Khanna (Center for Cancer Research National Institute, Bethesda, MD, USA), and the mouse MOS-J OS cell line was a kind gift of Prof. Schultz (Jackson Laboratory, Bar Harbor, ME 04609, USA).

In order to improve *ex vivo* visualization of metastatic nodules in affected tissues, all the cell lines were equipped with a *lacZ* gene as previously described (Arlt, Banke et al. 2011; Brennecke, Arlt et al. 2013).

143-B *lacZ* cells were retrovirally transduced with genes designed for stable expression of either SDF-1, or SDF-1-P2G, or SDF-1-KDEL. pcDNA3.1-derived plasmids containing sequences encoding SDF-1 and SDF-1-P2G were kind gifts of Prof. Dr. M. Thelen (IRB Bellinzona, Switzerland). The sequences were amplified by PCR for subcloning into the retroviral pMY-IRES-EGFP donor plasmid. The following primers were used: 5'CGC GAA TTC GCC ACC ATG GAC GCC AAG GTC GTC`3 and 5'GAC GAA TTC TCA CTT GTT TAA AGC TTT CTC CAG`3. The PCR products, 5'-EcoRI-SDF-1-EcoRI'3, 5'-EcoRI-P2G-EcoRI'3 or 5'-EcoRI-SDF-1-KDEL-EcoRI3' (a kind gift of Dr. Ueda and Prof. T. Kitamura, University of Tokyo, Japan) were ligated into pMYs-IRES-EGFP, from which EGFP is expressed from an internal ribosome entry site (IRES). Retroviral transduction of 143-B *lacZ* cells with these constructs and with empty pMYs-IRES-EGFP was followed by fluorescent activated cell sorting of EGFP expressing cells, giving rise to the 143-B *lacZ* EV, 143-B *lacZ* SDF-1, 143-B *lacZ* P2G and 143-B *lacZ* SDF-1-KDEL cell lines. Stability of the EGFP expression was regularly controlled under the microscope.

All the cells were cultured in DMEM/F12 medium (a 1:1 mixture of DMEM and Ham's F12 medium) supplemented with 10% FBS (GIBCO, Basel, Switzerland) in a humidified atmosphere of 95% air and 5% CO_2 at 37°C.

12.2 RNA isolation, reverse transcription reaction, semiquantative PCR and real time PCR

Total RNA isolation from the cell lysates or from primary tumor tissue homogenates with an RNA isolation spin technology kit (Qiagen, 19300 Germantown Road Germantown, MD, USA) was followed by reverse transcription reaction. On-column genomic DNA digestion was performed for each sample (Qiagen, USA). RNA concentration and purity were then analyzed by 260/280 nm optical density measurements using the NanoDrop Spectrophotometer (Thermo Scientific, 02451 81 Wyman StreetWaltham, MA USA). For cDNA synthesis, 1 µg of isolated RNA was added to the reverse transcription reaction performed with a High Capacity cDNA Reverse Transcription Kit (Applied Biosystems by Life Technologies, Van Allen Way, Carlsbad, CA 92008, USA).

Gene expression was quantified using the real time PCR SYBR Green method (SYBR Select Master Mix, Applied Biosystems, USA) according to the manufacturer's recommendations. The step One Plus Real-Time PCR system was used. All reactions were run in triplicates and negative controls included (reverse transcription reaction without reverse transcriptase and water control). The results were calculated with the ΔΔCt method (Livak and Schmittgen 2001) and normalized to the expression level of endogenous GAPDH transcripts.

Primers used are presented in the Table 1.

Table 1. Primers used for semi-quantitative and/or real-time PCR

Gene	Forward primer	Reverse primer
SDF-1	5'ATGTGAGAACATGCCTAGATTTACCC'3	5'GCTTCATGGCAAGATTCTGGCTTA'3

SDF-1-KDEL	5’GATCCCAGTGTGGTGGTACGGGAAATC’3	5’GAATCCTTACACCTCGTCCTTCTCGCT’3
CXCR4	5’ACTTGTGGGTGGTTGTGTTCCAGTTTC’3	5’AAGGAGTCGATGCTGATCCCAATGTAGT’3
CXCL14	5’ GTGGACGGGTCCAAATGCAA‘3	5’CTGACCTCGGTACCTGGACAC‘3

12.3 Immunocytochemistry

Cells were grown on a glass microscope cover slip to 70-80% confluency. Cells stained for an intracellular marker were first fixed with 4% formalin in PBS for 20 min at room temperature followed by permeabilization with 0.1% saponin in F12/DMEM/0.1% BSA medium. These two steps were omitted for the staining of molecules at the cell surface. Cells were incubated with the appropriate primary antibody (anti-SDF-1, or 12G5 or UMB-2, please see table 2) for 2 hours and subsequently with the respective secondary antibody coupled with Alexa Fluor 546 (Invitrogen by Life Technologies, USA). Cell nuclei were labelled with DAPI stain. The staining was analysed under Nikon Eclipse E600 microscope (Schipholweg 321 P.O. Box 222 N 1170 AE Badhoevedorp, The Netherlands) with appropriate filter blocks at 20-fold or 40-fold magnification.

12.4 Flow cytometry

The levels of cell surface located and cytoplasmic CXCR4 were estimated by flow cytometry in *in vitro* cultured 143-B cells and in 143-B cells derived from primary tumor tissue or lung. Cells in tissue culture were grown to 50-60%, 70-80% or 95-100% confluency and gently detached in MACS buffer (1xPBS, 0.05% EDTA and 2% FBS). After washing step in MACS buffer, the cells were stained with 12G5 or 6H8 anti-CXCR4 primary antibody (please see table 2) for 30 min. Alternatively, cells selected for immunostaining of intracellular CXCR4, were incubated in fixation/permeabilization solution (BD Biosciences, 1 Becton Drive Franklin Lakes, NJ 07417, USA) before incubation with primary 6H8 CXCR4 antibody (table 2). Immunostaining of all cells was then completed by incubation with mouse Alexa Fluor

647 (Abcam, UK) labelled secondary antibodies in MACS buffer for 20 min. Cells incubated with secondary antibodies alone were used as a negative control in every experiment. Mouse IgG1 antibody was used as an additional control for non-specific 6H8 CXCR4 antibody binding. All incubations were carried out at 4°C. Finally, the cells were filtered with a 20 μm membrane filter and CXCR4 immunostaining was analysed with a BD LRS Fortessa flow cytometer (Fortessa by BD Biosciences, 1 Becton Drive Franklin Lakes, NJ 07417, USA).

The analysis of cell surface CXCR4 expression in 143-B cells isolated from primary tumors and metastasis-bearing lungs started with the digestion of primary tumor and lung tissues in 2 mg/ml collagenase IV solution (Gibco by life Technologies, Van Allen Way, Carlsbad, CA 92008, USA) in TBS (Tris-buffered saline) for 1 hour at room temperature. Next, the cells were resuspended through a 20 G needle, restrained through a 100 μm filter, centrifuged at 1250 rpm for 3 min and washed with MACS buffer. The immunostaining procedures were the same as those described for 143-B cells grown in tissue culture. In addition, samples were incubated with the Fixable Viability Dye eFluor 450 (Affymetrix by eBioscience, 3420 Central Expressway Santa Clara, CA 95051, USA) for 30 min at 4°C in order to exclude dead cells from the analysis. Finally, the cells were fixed with 4% paraformaldehyde in PBS at room temperature and analyzed by flow cytometry with a BD LRS Fortessa instrument (Fortessa by BD Biosciences, USA). EGFP-expressing tumor cells were selected from the analyzed cell population and dead cells were excluded from the analysis. FlowJo 10.0.8 Software (Flowjo LCC, 385 Williamson Way Ashland OR 97520, USA) was used for the data analysis.

Table 2. Antibodies used for the immunocytochemical and flow cytometry analyses.

Antibody	Concentration	Method	Company
goat polyclonal SDF-1	5 μg/ml	Intracellular	R&D Systems, Barton

antibody		ICC	Lane Abingdon Science Park Abingdon, OX14 3NB, UK
mouse anti-CXCR4 clone 12G5	10 µg/ml	cell surface ICC/Flow cytometry	R&D Systems, Barton Lane Abingdon Science Park Abingdon, OX14 3NB, UK
rabbit anti-CXCR4 clone UMB-2	23,4 µg/ml	Intracellular ICC	Abcam, 330 Cambridge Science Park Cambridge CB4 0FL, UK
mouse anti-CXCR4 6H8	0.68 µg/ml	Flow cytometry	kind gift of Prof. Dr. M. Thelen, IRB Bellinzona, Switzerland

12.5 SDF-1 ELISA

The amount of the peptides SDF-1, P2G and SDF-1-KDEL expressed by 143-B cell line derivatives were quantified with an SDF-1 ELISA (SDF-1 ELISA DuoSet® development kit, R&D Systems, USA) in conditioned medium collected at 48 h after cell seeding or in extracts of primary tumours grown from the different cell lines and collected from the mice at sacrifice. Tumour tissue was extracted with 1 ml of ice-cold extraction buffer (Pierce by Thermo Scientific, 02451 81 Wyman Street, Waltham, MA USA) supplemented with a protease inhibitor cocktail (Roche, CH-4070 Basel, Switzerland) and cleared by centrifugation at 10’000 g and 4°C for 5 min. In order to release the analyzed peptides from mucopolysaccharides in cell fragments, tissue sediments were washed once with acidic buffer (Glycine, pH 2). The ELISA plates were coated with biotinylated antibodies to SDF-1 (R&D

Systems, UK) and 100 µl of cell supernatants diluted 1:10, 1:20 and 10:40 in fresh culture medium or 100 µl of tumor extracts diluted 1:2, 1:4 and 1:8 in tissue extraction buffer were applied to individual wells. The ELISA plates were incubated at room temperature for 2 hours. Standard curves were prepared with SDF-1 standard solutions (R&D Systems, UK). All measurements were run in duplicates and repeated three times. The ELISA plates were analyzed with a Microplate Reader (Benchmark by Bio-Rad, 1000 Alfred Nobel Drive Hercules, California 94547, USA) and the amount of peptides released by 10^6 cells into 1 ml of conditioned medium during 48 hours was calculated. Alternatively, the amount of peptides isolated from tumor extracts was normalized to 1 µg of total protein measured with a Bradford assay (BioRad, 1000 Alfred Nobel Drive Hercules, California 94547, USA) according to the manufacturer's instructions.

12.6 SDF-1 chemotaxis assay

SDF-1 dependent chemotaxis of the 143-B OS cell lines was performed in a 48-well transmembrane Boyden Chamber with polyvinylpyrrolidone-free polycarbonate membranes of 8 µm pore size (NeuroProbe, 16008 Industrial Drive Gaithersburg, MD 20877, USA). 143-B cells were grown to 50-60% confluency, gently detached in trypsin-EDTA buffer and resuspended in chemotaxis medium consisting of DMEM/F12 (1:1) supplemented with 0.2% FBS. $2x10^4$ cells resuspended in 50 µl of chemotaxis medium were carefully added to the upper compartment of individual wells, whereas the bottom compartments of the wells were filled with chemotaxis medium containing chemo-attractant SDF-1 at concentrations ranging from 10 nM and 1000 nM. Chemotaxis medium without SDF-1 was used as a control. The cells were allowed to transmigrate for 4 hours under tissue culture conditions at 37°C. Nonmigrated cells on the upper surface of the membrane were carefully removed with a rubber scraper. Migrated cells located on the lower surface of the membrane were fixed and stained with Diff-Quik® (Medion Diagnostics AG, Bonnstrasse, 9, Düdingen Switzerland) and counted under a Nikon Eclipse E600 microscope (Nikon, The Netherlands) at 100-fold

magnification in five randomly selected membrane areas of 0.015 mm^2. The experiment was repeated 3 times.

12.7 Cell proliferation assay

Doubling times of the 143-B cell line derivatives were determined in a cell proliferation assay as previously described (Berndt, Campanile et al. 2013; Gvozdenovic, Arlt et al. 2013). Briefly, $5x10^5$ cells were seeded in 12.5-cm^2 dishes on day 0. The cells were counted with a hemocytometer at 24 hours (day 1), 48 hours (day 2), 72 hours (day 3), and 96 hours (day 3) after seeding. Five flasks were used per each time point and per cell line. The experiment was repeated 3 times. The doubling time was calculated using the following formula: $t_{1/2}=\ln 2/\gamma$, where $t_{1/2}$ is the doubling time and γ is the slope of the linear regression curve.

12.8 Animal experiments

All animal experiments were performed according to the institutional guidelines and approved by the Ethics Committee of the Veterinary Department, Canton of Zurich, Switzerland (Animal application license numbers 129/2009, 169/2009, 41/2013, 42/2013).

Cells were grown to 70-80% subconfluency and then gently detached with Trypsin/PBS/0.05% EDTA and resuspended in PBS/0.05% EDTA. Derivatives of the human 143-B OS cell line were authenticated with polymorphic short tandem repeat loci profiling (Microsynth, Switzerland) less than six months before the animal experiments and correct expression of the constructs was verified by PCR as described in the section “cell lines” of the material and methods.

In each animal experiment mice were randomized in different experimental groups. Ten microliters containing 10^5 (143-B *lacZ* EV/SDF-1/P2G/SDF-1-KDEL, K12 *lacZ*, and K7M2 *lacZ*), or $3*10^5$ (K12 *lacZ* and K7M2 *lacZ*), or $5*10^5$ (MOS-J *lacZ*) cells were injected into the medullar cavity of the left tibia of individual mice.

Tumor growth was monitored once a week by X-ray and caliper measurement. The tumor volume was calculated as the volume difference between tumor-bearing and control leg with the following formula: leg volume = L x W^2 x 0.5; (L length and W width of the leg).

On the day of sacrifice, mouse organs were collected and prepared as reported (Brennecke, Arlt et al. 2014). Metastatic tumor cells were visualized as described previously (Arlt, Banke et al. 2011). Briefly, organs were fixed in 2% formaldehyde solution followed by staining in 5-bromo-4-chloro-3-indolyl-b-D-galactoside (X-Gal) solution at 37 °C for 3 hours. Blue stained metastases on the surface of whole-mounts of mouse lungs were counted under the microscope (Nikon, The Netherlands) at 4X magnification.

For *in vivo* selection of highly metastatic murine OS cell lines, primary tumors or whole mouse lungs were collected at autopsy, carefully minced with scissors and incubated in 2 mg/ml collagenase B (Roche, Switzerland) in TBS at 37°C for one hour with gentle and constant agitation. The cells were then re-suspended through a 20 G needle and seeded into six-well plates and left to adhere overnight in F12/DMEM medium supplemented with 10% FBS and 0.1% Penicillin Streptomycin (Gibco by Life Technologies, USA). When the cells adhered and started growing, 800 mg/ml of neomycin G418 was added to the medium in order to obtain homogenous populations of tumor cells. The cells were allowed to grow to 70-80% of confluency. *LacZ* gene expression was verified by X-gal staining. For the staining the cells were washed in PBS three times and incubated in 2%-formaldehyde solution for 5 min. Next, the cells were washed again and incubated in X-gal solution for one hour at 37°C. Images of *lacZ* expressing cells were taken with a camera attached to a Nikon Eclipse E600 microscope (Nikon, The Netherlands). Living tumor cells selected for further analyses were collected, frozen and stored in liquid nitrogen.

In order to estimate the efficiency of intranasal and intratracheal ways of lung-specific drug administration and to compare these two techniques, mice were treated with 0.5% Evans blue solution (Sigma-Aldrich, USA). For intranasal drug application, a mouse was anesthetized with 112.5 mg/kg Ketamin, 16.5 mg/kg Xylazin and 15 mg/kg Acepromazin in PBS, applied by i.p. injection, and carefully hold in a hand with its head up. Drops of either 12.5 µl or 25 µl of Evans blue solution were applied on a mouse nostril. After approximately 5 min when the first drop was inhaled, a second drop of the same volume was applied on the second nostril of the mouse. In total, 25 µl or 50 µl of Evans blue solution were administrated in mice intranasally. We performed intratracheal intubation by using a special MicroSprayer® Aerosolise specially designed for mice (Penn-Century, Inc. 7670 Queen Street, Suite 200 Wyndmoor, PA 19038 USA). The mice were first anesthetized with 2% gas isoflorane and placed on their back on a special platform at approximately 45° grade. In order to ensure safe delivery of the solution, we assisted ourselves with a laryngoscope designed for use in mice (Hallowell EMC, 63 Eagle St, Pittsfield, MA, USA). The tip of the MicroSprayer® Aerosolise was carefully placed into the mouse trachea up to the carina, the first tracheal bifurcation, and 25 µl of Evans blue solution was released into the mouse lungs. After the treatment, mice were immediately sacrificed and the distribution of the dye in the lungs was analyzed.

In order to examine the tissue distribution of P-chalcone or CN-chalcone (kind gifts of Prof. J.-L. Galzi, University of Strasbourg, France) upon pulmonary administration, the compounds were administrated at a concentration of 300 µM diluted in PBS/10% 2-hydroxylpropyl-βcyclodextrin (Sigma-Aldrich, USA) solution. Twenty-five µl of P-chalcone or CN-chalcone were applied through the nose or through the trachea as described above. Mouse lungs, liver, kidneys and brain were collected at autopsy, snap frozen in liquid nitrogen and stored at 80°C for further analysis.

12.9 *In vivo* micro-Computed Tomography-derived mouse tibia morphometry

Changes in bone morphology were assessed by micro-computed tomography (μCT) in tumor-bearing and control mouse tibiae during the final stage of tumor development in at least four randomly selected mice per experimental group. The SkyScan 1176 *in vivo* μCT system (SkyScan/Bruker Corporation, 40 Manning Road, Manning Park Billerica, MA 01821, USA) with a digital X-ray camera of 12.63 pixels/μm operating under a 17 mm field of view was used. Mice were anesthetized with 5% isoflurane/oxygen (Forene Isoflurane, AbbVie, North Chicago, IL, USA) and maintained anesthetized during scanning with 2% isoflurane/oxygen using the SP-5002 combined Y-connector and a face mask (Gloor Instruments, Uster, Switzerland) connected to a V3000PK rodent anesthesia machine/isoflurane vaporizer (Parkland Scientific, FL, USA). Mice were placed in supine position in a polystyrene bed extending from the carbon fiber "rat bed" and hind legs were fixated between two pieces of polystyrene foam secured with Micropore paper tape (Provet, Glattbrugg, Switzerland). To prevent cornea from drying out, Coliquifilm eye cream (Allergan, Dublin, Ireland) was applied. During scanning, mice were continuously monitored with a camera system mounted on an in-house developed platform. Scanning was performed in air at 35°C with a working source voltage of 50 kV and a source current of 500 μA. Two measurements per one tomography projection were performed. The exposure time per projection was 80 ms. Each shot required a source rotation step of 0.8°. It allowed sharpness of the final reconstituted model of 35 μm per voxel (isotropic voxel size 35x35x35 μm^3). Approximately 6 min were needed for each scan, and 360° sample rotation was used. An aluminium (Al 0.5 mm) filter was used in order to reduce beam hardening effects.

The data processing started with three-dimensional reconstitution of the acquired images using NRecon software v1.6.8.0 (Skyscan/Bruker Corporation, USA). Beam-hardening correction was set to 20%, smoothing to 2 and ring artifact reduction to 1. The image

conversion value was set to 0.07. Following reconstruction, tumor-bearing hind legs were aligned *in silico* using Data Viewer v1.5.0 (Skyscan/Bruker Corporation, USA). Next, a region of interest (ROI) was determined in the z-stack by manually creating a constant contour that included as starting point the tibial plateau, and as end point the convergence of the fibula with the tibial shaft (CTAn v1.13.11.0 software; Skyscan/Bruker Corporation, USA). Finally, after global segmentation, the bone volume (BV) within the selected ROI was calculated. Three-dimensional images of the mouse tibiae were made using Ctvox v.2.7.0 (Skyscan/Bruker Corporation, USA).

12.10 Histology and immunostainings

Immunohistological stainings were performed as described (Campanile, Arlt et al. 2013). Briefly, tumors were collected at autopsy and fixed in 4% paraformaldehyde PBS solution. Incubation of the fixed tumors in decalcifying agent (Osteosoft, Merck, 2000 Galloping Hill Road Kenilworth NJ, USA) for one week was followed by tumor dehydration. Next tumors were embedded in paraffin and six μm paraffin sections were made. Three randomly selected six μm primary tumor tissue cross-sections per group were stained with hematoxylin and eosin and imaged at 20-fold magnification with a Nikon Eclipse E600 microscope (Nikon, The Netherlands) equipped with a Nikon camera (Kappa Optronics GmbH, Gleichen, Germany). The staining was repeated three times.

At least three cross-sections of primary tumors per group were incubated with either rabbit polyclonal CD31 (Abcam, 330 Cambridge Science Park Cambridge CB4 0FL, UK) or rabbit polyclonal Ki67 (Abcam, UK), or rabbit monoclonal ERG (ETS-related gene) (Abcam, UK) primary antibody overnight at 4°C. CD31 and Ki67 primary antibodies were diluted 1:100 in TBS supplemented with 10% goat serum (Vector Laboratories, 30 Ingold Road Burlingame, CA 94010, USA). ERG antibody was diluted 1:50 in TBS supplemented with 10% goat serum (Vector Laboratories, USA). Immunostainings were visualized either with anti-rabbit 547

fluorescence secondary antibody (Thermo Scientific 02451 81 Wyman StreetWaltham, MA USA) (slides were incubated with the secondary antibody for two hours at room temperature) or with secondary peroxidase-conjugated anti-rabbit antibodies (Vector Laboratories Inc., USA), Vectastain Elite ABC (Vector Laboratories Inc., USA) and a substrate-chromogen system (Dako, DK-2600 Glostrup, Denmark) according to the manufacturer's instructions. Cell nuclei were stained with DAPI. The immunostainings were repeated three times, each time using a different randomly selected primary tumor of each group. Pictures were taken with a Nikon Eclipse E600 microscope (Nikon, The Netherlands) or a Zeiss microscope (Observer Z1, Zeiss Microscopy, Jena, Germany) equipped with correspondent cameras.

Micro-vessel density visualized by CD31- or ERG immunostaining was analyzed for all groups in three randomly selected fields (0.14 mm^2) per slide at 20-fold magnification using three representative slides per group. The micro-vessel density was calculated as the ratio between the area occupied by blood vessels and the total area of viable tissue per slide using a custom-made program (ETH, Zurich) for Image J software (NIH, Bethesda, MD, USA).

Ki67 staining, indicating proliferating cells, was analyzed in at least two randomly selected fields (0.37 mm^2) per slide at 20-fold magnification using three representative slides per group. A Ki67 proliferation index was calculated with Image J software (NIH, USA) as the proportion between the number of Ki67-stained cells and the total number of tumor cells counted in the selected field.

12.11 Data analysis

Obtained data were analyzed with GraphPad PRISM v5.01 software (GraphPad Software, 7825 Fay Avenue, Suite 230. La Jolla, CA 92037 USA). One-way variance analysis was used when variables in three or more groups were analyzed. Two-way analysis of variance was used when analyzing two independent variables. Student's t-test was used when data from two individual groups were compared. Data were correlated by using Pearson correlation. All

experiments were repeated at least three times. The results are presented as mean values ± standard error of the mean (SEM) and considered to be significant when $p<0.05$.

13. References

Abe, P., W. Mueller, et al. (2014). "CXCR7 prevents excessive CXCL12-mediated downregulation of CXCR4 in migrating cortical interneurons." Development **141**(9): 1857-1863.

Abi-Younes, S., A. Sauty, et al. (2000). "The stromal cell-derived factor-1 chemokine is a potent platelet agonist highly expressed in atherosclerotic plaques." Circulation research **86**(2): 131-138.

Adams, D. H. and A. R. Lloyd (1997). "Chemokines: leucocyte recruitment and activation cytokines." Lancet **349**(9050): 490-495.

Aiuti, A., I. J. Webb, et al. (1997). "The chemokine SDF-1 is a chemoattractant for human CD34+ hematopoietic progenitor cells and provides a new mechanism to explain the mobilization of CD34+ progenitors to peripheral blood." The Journal of experimental medicine **185**(1): 111-120.

Amara, A., O. Lorthioir, et al. (1999). "Stromal cell-derived factor-1alpha associates with heparan sulfates through the first beta-strand of the chemokine." The Journal of biological chemistry **274**(34): 23916-23925.

Arlt, M. J., I. J. Banke, et al. (2011). "LacZ transgene expression in the subcutaneous Dunn/LM8 osteosarcoma mouse model allows for the identification of micrometastasis." Journal of orthopaedic research : official publication of the Orthopaedic Research Society **29**(6): 938-946.

Asai, T., T. Ueda, et al. (1998). "Establishment and characterization of a murine osteosarcoma cell line (LM8) with high metastatic potential to the lung." International journal of cancer. Journal international du cancer **76**(3): 418-422.

Bacchetti, S. and F. L. Graham (1977). "Transfer of the gene for thymidine kinase to thymidine kinase-deficient human cells by purified herpes simplex viral DNA." Proceedings of the National Academy of Sciences of the United States of America **74**(4): 1590-1594.

Bachelerie, F., A. Ben-Baruch, et al. (2014). "International Union of Basic and Clinical Pharmacology. [corrected]. LXXXIX. Update on the extended family of chemokine receptors and introducing a new nomenclature for atypical chemokine receptors." Pharmacological reviews **66**(1): 1-79.

Bacon, K., M. Baggiolini, et al. (2002). "Chemokine/chemokine receptor nomenclature." Journal of interferon & cytokine research : the official journal of the International Society for Interferon and Cytokine Research **22**(10): 1067-1068.

Balkwill, F. (1998). "The molecular and cellular biology of the chemokines." Journal of viral hepatitis **5**(1): 1-14.

Balkwill, F. (2003). "Chemokine biology in cancer." Seminars in immunology **15**(1): 49-55.

Balkwill, F. (2004). "The significance of cancer cell expression of the chemokine receptor CXCR4." Semin Cancer Biol **14**(3): 171-179.

Baumhoer, D., J. Smida, et al. (2012). "Strong expression of CXCL12 is associated with a favorable outcome in osteosarcoma." Modern pathology : an official journal of the United States and Canadian Academy of Pathology, Inc **25**(4): 522-528.

Ben-Baruch, A. (2008). "Organ selectivity in metastasis: regulation by chemokines and their receptors." Clinical & experimental metastasis **25**(4): 345-356.

Ben-Baruch, A. (2008). "Organ selectivity in metastasis: regulation by chemokines and their receptors." Clin Exp Metastasis **25**(4): 345-356.

Ben-Baruch, A. (2009). "Site-specific metastasis formation: chemokines as regulators of tumor cell adhesion, motility and invasion." Cell adhesion & migration **3**(4): 328-333.

Berahovich, R. D., Z. Miao, et al. (2005). "Proteolytic activation of alternative CCR1 ligands in inflammation." Journal of immunology **174**(11): 7341-7351.

Bernards, R. and R. A. Weinberg (2002). "A progression puzzle." Nature **418**(6900): 823.

Berndt, K., C. Campanile, et al. (2013). "Evaluation of quercetin as a potential drug in osteosarcoma treatment." Anticancer research **33**(4): 1297-1306.

Berson, J. F., D. Long, et al. (1996). "A seven-transmembrane domain receptor involved in fusion and entry of T-cell-tropic human immunodeficiency virus type 1 strains." Journal of virology **70**(9): 6288-6295.

Bertolini, G., L. D'Amico, et al. (2015). "Microenvironment-Modulated Metastatic CD133+/CXCR4+/EpCAM- Lung Cancer-Initiating Cells Sustain Tumor Dissemination and Correlate with Poor Prognosis." Cancer research **75**(17): 3636-3649.

Bleul, C. C., M. Farzan, et al. (1996). "The lymphocyte chemoattractant SDF-1 is a ligand for LESTR/fusin and blocks HIV-1 entry." Nature **382**(6594): 829-833.

Brennecke, P., M. J. Arlt, et al. (2014). "CXCR4 antibody treatment suppresses metastatic spread to the lung of intratibial human osteosarcoma xenografts in mice." Clin Exp Metastasis **31**(3): 339-349.

Brennecke, P., M. J. Arlt, et al. (2013). "Expression of the chemokine receptor CXCR7 in CXCR4-expressing human 143B osteosarcoma cells enhances lung metastasis of intratibial xenografts in SCID mice." PloS one **8**(9): e74045.

Burger, J. A. and T. J. Kipps (2006). "CXCR4: a key receptor in the crosstalk between tumor cells and their microenvironment." Blood **107**(5): 1761-1767.

Busillo, J. M. and J. L. Benovic (2007). "Regulation of CXCR4 signaling." Biochim Biophys Acta **1768**(4): 952-963.

Bussmann, J. and E. Raz (2015). "Chemokine-guided cell migration and motility in zebrafish development." The EMBO journal **34**(10): 1309-1318.

Campanile, C., M. J. Arlt, et al. (2013). "Characterization of different osteosarcoma phenotypes by PET imaging in preclinical animal models." Journal of nuclear medicine : official publication, Society of Nuclear Medicine **54**(8): 1362-1368.

Chambers, A. F., A. C. Groom, et al. (2002). "Dissemination and growth of cancer cells in metastatic sites." Nature reviews. Cancer **2**(8): 563-572.

Chatterjee, S., B. Behnam Azad, et al. (2014). "The intricate role of CXCR4 in cancer." Advances in cancer research **124**: 31-82.

Chen, Q., Z. Zhou, et al. (2015). "The importance of Src signaling in sarcoma." Oncology letters **10**(1): 17-22.

Chen, W. C., Y. S. Tzeng, et al. (2010). "Lung defects in neonatal and adult stromal-derived factor-1 conditional knockout mice." Cell and tissue research **342**(1): 75-85.

Christofori, G. (2006). "New signals from the invasive front." Nature **441**(7092): 444-450.

Crump, M. P., J. H. Gong, et al. (1997). "Solution structure and basis for functional activity of stromal cell-derived factor-1; dissociation of CXCR4 activation from binding and inhibition of HIV-1." The EMBO journal **16**(23): 6996-7007.

Dar, A., P. Goichberg, et al. (2005). "Chemokine receptor CXCR4-dependent internalization and resecretion of functional chemokine SDF-1 by bone marrow endothelial and stromal cells." Nature immunology **6**(10): 1038-1046.

Darash-Yahana, M., E. Pikarsky, et al. (2004). "Role of high expression levels of CXCR4 in tumor growth, vascularization, and metastasis." FASEB journal : official publication of the Federation of American Societies for Experimental Biology **18**(11): 1240-1242.

Daubeuf, F., M. Hachet-Haas, et al. (2013). "An antedrug of the CXCL12 neutraligand blocks experimental allergic asthma without systemic effect in mice." The Journal of biological chemistry **288**(17): 11865-11876.

Dealwis, C., E. J. Fernandez, et al. (1998). "Crystal structure of chemically synthesized [N33A] stromal cell-derived factor 1alpha, a potent ligand for the HIV-1 "fusin" coreceptor." Proceedings of the National Academy of Sciences of the United States of America **95**(12): 6941-6946.

Debnath, B., S. Xu, et al. (2013). "Small molecule inhibitors of CXCR4." Theranostics **3**(1): 47-75.

Delgado-Martin, C., C. Escribano, et al. (2011). "Chemokine CXCL12 uses CXCR4 and a signaling core formed by bifunctional Akt, extracellular signal-regulated kinase (ERK)1/2, and mammalian target of rapamycin complex 1 (mTORC1) proteins to control chemotaxis and survival simultaneously in mature dendritic cells." The Journal of biological chemistry **286**(43): 37222-37236.

Domanska, U. M., R. C. Kruizinga, et al. (2013). "A review on CXCR4/CXCL12 axis in oncology: no place to hide." Eur J Cancer **49**(1): 219-230.

Dunn, T. B. and H. B. Andervont (1963). "Histology of Some Neoplasms and Non-Neoplastic Lesions Found in Wild Mice Maintained under Laboratory Conditions." Journal of the National Cancer Institute **31**: 873-901.

Fahham, D., I. D. Weiss, et al. (2012). "In vitro and in vivo therapeutic efficacy of CXCR4 antagonist BKT140 against human non-small cell lung cancer." The Journal of thoracic and cardiovascular surgery **144**(5): 1167-1175 e1161.

Federsppiel, B., I. G. Melhado, et al. (1993). "Molecular cloning of the cDNA and chromosomal localization of the gene for a putative seven-transmembrane segment (7-TMS) receptor isolated from human spleen." Genomics **16**(3): 707-712.

Feng, Y., C. C. Broder, et al. (1996). "HIV-1 entry cofactor: functional cDNA cloning of a seven-transmembrane, G protein-coupled receptor." Science **272**(5263): 872-877.

Fidler, I. J. (1990). "Critical factors in the biology of human cancer metastasis: twenty-eighth G.H.A. Clowes memorial award lecture." Cancer research **50**(19): 6130-6138.

Fidler, I. J. (2002). "Critical determinants of metastasis." Seminars in cancer biology **12**(2): 89-96.

Forment, J. V., A. Kaidi, et al. (2012). "Chromothripsis and cancer: causes and consequences of chromosome shattering." Nature reviews. Cancer **12**(10): 663-670.

Fuchs, B. and D. J. Pritchard (2002). "Etiology of osteosarcoma." Clinical orthopaedics and related research(397): 40-52.

Furie, M. B. and G. J. Randolph (1995). "Chemokines and tissue injury." The American journal of pathology **146**(6): 1287-1301.

Garraway, L. A., H. R. Widlund, et al. (2005). "Integrative genomic analyses identify MITF as a lineage survival oncogene amplified in malignant melanoma." Nature **436**(7047): 117-122.

Gasparik, V., F. Daubeuf, et al. (2012). "Prodrugs of a CXC Chemokine-12 (CXCL12) Neutraligand Prevent Inflammatory Reactions in an Asthma Model in Vivo." ACS medicinal chemistry letters **3**(1): 10-14.

Giudice, A., M. Caraglia, et al. (2010). "Circadian rhythms, adrenergic hormones and trafficking of hematopoietic stem cells." Expert opinion on therapeutic targets **14**(5): 567-575.

Guan, G., Y. Zhang, et al. (2015). "The HIF-1alpha/CXCR4 pathway supports hypoxia-induced metastasis of human osteosarcoma cells." Cancer letters **357**(1): 254-264.

Guo, F., Y. Wang, et al. (2015). "CXCL12/CXCR4: a symbiotic bridge linking cancer cells and their stromal neighbors in oncogenic communication networks." Oncogene.

Guo, L., Z. M. Cui, et al. (2011). "Chemokine axes CXCL12/CXCR4 and CXCL16/CXCR6 correlate with lymph node metastasis in epithelial ovarian carcinoma." Chinese journal of cancer **30**(5): 336-343.

Guo, M., C. Cai, et al. (2014). "Hypoxia promotes migration and induces CXCR4 expression via HIF-1alpha activation in human osteosarcoma." PloS one **9**(3): e90518.

Gupta, G. P. and J. Massague (2006). "Cancer metastasis: building a framework." Cell **127**(4): 679-695.

Gupta, P. B., C. Kuperwasser, et al. (2005). "The melanocyte differentiation program predisposes to metastasis after neoplastic transformation." Nature genetics **37**(10): 1047-1054.

Gupta, S. K. and K. Pillarisetti (1999). "Cutting edge: CXCR4-Lo: molecular cloning and functional expression of a novel human CXCR4 splice variant." Journal of immunology **163**(5): 2368-2372.

Gvozdenovic, A., M. J. Arlt, et al. (2013). "Silencing of CD44 gene expression in human 143-B osteosarcoma cells promotes metastasis of intratibial tumors in SCID mice." PloS one **8**(4): e60329.

Hanson, L. R. and W. H. Frey, 2nd (2008). "Intranasal delivery bypasses the blood-brain barrier to target therapeutic agents to the central nervous system and treat neurodegenerative disease." BMC neuroscience **9 Suppl 3**: S5.

Hattermann, K. and R. Mentlein (2013). "An infernal trio: the chemokine CXCL12 and its receptors CXCR4 and CXCR7 in tumor biology." Ann Anat **195**(2): 103-110.

Heesen, M., M. A. Berman, et al. (1997). "Alternate splicing of mouse fusin/CXC chemokine receptor-4: stromal cell-derived factor-1alpha is a ligand for both CXC chemokine receptor-4 isoforms." Journal of immunology **158**(8): 3561-3564.

Hernandez, L., M. A. Magalhaes, et al. (2011). "Opposing roles of CXCR4 and CXCR7 in breast cancer metastasis." Breast cancer research : BCR **13**(6): R128.

Herzog, H., Y. J. Hort, et al. (1993). "Molecular cloning, characterization, and localization of the human homolog to the reported bovine NPY Y3 receptor: lack of NPY binding and activation." DNA and cell biology **12**(6): 465-471.

Hodohara, K., N. Fujii, et al. (2000). "Stromal cell-derived factor-1 (SDF-1) acts together with thrombopoietin to enhance the development of megakaryocytic progenitor cells (CFU-MK)." Blood **95**(3): 769-775.

Horuk, R. (2001). "Chemokine receptors." Cytokine Growth Factor Rev **12**(4): 313-335.

Huang, Y., J. Zhang, et al. (2013). "Expression of the CXCL12/CXCR4 and CXCL16/CXCR6 axes in cervical intraepithelial neoplasia and cervical cancer." Chinese journal of cancer **32**(5): 289-296.

Hung, C. S., H. Y. Su, et al. (2014). "High-level expression of CXCR4 in breast cancer is associated with early distant and bone metastases." Tumour biology : the journal of the International Society for Oncodevelopmental Biology and Medicine **35**(2): 1581-1588.

Isakoff, M. S., S. S. Bielack, et al. (2015). "Osteosarcoma: Current Treatment and a Collaborative Pathway to Success." Journal of clinical oncology : official journal of the American Society of Clinical Oncology **33**(27): 3029-3035.

Iwasa, S., T. Yanagawa, et al. (2009). "Expression of CXCR4 and its ligand SDF-1 in intestinal-type gastric cancer is associated with lymph node and liver metastasis." Anticancer research **29**(11): 4751-4758.

Janowski, M. (2009). "Functional diversity of SDF-1 splicing variants." Cell adhesion & migration **3**(3): 243-249.

Jazin, E. E., H. Yoo, et al. (1993). "A proposed bovine neuropeptide Y (NPY) receptor cDNA clone, or its human homologue, confers neither NPY binding sites nor NPY responsiveness on transfected cells." Regulatory peptides **47**(3): 247-258.

Jia, S. F., L. L. Worth, et al. (1999). "A nude mouse model of human osteosarcoma lung metastases for evaluating new therapeutic strategies." Clinical & experimental metastasis **17**(6): 501-506.

Jiang, W., P. Zhou, et al. (1994). "Molecular cloning of TPAR1, a gene whose expression is repressed by the tumor promoter 12-O-tetradecanoylphorbol 13-acetate (TPA)." Experimental cell research **215**(2): 284-293.

Joliat, M. J., S. Umeda, et al. (2002). "Establishment and characterization of a new osteogenic cell line (MOS-J) from a spontaneous C57BL/6J mouse osteosarcoma." In vivo **16**(4): 223-228.

Kajiyama, H., K. Shibata, et al. (2008). "Involvement of SDF-1alpha/CXCR4 axis in the enhanced peritoneal metastasis of epithelial ovarian carcinoma." International journal of cancer. Journal international du cancer **122**(1): 91-99.

Kansara, M. and D. M. Thomas (2007). "Molecular pathogenesis of osteosarcoma." DNA and cell biology **26**(1): 1-18.

Khanna, C., J. Prehn, et al. (2000). "An orthotopic model of murine osteosarcoma with clonally related variants differing in pulmonary metastatic potential." Clinical & experimental metastasis **18**(3): 261-271.

Kim, S. Y., C. H. Lee, et al. (2008). "Inhibition of the CXCR4/CXCL12 chemokine pathway reduces the development of murine pulmonary metastases." Clin Exp Metastasis **25**(3): 201-211.

Klein, M. J. and G. P. Siegal (2006). "Osteosarcoma: anatomic and histologic variants." American journal of clinical pathology **125**(4): 555-581.

Koshkina, N. V. and E. S. Kleinerman (2005). "Aerosol gemcitabine inhibits the growth of primary osteosarcoma and osteosarcoma lung metastases." International journal of cancer. Journal international du cancer **116**(3): 458-463.

Kroeze, W. K., D. J. Sheffler, et al. (2003). "G-protein-coupled receptors at a glance." Journal of cell science **116**(Pt 24): 4867-4869.

Kufareva, I., B. S. Stephens, et al. (2014). "Stoichiometry and geometry of the CXC chemokine receptor 4 complex with CXC ligand 12: molecular modeling and experimental validation." Proceedings of the National Academy of Sciences of the United States of America **111**(50): E5363-5372.

Kumar, V. S., N. Barwar, et al. (2014). "Surface osteosarcomas: Diagnosis, treatment and outcome." Indian journal of orthopaedics **48**(3): 255-261.

Laguri, C., F. Arenzana-Seisdedos, et al. (2008). "Relationships between glycosaminoglycan and receptor binding sites in chemokines-the CXCL12 example." Carbohydrate research **343**(12): 2018-2023.

Laing, K. J. and C. J. Secombes (2004). "Chemokines." Developmental and comparative immunology **28**(5): 443-460.

Laverdiere, C., B. H. Hoang, et al. (2005). "Messenger RNA expression levels of CXCR4 correlate with metastatic behavior and outcome in patients with osteosarcoma." Clinical cancer research : an official journal of the American Association for Cancer Research **11**(7): 2561-2567.

Lazennec, G. and A. Richmond (2010). "Chemokines and chemokine receptors: new insights into cancer-related inflammation." Trends in molecular medicine **16**(3): 133-144.

Liang, J. J., S. Zhu, et al. (2010). "High levels of expression of human stromal cell-derived factor-1 are associated with worse prognosis in patients with stage II pancreatic ductal adenocarcinoma." Cancer epidemiology, biomarkers & prevention : a publication of the American Association for Cancer Research, cosponsored by the American Society of Preventive Oncology **19**(10): 2598-2604.

Liao, Y. X., Z. Z. Fu, et al. (2015). "AMD3100 reduces CXCR4-mediated survival and metastasis of osteosarcoma by inhibiting JNK and Akt, but not p38 or Erk1/2, pathways in in vitro and mouse experiments." Oncol Rep **34**(1): 33-42.

Liao, Y. X., C. H. Zhou, et al. (2013). "The role of the CXCL12-CXCR4/CXCR7 axis in the progression and metastasis of bone sarcomas (Review)." Int J Mol Med **32**(6): 1239-1246.

Lin, F., S. E. Zheng, et al. (2011). "Relationships between levels of CXCR4 and VEGF and blood-borne metastasis and survival in patients with osteosarcoma." Medical oncology **28**(2): 649-653.

Liu, F., R. Lang, et al. (2009). "Increased expression of SDF-1/CXCR4 is associated with lymph node metastasis of invasive micropapillary carcinoma of the breast." Histopathology **54**(6): 741-750.

Lodowski, D. T. and K. Palczewski (2009). "Chemokine receptors and other G protein-coupled receptors." Curr Opin HIV AIDS **4**(2): 88-95.

Loetscher, M., T. Geiser, et al. (1994). "Cloning of a human seven-transmembrane domain receptor, LESTR, that is highly expressed in leukocytes." The Journal of biological chemistry **269**(1): 232-237.

Loetscher, P., J. H. Gong, et al. (1998). "N-terminal peptides of stromal cell-derived factor-1 with CXC chemokine receptor 4 agonist and antagonist activities." The Journal of biological chemistry **273**(35): 22279-22283.

Luo, J., Z. Luo, et al. (1999). "Attachment of C-terminus of SDF-1 enhances the biological activity of its N-terminal peptide." Biochemical and biophysical research communications **264**(1): 42-47.

Ma, Q., D. Jones, et al. (1998). "Impaired B-lymphopoiesis, myelopoiesis, and derailed cerebellar neuron migration in CXCR4- and SDF-1-deficient mice." Proceedings of the National Academy of Sciences of the United States of America **95**(16): 9448-9453.

Ma, Q., Y. Zhou, et al. (2012). "The clinical value of CXCR4, HER2 and CD44 in human osteosarcoma: A pilot study." Oncology letters **3**(4): 797-801.

Ma, Y., R. F. Hwang, et al. (2013). "Dynamic mast cell-stromal cell interactions promote growth of pancreatic cancer." Cancer research **73**(13): 3927-3937.

Mantovani, A. (1999). "Chemokines. Introduction and overview." Chemical immunology **72**: 1-6.

Mantovani, A., R. Bonecchi, et al. (2006). "Tuning inflammation and immunity by chemokine sequestration: decoys and more." Nature reviews. Immunology **6**(12): 907-918.

Marina, N., M. Gebhardt, et al. (2004). "Biology and therapeutic advances for pediatric osteosarcoma." The oncologist **9**(4): 422-441.

Masuda, T., M. Endo, et al. (2015). "ANGPTL2 increases bone metastasis of breast cancer cells through enhancing CXCR4 signaling." Scientific reports **5**: 9170.

McAllister, R. M., M. B. Gardner, et al. (1971). "Cultivation in vitro of cells derived from a human osteosarcoma." Cancer **27**(2): 397-402.

Meng, X., L. Wuyi, et al. (2010). "Expression of CXCR4 in oral squamous cell carcinoma: correlations with clinicopathology and pivotal role of proliferation." Journal of oral pathology & medicine : official publication of the International Association of Oral Pathologists and the American Academy of Oral Pathology **39**(1): 63-68.

Meyers, P. A., G. Heller, et al. (1993). "Osteogenic sarcoma with clinically detectable metastasis at initial presentation." Journal of clinical oncology : official journal of the American Society of Clinical Oncology **11**(3): 449-453.

Mialou, V., T. Philip, et al. (2005). "Metastatic osteosarcoma at diagnosis: prognostic factors and long-term outcome--the French pediatric experience." Cancer **104**(5): 1100-1109.

Miura, K., S. Uniyal, et al. (2005). "Chemokine receptor CXCR4-beta1 integrin axis mediates tumorigenesis of osteosarcoma HOS cells." Biochemistry and cell biology = Biochimie et biologie cellulaire **83**(1): 36-48.

Mohseny, A. B., K. Szuhai, et al. (2009). "Osteosarcoma originates from mesenchymal stem cells in consequence of aneuploidization and genomic loss of Cdkn2." The Journal of pathology **219**(3): 294-305.

Muller, A., B. Homey, et al. (2001). "Involvement of chemokine receptors in breast cancer metastasis." Nature **410**(6824): 50-56.

Munk, R., P. Ghosh, et al. (2011). "Involvement of mTOR in CXCL12 mediated T cell signaling and migration." PloS one **6**(9): e24667.
Murakami, T., W. Maki, et al. (2002). "Expression of CXC chemokine receptor-4 enhances the pulmonary metastatic potential of murine B16 melanoma cells." Cancer research **62**(24): 7328-7334.
Murdoch, C. (2000). "CXCR4: chemokine receptor extraordinaire." Immunol Rev **177**: 175-184.
Nagasawa, T. (2014). "CXC chemokine ligand 12 (CXCL12) and its receptor CXCR4." J Mol Med (Berl) **92**(5): 433-439.
Nagasawa, T. (2015). "CXCL12/SDF-1 and CXCR4." Frontiers in immunology **6**: 301.
Nagasawa, T., S. Hirota, et al. (1996). "Defects of B-cell lymphopoiesis and bone-marrow myelopoiesis in mice lacking the CXC chemokine PBSF/SDF-1." Nature **382**(6592): 635-638.
Nagasawa, T., H. Kikutani, et al. (1994). "Molecular cloning and structure of a pre-B-cell growth-stimulating factor." Proceedings of the National Academy of Sciences of the United States of America **91**(6): 2305-2309.
Nagasawa, T., T. Nakajima, et al. (1996). "Molecular cloning and characterization of a murine pre-B-cell growth-stimulating factor/stromal cell-derived factor 1 receptor, a murine homolog of the human immunodeficiency virus 1 entry coreceptor fusin." Proceedings of the National Academy of Sciences of the United States of America **93**(25): 14726-14729.
Namlos, H. M., S. H. Kresse, et al. (2012). "Global gene expression profiling of human osteosarcomas reveals metastasis-associated chemokine pattern." Sarcoma **2012**: 639038.
Naruse, K., M. Ueno, et al. (1996). "A YAC contig of the human CC chemokine genes clustered on chromosome 17q11.2." Genomics **34**(2): 236-240.
Nguyen, D. X., P. D. Bos, et al. (2009). "Metastasis: from dissemination to organ-specific colonization." Nature reviews. Cancer **9**(4): 274-284.
Noda, M., Y. Omatsu, et al. (2011). "CXCL12-CXCR4 chemokine signaling is essential for NK-cell development in adult mice." Blood **117**(2): 451-458.
Nomiyama, H., A. Mera, et al. (2001). "Organization of the chemokine genes in the human and mouse major clusters of CC and CXC chemokines: diversification between the two species." Genes and immunity **2**(2): 110-113.
Nomiyama, H., N. Osada, et al. (2010). "The evolution of mammalian chemokine genes." Cytokine & growth factor reviews **21**(4): 253-262.
Nomiyama, H., N. Osada, et al. (2011). "A family tree of vertebrate chemokine receptors for a unified nomenclature." Developmental and comparative immunology **35**(7): 705-715.
Nomura, H., B. W. Nielsen, et al. (1993). "Molecular cloning of cDNAs encoding a LD78 receptor and putative leukocyte chemotactic peptide receptors." International immunology **5**(10): 1239-1249.
Norton, L. and J. Massague (2006). "Is cancer a disease of self-seeding?" Nature medicine **12**(8): 875-878.
Oberlin, E., A. Amara, et al. (1996). "The CXC chemokine SDF-1 is the ligand for LESTR/fusin and prevents infection by T-cell-line-adapted HIV-1." Nature **382**(6594): 833-835.
Oda, Y., H. Yamamoto, et al. (2006). "CXCR4 and VEGF expression in the primary site and the metastatic site of human osteosarcoma: analysis within a group of patients, all of whom developed lung metastasis." Modern pathology : an official journal of the United States and Canadian Academy of Pathology, Inc **19**(5): 738-745.

Onai, N., Y. Zhang, et al. (2000). "Impairment of lymphopoiesis and myelopoiesis in mice reconstituted with bone marrow-hematopoietic progenitor cells expressing SDF-1-intrakine." Blood **96**(6): 2074-2080.

Otte, M., A. Kliewer, et al. (2014). "CXCL14 is no direct modulator of CXCR4." FEBS letters **588**(24): 4769-4775.

Pan, J., J. Mestas, et al. (2006). "Stromal derived factor-1 (SDF-1/CXCL12) and CXCR4 in renal cell carcinoma metastasis." Molecular cancer **5**: 56.

Patane, S., S. Avnet, et al. (2006). "MET overexpression turns human primary osteoblasts into osteosarcomas." Cancer research **66**(9): 4750-4757.

Pawig, L., C. Klasen, et al. (2015). "Diversity and Inter-Connections in the CXCR4 Chemokine Receptor/Ligand Family: Molecular Perspectives." Frontiers in immunology **6**: 429.

Peng, L., M. M. Damschroder, et al. (2015). "Molecular basis for the antagonistic activity of an anti-CXCR4 antibody." mAbs: 0.

Phillips, R. J., M. D. Burdick, et al. (2003). "The stromal derived factor-1/CXCL12-CXC chemokine receptor 4 biological axis in non-small cell lung cancer metastases." American journal of respiratory and critical care medicine **167**(12): 1676-1686.

Ponten, J. and E. Saksela (1967). "Two established in vitro cell lines from human mesenchymal tumours." International journal of cancer. Journal international du cancer **2**(5): 434-447.

Qin, L., I. Kufareva, et al. (2015). "Structural biology. Crystal structure of the chemokine receptor CXCR4 in complex with a viral chemokine." Science **347**(6226): 1117-1122.

Rimland, J., W. Xin, et al. (1991). "Sequence and expression of a neuropeptide Y receptor cDNA." Molecular pharmacology **40**(6): 869-875.

Ritter, J. and S. S. Bielack (2010). "Osteosarcoma." Annals of oncology : official journal of the European Society for Medical Oncology / ESMO **21 Suppl 7**: vii320-325.

Robertson, M. J. (2002). "Role of chemokines in the biology of natural killer cells." Journal of leukocyte biology **71**(2): 173-183.

Roland, J., B. J. Murphy, et al. (2003). "Role of the intracellular domains of CXCR4 in SDF-1-mediated signaling." Blood **101**(2): 399-406.

Saini, V., A. Marchese, et al. (2011). "Structural determinants of ubiquitin-CXC chemokine receptor 4 interaction." The Journal of biological chemistry **286**(51): 44145-44152.

Sakamoto, A. and Y. Iwamoto (2008). "Current status and perspectives regarding the treatment of osteo-sarcoma: chemotherapy." Reviews on recent clinical trials **3**(3): 228-231.

Sand, L. G., A. G. Jochemsen, et al. (2015). "Novel splice variants of CXCR4 identified by transcriptome sequencing." Biochemical and biophysical research communications.

Scadden, D. T. (2008). "Circadian rhythms: stem cells traffic in time." Nature **452**(7186): 416-417.

Scala, S. (2015). "Molecular Pathways: Targeting the CXCR4-CXCL12 Axis-Untapped Potential in the Tumor Microenvironment." Clinical cancer research : an official journal of the American Association for Cancer Research.

Schmidt, J., G. P. Strauss, et al. (1988). "Establishment and characterization of osteogenic cell lines from a spontaneous murine osteosarcoma." Differentiation; research in biological diversity **39**(3): 151-160.

Shah, A. and A. Mangaonkar (2015). "Idelalisib: A Novel PI3Kdelta Inhibitor for Chronic Lymphocytic Leukemia." The Annals of pharmacotherapy **49**(10): 1162-1170.

Shirozu, M., T. Nakano, et al. (1995). "Structure and chromosomal localization of the human stromal cell-derived factor 1 (SDF1) gene." Genomics **28**(3): 495-500.

Song, Z. Y., Z. H. Gao, et al. (2015). "Downregulation of the CXCR4/CXCL12 axis blocks the activation of the Wnt/beta-catenin pathway in human colon cancer cells." Biomedicine & pharmacotherapy = Biomedecine & pharmacotherapie **71**: 46-52.

Speetjens, F. M., G. J. Liefers, et al. (2009). "Nuclear localization of CXCR4 determines prognosis for colorectal cancer patients." Cancer microenvironment : official journal of the International Cancer Microenvironment Society **2**(1): 1-7.

Stafford, L. J., K. S. Vaidya, et al. (2008). "Metastasis suppressors genes in cancer." The international journal of biochemistry & cell biology **40**(5): 874-891.

Steinberg, M. and M. Silva (2010). "Plerixafor: A chemokine receptor-4 antagonist for mobilization of hematopoietic stem cells for transplantation after high-dose chemotherapy for non-Hodgkin's lymphoma or multiple myeloma." Clinical therapeutics **32**(5): 821-843.

Sun, X., C. Charbonneau, et al. (2013). "CXCR4-targeted therapy inhibits VEGF expression and chondrosarcoma angiogenesis and metastasis." Molecular cancer therapeutics **12**(7): 1163-1170.

Sun, X., G. Cheng, et al. (2010). "CXCL12 / CXCR4 / CXCR7 chemokine axis and cancer progression." Cancer Metastasis Rev **29**(4): 709-722.

Takabatake, Y., T. Sugiyama, et al. (2009). "The CXCL12 (SDF-1)/CXCR4 axis is essential for the development of renal vasculature." Journal of the American Society of Nephrology : JASN **20**(8): 1714-1723.

Tanegashima, K., K. Suzuki, et al. (2013). "CXCL14 is a natural inhibitor of the CXCL12-CXCR4 signaling axis." FEBS letters **587**(12): 1731-1735.

Tang, N., W. X. Song, et al. (2008). "Osteosarcoma development and stem cell differentiation." Clinical orthopaedics and related research **466**(9): 2114-2130.

Tashiro, K., H. Tada, et al. (1993). "Signal sequence trap: a cloning strategy for secreted proteins and type I membrane proteins." Science **261**(5121): 600-603.

Thelen, M. (2001). "Dancing to the tune of chemokines." Nature immunology **2**(2): 129-134.

Thelen, M., L. M. Munoz, et al. (2010). "Chemokine receptor oligomerization: functional considerations." Current opinion in pharmacology **10**(1): 38-43.

Thelen, M. and S. Thelen (2008). "CXCR7, CXCR4 and CXCL12: an eccentric trio?" Journal of neuroimmunology **198**(1-2): 9-13.

Thomas, R. M., J. Kim, et al. (2008). "The chemokine receptor CXCR4 is expressed in pancreatic intraepithelial neoplasia." Gut **57**(11): 1555-1560.

Tripathi, A., P. G. Vana, et al. (2015). "Heteromerization of chemokine (C-X-C motif) receptor 4 with alpha1A/B-adrenergic receptors controls alpha1-adrenergic receptor function." Proceedings of the National Academy of Sciences of the United States of America **112**(13): E1659-1668.

Valastyan, S. and R. A. Weinberg (2011). "Tumor metastasis: molecular insights and evolving paradigms." Cell **147**(2): 275-292.

Van Haastert, P. J. and P. N. Devreotes (2004). "Chemotaxis: signalling the way forward." Nature reviews. Molecular cell biology **5**(8): 626-634.

Wagner, P. L., E. Hyjek, et al. (2009). "CXCL12 and CXCR4 in adenocarcinoma of the lung: association with metastasis and survival." The Journal of thoracic and cardiovascular surgery **137**(3): 615-621.

Walkley, C. R., R. Qudsi, et al. (2008). "Conditional mouse osteosarcoma, dependent on p53 loss and potentiated by loss of Rb, mimics the human disease." Genes & development **22**(12): 1662-1676.

Wang, L. L. (2005). "Biology of osteogenic sarcoma." Cancer journal **11**(4): 294-305.

Wegner, S. A., P. K. Ehrenberg, et al. (1998). "Genomic organization and functional characterization of the chemokine receptor CXCR4, a major entry co-receptor for

human immunodeficiency virus type 1." The Journal of biological chemistry **273**(8): 4754-4760.

Wehler, T. C., C. Graf, et al. (2011). "SDF1beta expression in renal cell carcinoma correlates with grading and infiltration by CD8+ T-cells." Anticancer research **31**(9): 2797-2803.

Wheeler, Y. Y., S. Y. Chen, et al. (2003). "Intrabody and intrakine strategies for molecular therapy." Molecular therapy : the journal of the American Society of Gene Therapy **8**(3): 355-366.

Whelan, J. S., R. C. Jinks, et al. (2012). "Survival from high-grade localised extremity osteosarcoma: combined results and prognostic factors from three European Osteosarcoma Intergroup randomised controlled trials." Annals of oncology : official journal of the European Society for Medical Oncology / ESMO **23**(6): 1607-1616.

Williams, S. A., Y. Harata-Lee, et al. (2010). "Multiple functions of CXCL12 in a syngeneic model of breast cancer." Molecular cancer **9**: 250.

Xu, C., H. Zhao, et al. (2015). "CXCR4 in breast cancer: oncogenic role and therapeutic targeting." Drug design, development and therapy **9**: 4953-4964.

Young, K. C., E. Torres, et al. (2009). "Inhibition of the SDF-1/CXCR4 axis attenuates neonatal hypoxia-induced pulmonary hypertension." Circulation research **104**(11): 1293-1301.

Yu, L., J. Cecil, et al. (2006). "Identification and expression of novel isoforms of human stromal cell-derived factor 1." Gene **374**: 174-179.

Yu, Y., X. Shi, et al. (2013). "Stromal cell-derived factor-1 (SDF-1)/CXCR4 axis enhances cellular invasion in ovarian carcinoma cells via integrin beta1 and beta3 expressions." Oncology research **21**(4): 217-225.

Zeelenberg, I. S., L. Ruuls-Van Stalle, et al. (2001). "Retention of CXCR4 in the endoplasmic reticulum blocks dissemination of a T cell hybridoma." The Journal of clinical investigation **108**(2): 269-277.

Zeelenberg, I. S., L. Ruuls-Van Stalle, et al. (2003). "The chemokine receptor CXCR4 is required for outgrowth of colon carcinoma micrometastases." Cancer research **63**(13): 3833-3839.

Zhang, Y., A. Foudi, et al. (2004). "Intracellular localization and constitutive endocytosis of CXCR4 in human CD34+ hematopoietic progenitor cells." Stem cells **22**(6): 1015-1029.

Zhao, H., L. Guo, et al. (2015). "CXCR4 over-expression and survival in cancer: a system review and meta-analysis." Oncotarget **6**(7): 5022-5040.

Zhou, W., Z. Jiang, et al. (2009). "Down-regulation of CXCL12 mRNA expression by promoter hypermethylation and its association with metastatic progression in human breast carcinomas." Journal of cancer research and clinical oncology **135**(1): 91-102.

Ziarek, J. J., C. T. Veldkamp, et al. (2013). "Heparin oligosaccharides inhibit chemokine (CXC motif) ligand 12 (CXCL12) cardioprotection by binding orthogonal to the dimerization interface, promoting oligomerization, and competing with the chemokine (CXC motif) receptor 4 (CXCR4) N terminus." The Journal of biological chemistry **288**(1): 737-746.

Zlotnik, A., A. M. Burkhardt, et al. (2011). "Homeostatic chemokine receptors and organ-specific metastasis." Nature reviews. Immunology **11**(9): 597-606.

Zlotnik, A. and O. Yoshie (2000). "Chemokines: a new classification system and their role in immunity." Immunity **12**(2): 121-127.

(2002). "Chemokine/chemokine receptor nomenclature." Journal of immunological methods **262**(1-2): 1-3.

14. Acknowledgments

First of all, I would like to thank my supervisors Prof. Bruno Fuchs and Prof. Walter Born for the continuous support and excellent guidance of my PhD study. I am very grateful to you for giving me the opportunity to perform my PhD research in your laboratory, for your patience and motivation.

I would like to thank all my committee members, Prof. Ernst Hafen, Prof. Josef Jiricny, Prof. Pancras Hogendoorn and Prof. Marcus Thelen for their precious comments and insightful discussions during my committee meetings. I very much appreciate your help and support you gave me.

In particular, I would like to express my deepest gratitude to Prof. Dr. Ernst Hafen for having accepted to be my thesis director and for his support and encouragement during the time of my PhD study.

I would like to give special thanks to Prof. Marcus Thelen for his great contribution to my PhD research, for his knowledge, and for challenging and inspiring discussions which helped me broaden my knowledge in the field of chemokines and widen my research. I am very grateful to you for having accepted to be my advisor. This thesis would not have been possible without your support.

I thank my colleagues and labmates for their advice and support. In particular, I would like to thank Dr. Ana Gvozdenovic, Dr. Aleksandar Boro, Dr. Adam Sabile, Dr. Sander Botter, Prof. Roman Muff, Dr. Knut Husmann, Dr. Ram Kumar, Dr. Aleksandar Kuzmanov, Daniela Meier, Bernhard Robl, Viola Puddinu, Egle Radice, Dr. Carmen Campanile, Chris Bühler, Josefine Bertz, Simon Häberle, Else-Marie Pedersen, Philomina Selvam and Joaquin Urdinez. Special thanks go to Dr. Matthias JE Arlt for his great contribution to my PhD project and related research.

Many thanks go to Dr. Patrick Brennecke who introduced me in the research of chemokines and helped and supported me during the whole time of my PhD study.

Furthermore, I would like to thank Dr. David Jarrossay and Dr. Malgorzata Kisielow for their help with flow cytometry assay.

Last but not the least I would like to thank my family and my boyfriend for patiently supporting me spiritually throughout the years of my PhD study.